Doctoral Dissertation
Doctoral Program in Energy Engineering (30th Cycle)

Hyperspectral Imaging for Landmine Detection

Ihab Makki

* * * * * *

Supervisors

Prof. Rafic Younes, Supervisor
Prof. Massimo Zucchetti, Supervisor
Prof. Tiziano Bianchi, Co-Supervisor
Prof. Clovis Francis, Co-Supervisor

Doctoral Examination Committee:

Prof. Maria Sabrina Greco, Reviewer, University of Pisa
Prof. Ali El-Zaart, Reviewer, Beirut Arab University
Prof. Luisa Verdoliva, Referee, University of Napoli Federico II
Prof Georges Sakr, Referee, University Saint Joseph
Prof. Fahed Abdallah, Invited, Lebanese University
Col. Pierre Bou Maroun, Invited, Lebanese Army

Politecnico di Torino
December 12, 2017

I hereby declare that, the contents and organisation of this dissertation constitute my own original work and does not compromise in any way the rights of third parties, including those relating to the security of personal data.

………………………….....
Ihab Makki
Beirut, December 12, 2017

Summary

This PhD thesis aims at investigating the possibility to detect landmines using hyperspectral imaging. Using this technology, we are able to acquire at each pixel of the image spectral data in hundreds of wavelengths. So, at each pixel we obtain a reflectance spectrum that is used as fingerprint to identify the materials in each pixel, and mainly in our project help us to detect the presence of landmines.

The proposed process works as follows: a preconfigured drone (hexarotor or octorotor) will carry the hyperspectral camera. This programmed drone is responsible of flying over the contaminated area in order to take images from a safe distance. Various image processing techniques will be used to treat the image in order to isolate the landmine from the surrounding. Once the presence of a mine or explosives is suspected, an alarm signal is sent to the base station giving information about the type of the mine, its location and the clear path that could be taken by the mine removal team in order to disarm the mine.

This technology has advantages over the actually used techniques:

- It is safer because it limits the need of humans in the searching process and gives the opportunity to the demining team to detect the mines while they are in a safe region.

- It is faster. A larger area could be cleared in a single day by comparison with demining techniques

- This technique can be used to detect at the same time objects other than mines such oil or minerals.

First, a presentation of the problem of landmines that is expanding worldwide referring to some statistics from the UN organizations is provided. In addition, a brief presentation of different types of landmines is shown. Unfortunately, new landmines are well camouflaged and are mainly made of plastic in order to make their detection using metal detectors harder. A summary of all landmine detection techniques is shown to give an idea about the advantages and disadvantages of each technique.

In this work, we give an overview of different projects that worked on the detection of landmines using hyperspectral imaging. We will show the main results achieved in this field and future work to be done in order to make this technology effective.

Moreover, we worked on different target detection algorithms in order to achieve high probability of detection with low false alarm rate. We tested different statistical and linear unmixing based methods. In addition, we introduced the use of radial basis function neural networks in order to detect landmines at subpixel level. A comparative study between different detection methods will be shown in the thesis.

A study of the effect of dimensionality reduction using principal component analysis prior to classification is also provided. The study shows the dependency between the two steps (feature extraction and target detection). The selection of target detection algorithm will define if feature extraction in previous phase is necessary.

A field experiment has been done in order to study how the spectral signature of landmine will change depending on the environment in which the mine is planted. For this, we acquired the spectral signature of 6 types of landmines in different conditions: in Lab where specific source of light is used; in field where mines are covered by grass; and when mines are buried in soil. The results of this experiment are very interesting. The signature of two types of landmines are used in the simulations. They are a database necessary for supervised detection of landmines. Also we extracted some spectral characteristics of landmines that would help us to distinguish mines from background.

Acknowledgment

Thank you

Contents

List of Figures

List of Tables

Chapter One

1.Introduction

Landmines and cluster munition constitute a main obstacle against the development of the societies and return to normal life after the ceasefire is achieved. The fear of death and the destruction won't stop with the end of war, but will continue with the existence of threat of cluster munitions, landmines, unexploded ordnance and improvised explosive devices. This type of weapons doesn't know when the war is ended and remain active for years or even decades menacing innocent people in their everyday life

According to recent statistics [1], 80% of the casualties of landmines are from children that have nothing to do with the war or its causes. Therefore, there is a need to ban the use of this type of blind weapons. The efforts to ban landmines has started and we have an international campaign to ban landmines and cluster munitions with numeral signees countries [130]. However, nobody can control the situation during the war and the landmines are being used during recent conflicts (ex. In Libya and Syria 2016). Therefore, there is a need to find detection techniques that are fast and reliable.

Different techniques have been addressed in order to detect landmines. Each method has its advantages and inconveniences. One of the earlier and most used methods is the metal detector. Due to electrical induction phenomena, this type of detectors is able to detect the objects that contains metal under the soil. Although this technique is cheap, it has several drawbacks: it detects all metals, either landmines or inert metals so it has very high false alarm rate; new landmines contains less metals so they are harder to be detected. Other techniques used for landmine detection will be mentioned in the next chapters.

 In this thesis, we are addressing this problem with a new technique named Hyperspectral Imaging or Imaging spectroscopy. This technique gives the ability to measure at each image unit (pixel) the portion of light reflected in hundreds of wavelengths. Thus, we will obtain a hypercube composed of two spatial dimensions and a third dimension that contains spectral information. This technique is well used in remote sensing field for different purposes like mapping, agriculture, astronomy, food monitoring, surveillance and others.

When light hits an object, it is either absorbed or reflected. The portion of light that is reflected depends on the size of the molecules of the object that is reflecting on, the intermolecular distances in addition to the wavelength of the radiation. Each material composed of different components could reflect light of various wavelengths in a different

manner. Therefore, we have the ability using this technology to identify the materials remotely. In our case, we will use the spectral and spatial information of the hyperspectral images to detect landmines and cluster munitions without the presence of deminers on field.

Several approaches exist for target detection using hyperspectral imaging: some are supervised where the spectrum of the data is known before; other are unsupervised based on searching for targets that are spectrally different from their surroundings. The latter type of information does not necessitate the knowledge of the target spectrum in advance. However, this type of detectors is characterized by a high false alarm rate as we will see in the next chapters because rare events in the image different from their background will be marked as targets.

During the work on this PhD thesis, we studied different scenarios of supervised and unsupervised detection, taking into consideration image preprocessing techniques like feature selection and dimensionality reduction. Knowing the target reflectance spectra will not make its detection a straightforward process due to several reasons:

1) Spectral variability: the spectrum registered in lab conditions will not be necessary the same in field condition due to effect of weather and illumination conditions.

2) Noisy images.

3) Low spatial resolution that make the reflectance detected in a pixel composed by a mixture of endmembers reflectance spectra.

We worked on different types of supervised and unsupervised detection algorithms based on probabilistic and linear mixture models. In addition, we worked on artificial neural networks in order to detect landmines using hyperspectral images in a fast and more accurate way.

In Chapter 2, we analyze the problem of landmines and show the existing methods currently used to address this issue. An introduction to hyperspectral imaging with stat of art of landmine detection using hyperspectral imaging and different tools used in hyperspectral image treatment are shown in Chapter 3. In Chapter 4, we present all experiments done during my work on the thesis with the results achieved. The conclusions are drawn in Chapter 5.

Chapter Two:

2. Problem of landmines and existing solutions

2.1.   Problem of Landmines

This chapter presents an introduction concerning landmines contamination issues, crisis, legacy, and action. We conduct an analysis of mine action, national and international programs. It is consequential to survey the foundation of the mine activity area since its start. We introduce the problem of landmines and how action is taken to face these problems. A concise abridgement of the expedition to ostracize killing mines is additionally included. In addition, we show the main types of landmines.

Part of the information shown here is published in [129].

2.1.1. Landmine contamination and impact

Several countries suffer from the existence of millions of landmines in their territories. These landmines have indefinite life, and may still cause horrific personal injuries and economic dislocation for decades after a war has finished. Therefore, there is a growing demand by these countries for reliable landmine inspection systems.

 This problem affects the social and economic development of the regions, diminishes the areas to be cultivated [2], [3], [4], [5]], and also risks killing innocent people; triggered by the fact that mines do not know truce [[6], [7], [8], [9]]. As known, mines lead to hundreds of thousands of deaths or to amputation of limbs. For instance, in Cambodia there are more than 35000 amputees affected by landmine explosion [[2], [5]]. Some of the injured people die in the fields from bleeding or lack of transport to reach the hospital [5]. Mines can decrease the area to be cultivated, also prevent the income of valuable foreign currency coming from tourist's visit, which lead to economic regression.

Various obstacles are faced in removing these landmines, such as the loss or absence of maps or information about the landmine types used or the areas where they were originally emplaced,

the change of landmines locations due to climatic and physical factors, the large variety of types of landmines, and the high cost of locating and removing landmines. The landmines sensitivity to explosion with time or atmospheric factors also poses a great danger to individuals.

Landmines are victim-activated and indiscriminate. Mines emplaced during a conflict against enemy forces can still kill or injure civilians decades later. Land mines, cluster munitions, and other explosive remnants of war (ERW) continue to kill or injure at least 4,300 people every year [3]. The vast majority of recorded casualties are civilians (80% in 2015) as shown in Fig. 1 of which 39% are children (Fig 2). Between 1999 and 2012, more than 1,000 deminers have been killed or injured while undertaking demining operations [10].
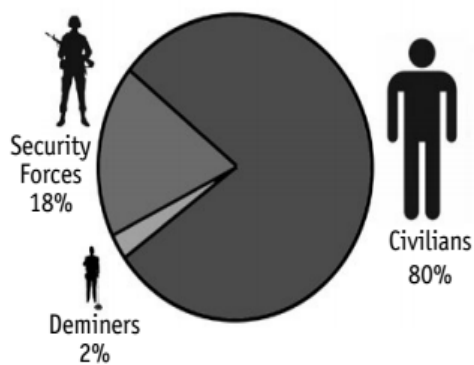
Figure 1: Mines/erw casualties by civilian/military status in 2014
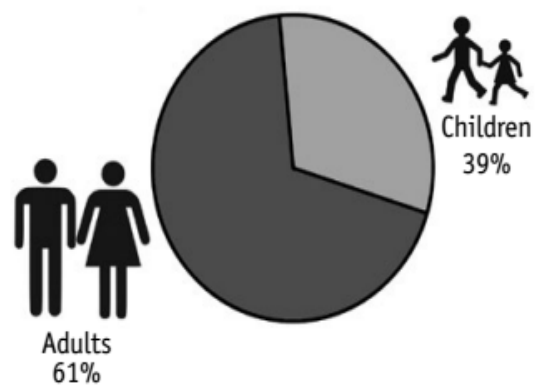
Figure 2: Mines/erw casualties by age in 2014

States with causalities in 2015 are shown in the next table:

Table 1: States/Areas With Mine/Erw Casualties In 2014

Sub-Saharan Africa	Americas	East and South Asia, and Pacific	Europe, the Caucasus, and Central Asia	Middle East and North Africa
Angola	Colombia	**Afghanistan**	**Albania**	**Algeria**
Chad	**Peru**	**Cambodia**	Armenia	Egypt
Congo, DR		India	Azerbaijan	Iran
Côte d'Ivoire		Lao PDR	**Belarus**	**Iraq**
Guinea-Bissau		Myanmar	**Bosnia and**	**Kuwait**
Kenya		Nepal	**Herzegovina**	Lebanon
Mali		Pakistan	**Croatia**	Libya
Mozambique		**Philippines**	**Poland**	Morocco
Namibia		Sri Lanka	Russian Federation	Palestine
Niger		**Thailand**	**Serbia**	Syria
Senegal		Vietnam	**Tajikistan**	**Yemen**
Somalia			**Turkey**	*Western Sahara*
South Sudan			**Ukraine**	
Sudan			*Kosovo*	
Tunisia			*Nagorno-Karabakh*	
Uganda				
Zambia				
Zimbabwe				
Somaliland				

The total casualties in 2015 denoted the most yearly recorded losses since 2006. Year 2015 additionally denoted the most noteworthy number of yearly losses by extemporized mines recorded by the Monitor [5].

When a landmine explodes, the impact of the explosion weakens as the distance increases from the mine. The blast wave generated by to explosion has a peak power at the beginning and loses its power while moving in the atmosphere. Accordingly, it is possible that get a high killing power from a mine containing small amount of explosives in close contact, (for example, a mine under the foot) while encountering considerably less damage from a significantly bigger dangerous charge a few meters away. There is consequently a colossal assortment in the scope of touchy wounds from landmines and UXO. Mine/UXO wounds have two fundamental effects. Firstly, they influence the lives of the wounded and their family; furthermore, they have impacts on the medicinal foundation of the influenced nation. The fundamental monetary impact on the casualty is the constraining of capacity to acquire wage to bolster themselves and their family. In addition to evident physical wounds, the setback may endure mental harm. Female setbacks are viewed as being especially helpless as the broad physical harm can seriously restrict their odds of marriage. The impacts are not constrained to the setback or their close families. Treating mine wounds depletes the neighborhood therapeutic foundation of developing nations, as these sorts of wounds unavoidably wind up noticeably tainted and typically requires 2-3 operations to debride the wounds. Every loss will

require prosthesis or a wheelchair on the chance to recover portability. The prostheses will likewise require concentrated physiotherapy to figure out how to utilize the counterfeit appendage. Moreover, most amputees will require another appendage ever 2-3 years as the old ones destroy.

2.1.2. Types of landmines

Mines can be outlined either as 'anti-personnel' or as 'anti-tank'. Anti-personnel (AP) mines are intended to be actuated by individuals, while anti-tank (AT) mines are expected to thrash tanks or other shielded vehicles [11].

Anti-tank mines are designed to be triggered by heavy vehicles such as tanks. They are large (usually bigger than a person's shoe) and heavy (weighing more than 5 kilos). These mines contain enough explosives to destroy the vehicle that runs over them and as a result also frequently kill people in or near the vehicle. Anti-tank mines are laid where enemy vehicles are expected to travel: on roads, bridges and tracks.

Anti-personnel mines are triggered much more easily and are designed to wound people. They have less explosives and are much smaller and lighter than anti-tank mines—they could be as small as a packet of cigarettes, weighing as little as 50 grams. Anti-personnel mines come in all shapes and colors and are made from a variety of materials.

Although AP mines may kill a person, they are primarily designed to cause severe injury—a wounded person must be assisted and this takes more of the enemy's time and resources. Anti-personnel mines can be laid anywhere and can be set off in a number of ways—stepping on them, pulling on a wire or simply shaking them. Anti-personnel mines may also explode when an object placed over them is removed. [12]

type	AP landmine	AT landmine
weight	Light(100g-4Kg)	Heavy(6Kg-11Kg)
size	6-20cm	20-50cm
target	Human	Vehicle
Case material	Plastic,metal,wood	Plastic,metal
Operating pressure	5Kg	120Kg

Figure 3: Comparison between AT and AP landmines

Generally, there are two types of AP mines: blast mines and fragmentation mines.

BLAST MINES

> Blast landmines are buried close to the surface of the soil and are generally triggered by pressure. When a person steps on a blast mine and activates it, the mine's main charge detonates, creating a blast shock wave consisting of hot gases travelling at extremely high velocity. A famous type of blast mines is scatterable mines.[13]

FRAGMENTATION MINES

This type of landmines release fragments in all directions, or can be arranged to send fragments in one direction. These landmines can cause injuries up to 200m away and kill at closer distances. The fragments used in these landmines are either metal or glass. [13]

Anti-tank mines are designed to immobilize or destroy vehicles. All anti-tank mines are blast mines, because the goal of the anti-tank mine is to destroy the tank's tracks and body. There's no need for a fragmentation anti-tank mine.

Most countries and armies try to possess landmines to protect the main installations and key basis from enemy intruders. When a military base is constructed in an open area, it will be vulnerable to attacks by the enemy from all sides. In such cases, the landmines are used to limit the reachable zones and focus the defensive forces in one side. Mines can also be used as part of the support system for heavy artillery.

However, while landmines may have readily identifiable military applications, the nature, design, and deployment of large numbers of mines will necessarily lead to civilian casualties

The neutralization of mines requires specialized training and remains a tedious and dangerous process. Mines are often designed and deployed in order to make their detection as difficult as possible. Furthermore, advances in technology are exacerbating the problem because most modern mines are now made with plastics and may contain only traces of metal, if any. Newer models may also contain sophisticated electronic fuses that make them more hazardous to remove.

2.2. Landmine detection techniques

In this section, we show the main detection techniques used in the detection of landmines. The goal of this section is to show the techniques already used, their pros and cons and compare their performance with the hyperspectral image technique.

The most widely used method for detecting mines follows the same techniques developed during the Second World War, and directly involves human beings. The typical deminer's tool kit today largely resembles those used more than 50 years ago (It consists of a metal detector and a prodding instrument).

Several techniques have been designed and developed for demining. Each technique is suitable for detection under some conditions depending on the type of the mine case, the explosive material and the soil.

As we are studying the potential of hyperspectral imaging for landmine detection, we will describe the detection techniques currently used. The rationale of this section is not to go through the complicated physics principles of how the sensors work but to give some brief information about these techniques stating their strengths and limitations, in order to highlight the advantages of hyperspectral imaging over other techniques.

Generally, most of the landmine detection techniques consist of three main units; a sensor to capture a signature of the landmine, a signal or image processing unit to arrange the acquired data and a decision making unit to decide whether a landmine exists or not.

The sensor may be electromagnetic, acoustic, nuclear, biological, chemical or mechanical.

2.2.1. Electromagnetic Methods

The deminer holds the handle of Electro-Magnetic Induction (EMI) detector (Fig.4) close to the ground and sweeps it slowly around the area being investigated. Electrical current flowing through the first coil, the "transmit coil," induces a time-varying magnetic field in the ground. This primary magnetic field, in turn, induces electrical (eddy) currents in buried metal objects. The currents from the buried objects create a weaker, secondary magnetic field. The second coil, the "receiver coil," detects changes in voltage induced by the secondary magnetic field as shown. The detector then converts these changes in the electric potential to an audible signal. [13]

Figure 4: Landmine detection with metal detector

2.2.2. Ground Penetrating Radar (GPR)

Difficulty in detecting tiny amounts of metal in a plastic land mine with a metal detector has led to the development of this technique. GPR detects buried objects by emitting radio waves (ranging from about 10 MHz to a few GHz) into the ground and then analyzing the return signals generated by reflections of the waves at any subsurface discontinuity with different indexes of refraction such as at the boundary between soil and a landmine or between soil and a large rock. The GPR technique (Fig.5) uses an antenna pair (transmitter and receiver separated by a small fixed distance) to send short pulses of electromagnetic energy into the subsurface and then record the returning signals. The return signal is interpreted using a computerized signal processing system that gives an audio image to determine the object's shape and position. [[13],[14]
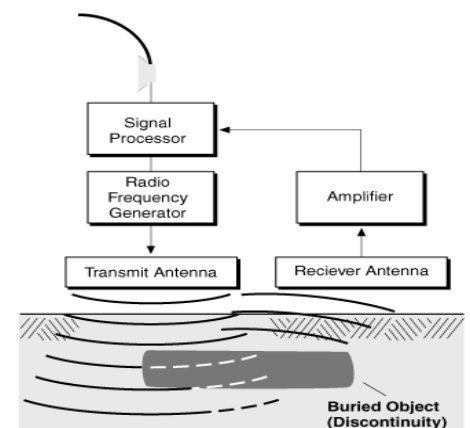
Figure 5: GPR principle

2.2.3. Infrared/Hyperspectral Systems

Infrared radiation consists of wavelength of $0.7\mu m$ to $1mm$ in microwave regions. Infrared/hyperspectral methods detect anomalous variations in electromagnetic radiation reflected or emitted by either surface mines or the soil and vegetation immediately above buried mines. Two modes of action, including active and passive irradiation using a broad range of electromagnetic wavelengths: A passive IR system detects natural radiation from the object whereas active systems are provided with heat source and detects radiation from heated object. Thermal detection methods exploit diurnal variations in temperatures of areas near mines relative to surrounding areas. The physical activity of emplacing mines changes the natural soil particle distribution by bringing small particles to the surface, which in turn affects the way in which the soil scatters light. Systematic changes in vegetation moisture levels immediately above buried mines also may have influence [13].

2.2.4. Acoustic/Seismic method

These methods are unique among detection methods that identify the mine casing based on the mechanical properties and are not based on electromagnetic properties. The A/S technique is used for the detection of landmines by vibrating them with acoustic or seismic waves that are generated and received by non-contact (acoustic) and contact (seismic) transducers, respectively. The transmitting system may be composed of acoustic loudspeakers or electrodynamic shakers. When the receiver senses a reflected energy that means an object possibly a landmine is buried. (Fig.6) [15].
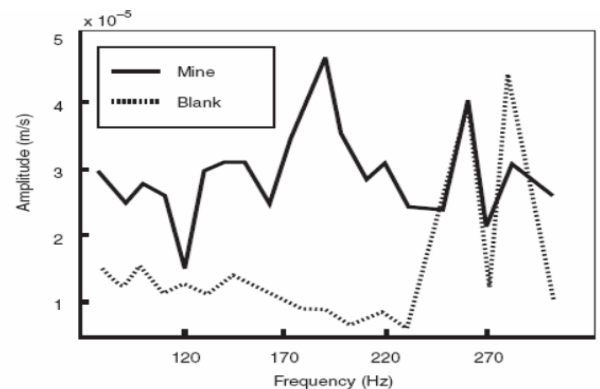
Figure 6: Amplitude of Surface Vibration of Ground in response to sound waves: over a Mine (solid line) and a Blank (dashed line)

2.2.5. Nuclear Quadruple Resonance (NQR)

This is a radiofrequency-based technique used to detect specific chemical compound like explosives. It is composed of an emitter that sends a radiation with a frequency that corresponds to the frequency of resonance of the explosive material. By this, the nuclei of the component is excited and when it returns to the stable state, it emits another radiation that induces an electric potential at the receiver coil. By this, the presence of a landmine is noticed by the detection of the presence of explosives [16].

2.2.6. Vapor sensors

A small percentage of the explosive manages to get out, as vapor, through fissures and shield structures of mines. The idea is to detect the presence of vapor from explosives. There are two research lines in this topic: biological and chemical.

Biological detection methods involve the use of mammals, insects, microorganisms, or plants to detect explosives. Each of the different methods operates on a different set of principles and is at a different stage of development.

A variety of possible non-biological mechanisms for detecting low concentrations of explosives in air or in soil samples have been investigated in recent years leading to the development of highly sensitive odor detection devices. When a sample of air containing explosives passes between the slides of the sensor, some of the explosive binds to the polymer and reduces the amount of fluorescent light that one slide emits. This reduction in the intensity of radiation received is detected by a small photomultiplier device giving notice the existence of explosive material.[13],[15]

2.2.7. Mechanical methods

In some cases, if the terrain and soil conditions are suitable, it is possible to use large armored vehicles in order to clean the minefields. This method is preferred by the army during the time of conflict as there is no much time to localize, identify and isolate the mines. It necessitates the use of large and expensive vehicles. The risk is minimized as the demining personnel are either in a well shielded place or are remotely controlling the vehicles. However, this technique leaves the area virtually destroyed. In addition, a landmine may be buried deeper or partly damaged making it more dangerous. [15]

Chapter Three

3. Hyperspectral Imaging: Introduction to landmine detection and processing techniques

3.1. Introduction to Hyperspectral imaging

Hyperspectral imaging is a trending technique in the field of remote sensing. It is based on acquiring images in quasi-continuous bands in the visible and infrared domain. By this, we get at each pixel a reflectance spectrum that help us to identify the constituents of the materials in the image. This type of imaging is a developed version of the multispectral imaging technique. In this section, we would like to show the origin of hyperspectral imaging, different data acquisition processes used to acquire the hypercube in addition to main hyperspectral imaging cameras used in this field.

3.1.1. Broadband, Multispectral, Hyperspectral and Ultraspectral Imaging

Hyperspectral imaging is the result of development in the field of electro optics. The development in sensor manufacturing made the image acquisition in hundreds of wavelengths possible. The first imagers were broadband imagers that sense the light intensity in a wide range of spectrum. These imagers detect the light intensity in a wide range of frequencies in the visible or infrared domain. After that, the eighties and nineties became the era of multispectral imagers were the imagers were able to acquire image slices in tens of frequencies (Fig.7). The development of photodetectors made possible to acquire image slices in even narrower bands. This have increased the spectral resolution of the imager and improved the possibility to distinguish more materials.
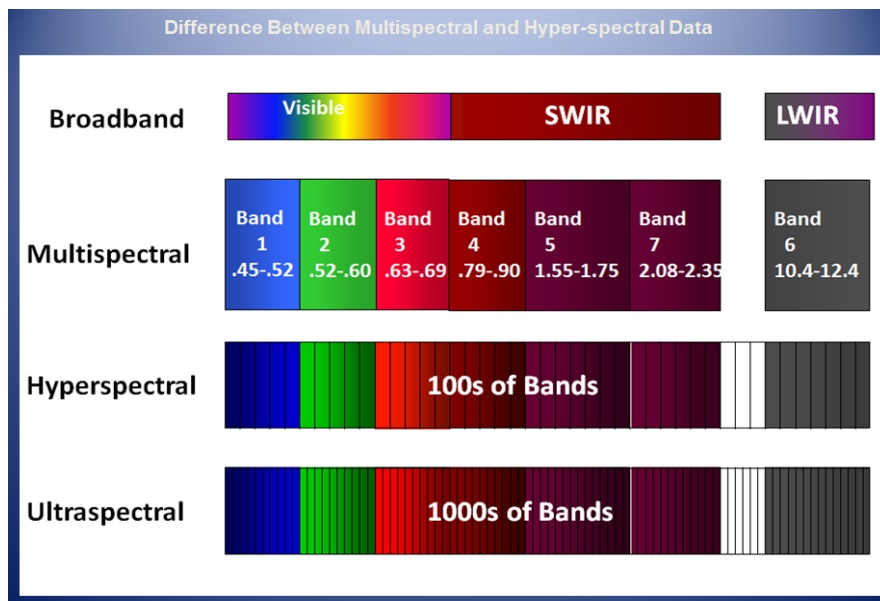
Figure 7: Difference between broadband, multispectral, hyperspectral and Ultraspectral Imaging

3.1.2. Hyperspectral Image Scanning Modes

Generally, to acquire a multispectral or hyperspectral images, two types of scanners are usually used: Wiskbroom scanners and Pushbroom scanners. These two scanners differs in the technology used to detect the light of different wavelengths. In both techniques, we use the forward motion of the platform to record successive scan lines and build up the 2 dimensional images. In the following, we will some of the characteristics of each technology.

3.1.2.1. *Whiskbroom or Across Track scanner*

Whiskbroom scanners collect measurements from one pixel in the image at a time. A rotating reflecting device moves forth and back to reflect the incident light from different angles to the single sensor that the scanner have. This allows the scanner to measure the energy from one side of the aircraft to the other. The Instantaneous Field of View (IFOV) is scanned perpendicular to the direction of motion of the sensor to form one spatial rom of the spectral image [132]. The incoming energy is separated into several spectral components that are independently sensed.
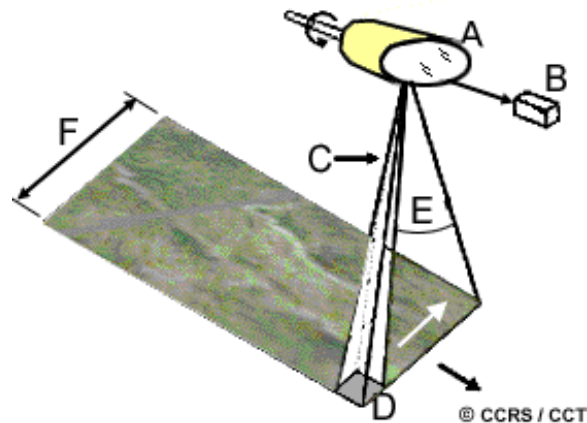
Figure 8: Wiskbroom scanning principle [132]

3.1.2.2. ***Pushbroom or Along Track scanner***

A push broom scanner collects data along track using a row of sensors arranged perpendicular to the direction of travel. The data are collected row by row. The imager scans a slit on the ground in across-track direction. The slit image is focused and spectrally dispersed onto a two dimensional array of image sensors.
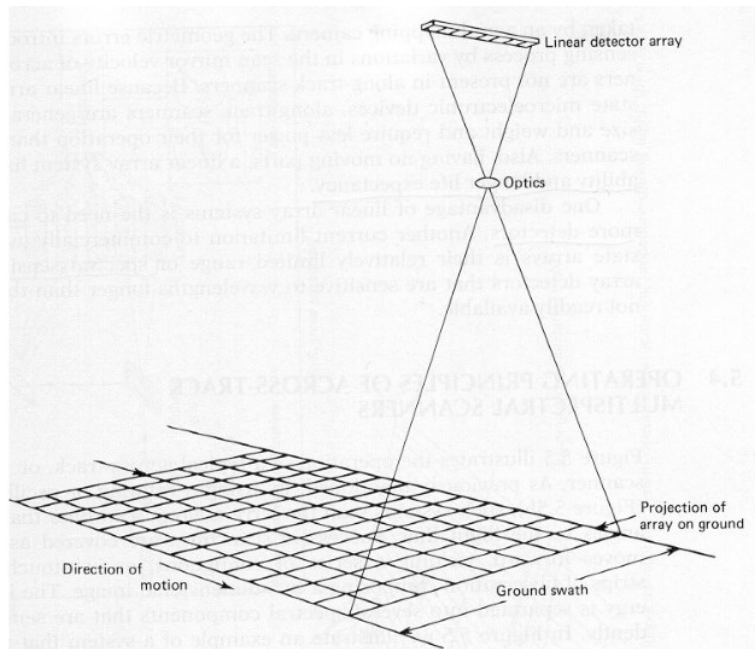
Figure 9: Pushbroom scanner principle

Whiskbroom imager have inherently inferior spatial resolution compared to pushbroom imagers. In addition, pushbroom imager has better geometry than wiskbroom imagers due to fixed distance among detector elements. However, in pushbroom imager more detectors need to be calibrated before use.

In new hyperspectral imagers, instead of using the dispersive elements to measure the energy in different wavelengths, spectral filters in the fore optics at the focal plan are used to switch between wavebands.

3.1.3. Important hyperspectral camera

Several hyperspectral imagers gained a large reputation in the field of hyperspectral imaging. The number of companies that manufacture hyperspectral cameras is increasing as the use of this technology is expanding to new domains. Now this technique is used in different unrelated domains like chemistry, mapping, military, food quality monitoring, agriculture and other. Therefore, the number of buyers is increasing and the number of the manufacturers so. Some of the main hyperspectral cameras are:

➢ AVIRIS: Airborne Visible Infrared Imaging Spectrometer is operated by Jet Propulsion Lab (JPL) of NASA. This sensor acquires hyperspectral images in 224 bands between 0.4 and 2.5 μm. the spectral resolution is about 10nm. It is a pushbroom sensor that have field of View FOV=30° distributed on 614 pixels. The instantaneous field of view IFOV equal to 1mrad and could be calibrated to 0.1mrad.

➢ HyMap sensor: it works from visible to thermal infrared range. The spectral resolution is about 10-20nm in the VNIR and SWIR regions and about 100-200nm in TIR. The FOV vary between 30 and 65° distributed on 512 sample with IFOV between 1 and 3 mrad. This sensor is fabricated by Integrated Spectronics and mainly used for earth observation.

➢ COMPASS: this sensor is developed by the Night Vision and Electronic Sensors Directorate (NVESD) of the US army. It works between 400 and 2350nm in 256 samples.

➢ HYDICE: Hyperspectral Digital Imagery Collection Experiment. It acquires hyperspectral images in 210 bands between 400 and 2500 nm. It is manufactured by the NAVAL Research Lab.

➢ CASI: Compact Airborne Spectrographic Imager. It is one of series of sensors manufactured by ITRES research limited in collaboration with Defence Research and Development Canada (DRDC). It detects image slices between 400 and 1000nm with 10 nm spectral resolution. Other imagers also manufactured by the same company cover other ranges like SASI (1000 to 2500nm) and microTABI (3700 to 4800nm).

➢ NVIS: Night Vision Imaging Spectrometer is a pushbroom imager that uses two co-aligned imaging spectrometers covering together the range between 400 and 2350 nm with 384 spectral bands. The cross-track FOV is 13° composed of 256 pixels with IFOV about 0.9 mrad.

➢ EPS-H: It is a sensor manufactured by GER Corporation. It is composed of several imagers that covers the range between visible 430nm to thermal infrared 12500nm. The spectral resolution changes in each range.

3.2. Previous projects on landmine detection using HI

This research was published in the journal paper ISPRS journal of photogrammetry and remote sensing [17].

Our goal in this section is to describe past projects that used infrared hyperspectral imaging for landmine detection and that have been presented in conferences proceedings and journal articles. Note that additional military research may exist in this field. Such projects, however, are not described herein due to lack of information.

3.2.1. Defence Research and Development Canada projects

One of the earlier projects doing research on landmine detection using infrared wavelengths took place at Defence Research & Development Canada (DRDC). DRDC started their research, in support of the Canadian army on landmine and unexploded ordnance detection in 1978 and, in collaboration with Itres Research, on hyperspectral imaging for landmine detection in 1989. Detection of sparse targets using optical imaging was previously studied. Algorithms developed during this project could be applied to preprocessed images of hyperspectral imagers. An early project proposed a hierarchical image-processing algorithm to detect sparsely distributed bright region of several pixels wide in a monochromatic image [18]. A preprocessing operation is performed in order to remove distortions, dropouts, overlapping areas, misregistration, and any other artifacts and imperfections. Non suspected areas are discarded to reduce the data size. Then, suspected regions are segmented into homogeneous sub-regions and the morphological features of the sub-regions are extracted. Based on the extracted features, sub regions are classified. Finally, the spatial relationships between mine-like objects are determined. A supervised method analyzes these relationships and classifies the areas as a minefield providing a specific likelihood ratio. This hierarchical method can potentially achieve real-time detection of surface-laid mines. With the aim of improving the detection system, scientific research was focused on two topics: the first one dealt with the enhancement of the detection algorithms in order to achieve real-time detection, while the second one was related to the improvement of proper imaging technologies in order to obtain a higher image quality.

After the development of Visible and Near Infrared (VNIR) hyperspectral imagers (400-1000 nm), several experiments showed their compatibility with the detection of surface-laid and buried landmines. While testing the possibility to detect surface-laid mines, it was found that their spectral reflectance has similar behavior under different illumination conditions with different scaling factors and offsets. More precisely, a linear correlation exists between the mine spectra under different incident illuminations if the spectral vector is confined between 500nm and 680nm [21]. For classification purposes, the authors tested two methods: Linear Cross Correlation (LCC) and linear spectral unmixing. LCC is better in the case of high spatial resolution images. The linear unmixing method has a higher Probability of detection in the case of subpixel sized mines; but has also a higher false alarm rate.

Other tests led to study the possibility of detecting buried landmines using a VNIR imager. It was noticed that buried mines could not be detected by calculating the shift of the red edge of vegetative spectra. However, by using linear correlation, some mines with low vegetative cover

were detected [18]. It was also noticed that Anti-Tank surrogates were more detectable than Antipersonnel surrogates, presumably due to the increased area of disturbance required to bury the former [20]. The probability of detection (PD), intended as the number of mines detected over all existing mines in the image, obtained during the experiment varies between 33% and 100% and the False Alarm Rate (FAR), measured as the number of falsely detected mines per unit area, varies between 0.1 and $0.52/m^2$. According to the authors of [20], improving the classification algorithms and optimizing the spectral vectors, involving a systematic pattern classification study and emphasizing discriminant analysis and feature analysis, are possible steps to achieve better PD and lower FAR.

The spatial resolution of the image affects the performance of the detection algorithm [22]. As the pixel size gets closer to the size of the mine, the possibility to isolate landmines increases. This has been proven by the research team of DRDC in [23]. The authors acquired two types of images using a VNIR imager: Medium resolution images at the altitude of 300m and high-resolution images at the altitude of 6m in a different place. In the medium resolution experiment, they obtained a 100% PD and $0.00034/m^2$ FAR. In the high-resolution experiment, all mines were detected with a false alarm rate of $0.0043/m^2$. Linear Cross Correlation (LCC) and Orthogonal subspace projection (OSP) were used in classification. The best detection is achieved when taking the result of the combination of the two techniques.

In order to have quasi real-time detection of surface-laid mines using a VNIR imager, the authors in [24] proposed a system consisting of two modes: in the first mode, the system learns the target spectra. In the second mode, the system looks for the targets by acquiring spectral data for each pixel and then applying comparative algorithms to the candidate pixels, using the stored reference spectra. The processing platform involves a system that generates the results of data acquisition and target analysis to an operator by displaying probability information alongside the base imagery. The entire process (data acquisition - radiometric correction - data fusion from different systems) finishes within few time frames of acquisition (a time frame is approximately 15-35 ms). The radiometric and target identification processes can be applied independently to each frame, so the processing of a frame will not affect the results related to the processing of other frames [24].

In [25], which is a continuation of the research in [24], we find the first experiment that aims at detecting landmines from an airborne hyperspectral imaging system in real time. The above paper describes how software and hardware improvements can achieve real time detection from an airborne platform. First, radiometric correction is applied on raw data, then custom classification algorithms are applied to the corrected data. A spectral signature library provides reference spectral vectors. The classification results are stored and displayed in real time. The first real time landmine detection system was mounted on a slow vehicle (1-2 km/h) [24]. A display system shows selected bands including corrected spectral bands, partial data results or final target bands. The second real-time detection system was an improvement of the first system to be compatible with airborne imaging data rates. A hardware/software system was implemented measuring the change in slit contamination (filings, dust, paint flecks) relative to the slit performance during calibration and modifying the correction matrix accordingly during radiometric conversion. Detection rates were not the prime concern of the test. The authors wanted to test the ability to detect landmines from an airborne platform in real time. There are no indications regarding the algorithms used for data correction, band selection, and classification.

Short wave infrared (SWIR) bands (1000-2500nm) have also been considered to detect landmines. As the spectrum is wider with the inclusion of SWIR bands, the possibility to distinguish landmines is higher. A simple classification boundary should be able to distinguish surface-laid mines from many human-made artifacts and natural materials. However, old buried landmines are hard to be detected using SWIR [26].

A project studying Long Wavelength Infrared (LWIR) hyperspectral imaging of landmines led to the development of a commercially available LWIR hyperspectral imager suitable for airborne landmine detection [27]. The instrument was used to collect imagery of surface and buried mines and improvised explosive devices over full diurnal cycles in arid, desert-like conditions and was found to provide some advantages over broad-band imaging in the detection of buried threat objects [28].

The team of DRDC started in 1997 a project testing the combination of various detection technologies called Improved Landmine Detector Project ILDP. Since a single detection technique will not be able to detect all types of landmines in all conditions, the fusion of various techniques can be more effective [29],[30]. The authors tested a small teleoperated vehicle carrying four types of detectors: Forward Looking Infrared imager, down looking electromagnetic induction detector, down-looking Ground Penetrating Radar (GPR) and finally a thermal neutron activation detector used as confirmatory detector of suspected targets. In order to apply sensor data fusion, several methodologies were used, including spatial correspondence and custom designed navigation. The above system was intended for anti-vehicle landmines, but not for anti-personnel mines. In order to address the latter, a smaller system with different sensors was proposed. Therefore, using a high mobility robotic platform, the authors proposed a system that contains five separate technologies: 2 hyperspectral cameras (thermal infrared (TIR) and VNIR), a scanning sensor imaging system which is mounted on a custom built articulated robotic scanner, and a nuclear confirmation sensor [31]. The role of each technique is as follows:

> ➢ Forward looking SWIR or TIR cameras should detect thermal contrast between a landmine and its surroundings.
> ➢ VNIR camera should detect spectral reflectance differences between disturbed and undisturbed soil and the presence of a trip wire.
> ➢ Articulated Robotic Scanner affords the mechanical precision to provide images from scans of a lightweight non imaging sensor.
> ➢ Nuclear imaging is used for confirmation.
> ➢ High mobility platform helps in moving the sensor payload.

In order to handle the enormous volume of data generated by hyperspectral imaging, the authors proposed to use real-time techniques and algorithms described in [24],[25] to compress the hyperspectral images into single band images, which could then be processed by the minefield detection algorithms described in [18]. The results of these projects were encouraging and show that a teleoperated replacement of a human operator may be possible in the future.

A discussion of the results obtained after landmine detection tests using VNIR, SWIR, and TIR imagers by DRDC and Itres was presented in [32]. Reliable surface-laid mine detection in various weather conditions was achieved using VNIR and SWIR spectra, even if not in real time. Reliable buried landmine detection was not achieved. There is no huge difference in the

VNIR range between the signatures of buried landmines and background materials, however they could be indirectly detected by observing differences in reflectance between compact soil over mines and background.

DRDC and Itres presented a review of the research on infrared and hyperspectral technologies for landmine detection in [33]. Besides providing the theoretical background for the detection of surface-laid and buried mines and the results of their experiments, the authors also described examples of Hyperspectral Imagery (HSI) images of trace amounts trinitrotoluene (TNT) and Cyclotrimethylenetrinitramine (RDX) distributed on the ground surface. The mechanism of the distribution of the trace explosives by ants is further discussed in [34], [35].

The Canadian research and development conducted a project between 2004 and 2008 called Shield ARP 12rl in order to develop and exploit optical imaging sensors for mine detection. Airborne tests of real time hyperspectral imaging and a SWIR HSI imaging phenomenology study were completed in October 2006. Tests on vehicle mounted optical tripwire imager and development of Thermal infrared hyperspectral imager were completed on March 2008 [36]. After the realization of simultaneous imaging in VNIR and SWIR bands, the ability of classifiers to separate camouflage coatings from background improves when the VNIR and SWIR spectra are combined. Simultaneous collection of SWIR and TIR images from an airborne platform in an environment with minimal infrastructure has also been done. In vehicle-mounted trip wire detector tests, the SWIR provided better wire/background contrast than the VNIR band. The above report describes the tests and the results obtained during the project without mentioning the algorithms used or the way the real time airborne detection is performed.

DRDC and Itres proposed in [37] a new design of hyperspectral camera with a range-gated intensifier and combined the camera with selected pulsed lasers. The authors showed that it is possible to relate the reflected signal to specific light matter interactions, like induced fluorescence. This approach is independent of the ambient light conditions and can be customized to specific wavelengths. In addition, it could help in surveying a specific area in order to increase the SNR. The preliminary results indicate that the false alarm rate associated with this scenario might be too high for ground area scanning speeds of practical interest.

DRDC also began a project in 2005 to demonstrate the military utility of space-based reflective hyperspectral imagery (0.4-2.5 microns), especially in the domain of target detection and identification for land and marine mapping applications. The results achieved are encouraging and show that target abundance can be retrieved with high accuracy at the subpixel level using the Constrained Energy Minimization (CEM) algorithm. The fact that the estimated abundances are generally lower than the true abundances is consistent with an error introduced during the manual delineation of targets area, by assigning to targets larger areas than their true area [38].

3.2.2. Equinox Corporation fusion test

The fusion of visible and SWIR bands could give better detection results. A basic fusion of two spectrum bands produces acceptable segmentation of objects against background, irrespective of illumination conditions. In other words, selecting a set of two or three spectral image bands has been found to be just as effective in differentiating man-made objects from background as

using all spectral bands at once [39]. Such fusion has the potential to detect mine-like objects in an image using an integrated camera with visible and SWIR sensors and more sophisticated and specialized detection algorithms.

3.2.3. Hyperspectral Mine Detection program HMD

In [40], a Defense Advanced Research Project Agency (DARPA) sponsored experiment testing the potential to detect buried landmines using hyperspectral Mid-wave Infrared (MWIR) (3 to 5 µm) and Long-wave Infrared (LWIR) (8 - 12 µm) bands is described. The project emphasizes the detection of surface disturbances due to landmine burying. Previous experiments showed the capability of VNIR and SWIR imagers to detect surface disturbances [19], [20],[26]. However, the problem was the high false alarm rate induced by surrounding vegetation and rocks. According to the authors, the main rationale behind the detection of buried landmines using the spectral properties is that the surface proprieties are in some way different from the properties of subsurface soil. The soil exposure at the surface changes some of its physical and chemical properties. These experiments showed that spectral information are necessary for landmine detection.

In addition, the researchers of the Hyperspectral mine detection program HMD tried to detect buried landmines by evaluating the contrast in thermal reflectivity between the mine and the soil in just two bands of the thermal IR region [41]. They noticed that recently buried landmines could be seen in thermal infrared imaging as bright spots because the disturbed soil has an apparent temperature different from that of the surrounding undisturbed soil. In addition, they claimed that even mines buried for a very long time could be detected in some types of soil as the subsurface mine will have different thermal properties.

3.2.4. Hyperspectral Mine Detection Phenomenology program

The American army also started the project "Hyperspectral mine detection phenomenology program" (HMDP). Their main objective was to determine the existence of spectral characteristics that are useful for landmine detection [42]. Therefore, they collected high quality hyperspectral signatures of background materials and mines, measured temporal effects on buried landmines and measured a statistically significant set of hyperspectral signatures of surface and buried mines in natural soils, under variations of controlled variables. The spectral analysis results obtained during the HMDP project recordings are presented in [43]. The authors concluded that uncontrolled variables, mainly wind and rainfall, usually affect the results. The mines affected by more rainfall continue to produce a signature distribution that is different from the background. Also, it is remarkable that the temporal evolution of vegetation around landmines is too complex and makes the characterization of temporal signature evolution extremely difficult. The following general observations were made: 1) A light shower won't significantly reduce the signature; 2) The signature is reduced by one-half inch of rain, 3) One-inch of rain further reduces the signature, but does not eliminate it, and 4) For some conditions, several inches of rain may not eliminate the signature. Overall, the VNIR and LWIR spectral regions show the most consistent and highest performance. SWIR and LWIR show

good performance for some conditions. MWIR showed the least consistent and lowest performance.

3.2.5. Joint Multispectral Sensor Program (JMSP)

The goal of the research presented in [44] is to test the design of multispectral and hyperspectral imagers that are able to obtain better detection performance by respecting the requirements and conditions of target detection. For target detection, it is necessary to detect targets both in daylight and nighttime conditions. Panchromatic or multispectral images in VNIR and SWIR ranges give this capability during daylight. However, for military use, the MWIR and LWIR ranges are necessary for nighttime operation. Due to high correlation of spectral bands of background materials in all background conditions, the possibility to detect targets is high using MWIR and LWIR ranges. After testing dual bands in MWIR and LWIR ranges, the authors concluded that thermal multispectral images would give a better target detection and false alarm rate than a single band infrared sensor. Tests showed that appropriately chosen small bands could provide good detection, the optimal bands range being between 8 and 10.5 micrometers. There is a significant increased utility of using LWIR with MWIR compared to the use of MWIR alone. Thanks to the obtained results, the authors manufactured a new hyperspectral imager called SEBASS that works in the ranges 2.9 to 5.2 micron and 7.8 to 13.4 micron. The Aerospace Corporation is still using this sensor to take remote hyperspectral images in MWIR and LWIR ranges.

3.2.6. Night Vision and Electronics Systems Directorate (NVESD)

Night Vision and Electronics Systems Directorate (NVESD) has conducted during the fall of 2002 and spring of 2003 a wide variety of tests to examine airborne sensors for landmine detection [45]. The examined hyperspectral sensors were the Airborne Hyperspectral Imager (AHI) of the University of Hawaii, which is a Long-wave Infrared (LWIR) imager, and the Compact airborne hyperspectral sensor (COMPASS) which is an NVESD VNIR/SWIR sensor. In addition, a high frequency Synthetic Aperture Radar (SAR) and GPR have been used. The authors tested two methods for classification: Signature based and anomaly detection. Further, for anomaly detection two approaches were considered: Local like Reed-Xioli method and Global like NFINDR. The latter is an unmixing model method and alone is not sufficient for classification since it produces only abundance fractions as output. For that purpose, the authors proposed to use it with a Stochastic Target Detector (STD). The output of STD is a detection stochastic map that can be thresholded. The tests showed the capability of LWIR and reflection bands to detect landmines with the use of proper algorithms. The detection of landmines at subpixel level is challenging, but indeed possible with the use of high quality hyperspectral instruments and algorithms.

Using the LWIR hyperspectral images acquired by AHI, another test has been conducted by researchers at the Georgia Institute of Technology to detect a grid pattern of landmines and to use this information to improve the detection performance. First, an anomaly detector is applied to the hyperspectral data; in this case, the authors used the Dual Window-based Eigen Separation Transform (DWEST). Then, pattern parameters are extracted and used to form a pattern projection image. Finally, a pattern-based false alarm reduction is performed [46].

Using this process, higher probability of detection at lower false alarm rate is obtained. Therefore, the results prove that the inclusion of spatial pattern information in anomaly detection improves the detection of landmines in minefields [46].

3.2.7. Defense Science and Technology Laboratory DSTL countermine project

A project similar to those of DRDC and DARPA was started in Britain with the goal to detect landmines using a VNIR imager [47]. The program was called DSTL countermine project. Using the VNIR hyperspectral camera SOC 700 mounted on a tripod, the team took high spatial resolution images of landmines. However, the data is mainly used to investigate different processing methods and not to evaluate the PD and the FAR of the sensor. For data processing, the authors used Principal Component Analysis (PCA) for dimensionality reduction and anomaly detection method for classification. The authors avoid the use of spectral comparisons between the target and each pixel of the image, as it will be very time consuming due to the low target/background ratio. The results were still preliminary, however the authors concluded that VNIR has the potential to distinguish surface-laid landmines from background.

3.2.8. Indian Test to detect landmines using infrared images

In India, researchers proposed a hierarchical algorithm to detect landmines from infrared images that consist of preprocessing (contrast enhancement- filtering- smoothing), segmentation, feature extraction, and ANN based classification [48]. The authors tested the algorithm on surface-laid mines in two types of soil: black cotton and sand. During the preprocessing, the image is converted to gray level. The two most important preprocessing stages are the contrast enhancement and noise removal. Segmentation is the process of grouping homogenous pixels sharing some common attributes such as color, intensity or texture in an image. The aim is to separate the image into regions of interest and background, in order to make further analysis easier. Clustering, edge detection, and threshold based region growing are the main three categories encompassing the various existing image segmentation techniques [48]. Therefore, feature extraction and further processes are applied on the clusters that are deemed mine like. A Neural Network (NN) based algorithm is used to classify the mine from the surrounding. During the tests, the authors used a small NN of 1 hidden layer and 4 neurons. The results provided on a simple dataset are good, however the algorithm is not expected to work well on another field or type of soil as the data used during the phase of learning are not rich enough.

3.2.9. NATO project

In the Netherlands, a project took place in cooperation with NATO to make a remote detector of landmines. The main objective was to obtain near real time minefield detection during a conflict using an Unmanned Aerial Vehicle (UAV) at a typical altitude of 100 m. First, the authors presented the imaging technologies available at that time: Radar, Microwave radiometers, visible wavelengths, near, middle and far infrared. After that, the authors showed the principal signal processing techniques used for mine detection at that time. The main steps involved can be categorized as:

* image enhancement
* edge detection
* segmentation
* feature extraction and classification
* morphology

At the end of the report, the authors gave the following main recommendations based on various experimental results [49]

1. Conventional medium-resolution imaging radars are less suitable for remote mine detection.
2. Microwave radiometry detection principle is promising for remote mine detection.
3. The characteristics of visible and near infrared imaging are often requested. This is because imaging systems in these bands are often low cost, compact, have a high spatial resolution and can be used in real time detection.
4. The mid- or long-wave infrared wavelength band is a promising band for remote mine detection.
5. As Meteorological conditions (such as rain showers) can make mine and minefield detection in mid- and longwave infrared wavelength bands difficult, it is better to combine several wavelength bands.
6. A study on the best processing techniques and a reliable and accurate interpretation of the images of a remote mine detection system has to run in parallel with the development of a mine (field) detection system.

3.2.10. Humanitarian DEMining (HUDEM) and Belgian Mine Action Technology (BEMAT)

In Belgium, a research project focused on using the fusion of data from multiple sensors (Ground penetrating radar, metal detector and infrared sensor) [50]. In the above paper, the authors presented their views regarding multi-sensor data fusion potentials in improving the close-in detection of landmines and reduction of mined area. Modelling and fusion of the extracted features are based on belief function theory and possibility theory. After modelling, the fusion part is performed in two steps: the first step consists in analyzing all data measured by one sensor. The second step combines the results of the three sensors. The final part of the fusion approach is the decision. According to the authors, the final decision about the identity of the object should be left to a human observer with field experience. Therefore, the fusion output is an informative decision. The experience showed that the fusion gives better detection than any input sensor used alone.

3.2.11. FOI Multiple-Optical Mine detection System (MOMS) project

FOI, A Swedish defense research agency, worked on a project for the Swedish armed forces called Multi-Optical Mine detection System (MOMS). The objective of the project was to provide knowledge and competence for fast detection of surface-laid mines using multiple optical sensors [50]. The authors conducted research to test the feasibility of detecting

landmines using optical sensors and the possibility to combine multiple sensors. According to the authors, hyperspectral imaging is an encouraging candidate for automatic detection and recognition of exposed and semi-hidden mines, when a priori knowledge of the target spectral signature is available. However, the detection performance is limited when the targets are camouflaged by natural vegetation or hidden under other objects. In addition, the authors claim that no single detection architecture is able to meet the performance needed under all operating conditions; the choice of the particular sensors and algorithms will depend on environmental and operations conditions [51].

3.2.12. TELOPS test to detect buried object using airborne thermal hyperspectral images

In 2015, a Canadian research company specialized in infrared and hyperspectral imaging named TELOPS proved the possibility to detect buried objects using an airborne LWIR hyperspectral imager [52]. From an aircraft platform, they acquired thermal hyperspectral images of areas that contain man-made objects previously buried. They found that the disturbed soil right above a buried target is warmer than the undisturbed soil area next to it [52]. By comparing the emissivity data obtained through the Temperature-Emissivity separation, the buried target sites show up as part of the hottest ground area within the scene but further classification or additional information are needed to discriminate the buried objects from other naturally hot areas.

A summary of the above projects and of the results obtained is given in Table 2.

Table 2: Summary of projects studied landmine detection using infrared and hyperspectral imaging.

Research Project	Type of data	Techniques Used	Comments
Detection of surface-laid minefields using a hierarchical image processing algorithm (DRDC)	Infrared monochromatic Image	Hierarchical image processing	Method would be useful as follow-on stage to process airborne hyperspectral imagery after preprocessing in order to reduce the hyperspectral image to a single band.
Surface laid Landmine detection using VNIR (DRDC)	VNIR	LCC & Linear Unmixing	Surface-laid mines have consistent shape in VNIR bands; LCC performs well in case of high spatial resolution images; Unmixing techniques have higher PD in the case of subpixel target at the price of higher FAR
Buried Landmines detection using VNIR (DRDC)	VNIR	LCC	Using VNIR, buried mines are not directly detected, however the change of soil characteristics and vegetative stress due to mine burying is detectable.

Effect of Spatial resolution on mines detection (DRDC)	VNIR	LCC & OSP	LCC performs better when the pixel size is smaller than mine size. OSP is better when mine size is smaller than pixel size. Best detection is achieved when the result of two methods are combined.
Surface-laid Landmine detection using VNIR in real time (DRDC)	VNIR	Pipeline image processing	the proposed suite of algorithms proves the possibility to detect landmines in quasi real time using an airborne platform
Landmines detection using SWIR bands (DRDC)	SWIR	LCC	Similarly to VNIR bands, the use of SWIR is beneficial to detect surface-laid mines and recently buried landmines.
Landmines detection using LWIR bands (DRDC)	LWIR (TIR)	Spectral comparison	LWIR hyperspectral imaging provides advantages over broadband LWIR
Multiple sensors mounted on a robot (DRDC)	Fusion of VNIR, SWIR, LWIR HSI and other sensors	Dynamic range detector and contrast enhancement	A proposed system employing hyperspectral imagers for close-in anti-personnel mine detection.
Active hyperspectral imaging (DRDC/Itres)	VNIR	Casi imager with intensifier	With the addition of external illumination, the FAR increases as reflectivity of background increases.
Equinox Project	Fusion of visible and SWIR	Thresholded Ratio vegetation index	Here a ratio between two or three bands is used. More bands using other approaches may improve the results.
DARPA project to detect buried landmines	MWIR and LWIR	spectral comparison	LWIR and MWIR are more suitable to detect buried landmines.
Hyperspectral mine detection phenomenology program	VNIR,SWIR,MWIR,LWIR	Data collection using spectrometers	Weather conditions affect the intensity of the reflected spectra. The effect of rain is more important than other effects.
Joint Multispectral Sensor Program	VNIR,SWIR,MWIR,LWIR	Fourier Transform	Thermal sensor are beneficial for target detection at nighttime. LWIR bands are more effective than MWIR
airborne sensors tests (NVESD)	VNIR,SWIR,MWIR,LWIR	RX and NFINDR with STD anomaly detection. Grid pattern detection of landmines	LWIR gives a good detection with the use of proper algorithms. The inclusion of spatial pattern information in anomaly detection improves the detection performance.
DSTL countermine project	VNIR	PCA	more tests and other algorithms shall be tested to evaluate the effectiveness of VNIR bands in landmine detection

Indian Test to detect landmines using infrared image	Infrared Image	Hierarchical image processing	More images are needed to train the Neural network based classifier. A more complex one may be used in complex situations.
NATO project	VNIR,SWIR,MWIR, LWIR	Hierarchical image processing	Radars are less suitable for airborne mine detection. Combination of bands is necessary to overcome the meteorological effects. Improvement of algorithms and techniques in parallel is necessary.
Humanitarian demining (HUDEM & BEMAT)	GPR, metal detector, infrared sensor	belief and possibility theory	Fusion of sensors may give better results than single sensor.
FOI (MOMS)	VNIR,SWIR,MWIR, LWIR, 3D LADAR.	Anomaly detection, Support Vector Machines	Hyperspectral imaging is useful for automatic detection of open and semi-hidden mines. The choice of sensor suite and algorithms depends on environmental and operational conditions.
TELOPS	LWIR	Temperature-Emissivity separation, Linear Unmixing to study the mineral distribution	Soil above landmines is warmer than surrounding undisturbed soil. Complementary information are needed to reduce the FAR.

3.3. Hyperspectral Image Processing

In this section, we will introduce the detection algorithms used for target detection in hyperspectral imagery. In addition, we will introduce several preprocessing steps and hyperspectral data treatment usually used in a preliminary phase to simplify further detection or classification. Most of these methods were developed during research on general problems regarding the processing of hyperspectral images and are not specific for the landmine detection problem. However, advances in that research will directly affect the success of landmine detection using hyperspectral imaging. A review of different processing techniques used for data fusion, spectral unmixing, classification and target detection could be found in [53].

After the acquisition of a hyperspectral image, the data pass through several steps. First, the image is preprocessed to remove impurities, noise, and to reduce the size of the image. The main pre-processing steps are contrast enhancement, filtering and smoothing. Then, segmentation is done to separate useful data from background. After that, feature extraction is applied to extract the most appropriate features for classification. Finally, classification or clustering methods are applied to locate a target. In the following, we present the main algorithms used for target detection using hyperspectral images. Many other methods may be used in each phase. However, in this chapter we detail the most commonly used ones.

3.3.1. Contrast enhancement

The image enhancement process consists of a collection of techniques that try to improve the visual appearance of an image or to convert the image into a better form suited for analysis by a human or a machine [54]. Image enhancement methods are divided into two main categories: spatial domain methods and frequency domain methods. Spatial domain methods are applied directly on the pixels of the image. In frequency domain methods, the image is processed in the frequency domain after applying the Fourier transform on the original data. Contrast enhancement is one of the most commonly used image enhancement methods. For the mine detection case, the role of contrast enhancement is to enhance the difference between the landmine and the background materials [55]. The main contrast enhancement methods used are:

3.3.1.1. *Histogram equalization*

Histogram Equalization (HE) is the most widely used contrast enhancement technique due to its simplicity and effectiveness. The aim of HE is to make the probability distribution of gray levels approximately uniform in the output image. It is a global method that flattens the histogram and stretches the dynamic range using the cumulative density function of the image [55].

The probability of the kth gray level in an image f can be described as $p_f(f_k) = \frac{n_k}{n}$

where k $\in$ [0, L-1], L is the number of gray levels in an image, n_k is the number of times the kth level appears in the image, and n is the total number of pixels in the image. The histogram is the plot of $p_f(f_k)$ versus k, and the goal of the histogram equalization is to obtain an image with a uniform histogram. The uniform histogram can be achieved by

$$g_k = T(f_k) = \sum_{j=0}^{k} \frac{n_j}{n} = \sum_{j=0}^{k} p_f\left(f_j\right)$$

Keeping two conditions,

   (a) T(f_k) is single valued and monotonically increasing in the range k $\in$ [0, L-1].
   (b) T(f_k) should be T(f_k)$\in$ [0,L-1] for k $\in$ [0,L-1].

The drawback of HE is that the brightness of the image is changed. To overcome this drawback and improve the performance, many derivations of this method were proposed. Among them, we list the following:

Brightness Bi-Histogram Equalization (BBHE) [56], Dualistic Sub Image Histogram Equalization (DSIHE) [57], Minimum Mean Brightness Error Bi-Histogram Equalization (MMBEBHE)[58], Recursive Mean Separate Histogram Equalization (RMSHE)[59], Multi

Histogram Equalization (MHE)[60], Brightness Preserving Dynamic Histogram Equalization (BPDHE)[61], Recursive Separated and Weighted Histogram Equalization (RSWHE)[62], Global Transformation Histogram Equalization (GHE) [63] and Local Transformation Histogram Equalization (LHE)[63].

3.3.1.2. *Morphological Contrast Enhancement*

Morphological theory has been introduced in image processing to overcome a number of problems like image distortion due to noise. The first step in morphological contrast enhancement is to find peaks and valleys in the original image. Peaks are light shades of gray tone image, while valleys are dark ones. Peaks are obtained by subtracting the opening from the original image, and valleys are obtained by subtracting the original image from the closing as

$$p(f) = f - \gamma(f),$$
$$v(f) = \phi(f) - f,$$

where p(f) denotes the peaks, $v(f)$ denotes the valleys, $\gamma(f)$ denotes the opening, and $\phi(f)$ denotes the closing of an image function f. Basic definitions of morphological methods and operators (erosion, dilation, opening and closing) could be found in [59]. To improve the contrast, the peaks and valleys are multiplied by constants as follows:

$$p'(f) = p(f) \times c_1, \ v'(f) = v(f) \times c_2 \text{ where: } c_1 = \left| \frac{\max(f) - \max(I)}{\max[p(f)]} \right| \text{ and } c_2 = \left| \frac{\min(f) - \min(I)}{\max[v(f)]} \right|$$

where I indicates the gray level. In the case of 8 bit gray levels, max(I)=255 and min (I)=0.

The contrast-enhanced image is obtained as the summation of the original image, the peaks, and the negative valleys $f' = f + p'(f) - v'(f)$ [55].

3.3.2. Filtering

Filtering is an operation that allows to reduce the noise or to sharpen blurred areas in an image in order to make it clearer and more suitable for further processes. In the filtering of hyperspectral images, several techniques usually used in image processing have been upgraded to obtain multichannel restoration. For example, the well-known Wiener filter used in image processing has been extended to be used in hyperspectral images. There are two groups of filters: One is based on the assumption that the within-channel information is separable from between-channel information, i.e., spectral and spatial information are separable. These filters are called Hybrid filters. In this case, the first step is to decorrelate channels using Fourier Transform or PCA and then apply a classic 2D restoration method such as Wiener filter or Static Wavelet Transform. The other group consists of a few proposed filters that do not rely on the assumption of spectral and spatial separability [64].

3.3.2.1. *Wiener filter*

The Wiener filter is a widely used filter based on minimum mean square estimation. The original image is obtained from the received image by minimizing the mean square error. It assumes that the acquired image is composed of the original image and a white noise component that has a zero-mean Gaussian distribution [65].

g (t)= f(t) + n(t)   Where f(t) is the original image, g(t) the acquired image and n(t) the noise.

The estimation of f(t) is $\hat{f}(t) = \sum_{k=0}^{k=L-1} h(k)g(t-k)$. It is estimated using L samples taken from the received signal. h(k) is a variable independent of time to be found. It is calculated by minimizing the approximation error

$$J = E(e^2(t)) = E\left[\left(f(t) - \hat{f}(t)\right)^2\right] = E[\{f(t) - \sum_{k=0}^{k=L-1} h(k)g(t-k)\}^2]$$

The minimum is achieved by $\frac{\partial J}{\partial h(i)} = E\left[2\{f(t) - \sum_{k=0}^{k=L-1} h(k)g(t-k)\}\frac{de(t)}{dh(i)}\right] = 0$

and $\frac{de(t)}{dh(i)} = -g(t-i)$

We can reformulate it in a matrix form:

H=[h_0,h_1, h_2,…..,h_{L-1}]^T and G(k)=[g(k) g(k-1) … g(k-L+1)]^T

Thus $\frac{\partial J(H)}{\partial H} = 2$ RH-2P   => H*=R^{-1}P. This is called Wiener-Hopf equation.

Note that R is the autocorrelation of G. It is a symmetric Toeplitz matrix and therefore it is positive definite and non singular so R^{-1} has a solution. P is the cross-correlation between H and the input image.

3.3.2.2. *Adaptive 3D Wiener filter*

As most of the filters used while preprocessing hyperspectral images are based on the assumption of spectral and spatial separability, Gaucel et al [64]proposed a new filter for hyperspectral images   relying on spectral and spatial information simultaneously.

First the authors assume that the channel vector v(n_1,n_2) represents the zero-mean white Gaussian noise, uncorrelated with the original image f(n_1,n_2). The received image is g(n_1,n_2)=f(n_1,n_2)+v(n_1,n_2). Then, they apply the filter in local regions in which the signal-pixel vector f(n_1,n_2) is assumed homogeneous. So f could be modelled as f(n_1,n_2)= m_f +w(n_1,n_2), where m_f is the local mean of f(n_1,n_2) and w(n_1,n_2) a zero mean white noise.

The linear solution of Wiener filter is $\hat{f} = m_f + \Gamma_{fg}\Gamma_{gg}^{-1}(g - m_g)$ where Γ_{fg} is the covariance of f and g, and Γ_{gg} is the variance-covariance matrix of g. From the received image we could estimate Γ_{gg}. But as the noise and the signal are uncorrelated, $\Gamma_{gg} = \Gamma_{ff} + \Gamma_{vv}$ and $\Gamma_{fg} = \Gamma_{ff}$

Since the noise is zero-mean, m_f=m_g and the equation becomes

$$\hat{f} = m_g + H(g - m_g) \text{ and } H = (\Gamma_{gg} - \Gamma_{vv})\,\Gamma_{gg}^{-1}$$

Using the local region model, Γ_{gg} is estimated and m_g is updated at each pixel.

3.3.2.3.   *Multiway filtering*

Multiway filtering is another reformulation of the Wiener filter based on modelling the hyperspectral image by a third order Tensor.

The collected hyperspectral image *R* is modeled as the sum of the desired original image *X* and the additive white and Gaussian noise *N*

$$R = X + N$$

The goal is to estimate the original image by applying multidimensional filtering on the received data

$$\hat{X} = R \times_1 H_1 \times_2 H_2 \times_3 H_3$$

Where $\times_n$ represents the n-mode product. The *n*-mode product between a data tensor R and matrix H_n represents the consecutive matrix product between matrix H_n and the I_n-dimensional vectors obtained from R by varying index i_n and keeping the other indexes fixed [66].

In order to determine the optimal n-mode filters H_1, H_2 and H_3, the criterion used is the minimization of the mean squared error between the estimated signal $\hat{X}$ and the original one X.

$e(H_1, H_2, H_3) = E[\|X - R \times_1 H_1 \times_2 H_2 \times_3 H_3\|^2]$

To estimate H_n, an Alternative Least Square algorithm is used, consisting of the following steps [66]:

1. Initialization $k = 0$: $R^0 = R \Leftrightarrow H^0{}_n = I_{In}$ for all $n = 1$ to N *(=3* in this case).

2. ALS loop: while $\|X - R^k\|^2 > thr$, with thr > 0 fixed *a priori*.

(a) for $n = 1$ to N:

i. $R^k{}_n = R \times_1 H_1{}^k \cdots \times_{n-1} H_{n-1}{}^k \times_{n+1} H_{n+1}{}^k \ldots \times_N H_N{}^k$.

ii. $H_n{}^{k+1} = \text{argmin} \|X - R^k{}_n \times_n Q_n\|^2$ subject to $Q_n = H_1^T H_1 \otimes \ldots H_{n-1}^T H_{n-1} \otimes H_{n+1}^T H_{n+1} \otimes \ldots H_N^T H_N$ $Q_n \in R^{In \times In}$.

(b) $R^{k+1} = R \times_1 H_1{}^{k+1} \cdots \times_N H_N{}^{k+1}$, $k \leftarrow k + 1$.

3. Output: $\hat{X} = R \times_1 H_1 \times_2 H_2 \times_3 H_3$

Step (2)(a)(ii) of the ALS algorithm can be decomposed into the following sub-steps:

1.n-mode unfold $R^k{}_n$ into $R_n{}^k$ $= R_n(H_1{}^k \otimes \ldots H_n{}^{k-1} \otimes H_n{}^{k+1} \ldots \otimes H_N{}^k)$, and R into R_n;

2. Compute $\gamma_{RR}{}^n = E(R_n{}^k R_n{}^T)$, perform its eigenvector decomposition (EVD) and place the eigenvalues in $\lambda_\gamma{}^k$, for $k = 1$ to *In*;

3. Estimate K_n using Akaike Information Criterion or Minimum Description Length criterion.

4. Estimate $\sigma_\gamma^{(n)2}$ by computing $\frac{1}{I_n-K_n}\sum_{k=K_n+1}^{I_n}\lambda_k^\gamma$ and estimate β_i by computing $\lambda^\gamma{}_i - \sigma_\gamma^{(n)2}$ for $i = 1$ to K_n;

5. compute $\Gamma_{RR}^{(n)} = E(R_n\,{}^kR_n\,{}^{kT})$, perform its EVD, keep in matrix V_s^n the K_n eigenvectors associated with the K_n largest eigenvalues of $\Gamma_{RR}^{(n)}$, and keep the R_n largest eigenvalues $\lambda^n{}_{\Gamma k}$ for

$k = 1$ to K_n;

6. Compute the $(k+1)^{\text{th}}$ iteration of n-mode Wiener filter H_n^{k+1} using the expression of n-mode Wiener filter.

This method has been tested in [66] on different images and proved its efficiency by increasing the SNR by about 3dB. However, one of the main drawbacks is an increased complexity and computational time.

3.3.3. Segmentation

In the remote sensing community, segmentation is defined as the process of searching for homogenous regions in an image, that is later followed by the classification of these regions [67]. In image processing, there are many methods used for segmentation, however not all of them are applicable to multispectral and hyperspectral images. Some methods like watershed algorithms have been upgraded in order to segment hyperspectral images. Globally, segmentation algorithms are divided into two categories: Boundary-based and Region-based. Boundary based methods detect the boundary using the discontinuity property. In region-based algorithm, pixels in a region are grouped using the similarity property. In the following, we present the main methods used in hyperspectral image segmentation.

3.3.3.1.   *Watershed Algorithm*

The watershed algorithm is a powerful tool usually used for mathematical morphology segmentation. In [68] the authors proposed to use spatial gradients and spectral markers for segmentation. The algorithm works as follows:

First, to avoid obtaining a large number of minima while flooding the watershed using the gradient function (over-segmentation), they determine markers for each region of interest using Clara Clustering algorithm [69]. Then, the Factor Correspondence Analysis FCA [70] data reduction method is applied to remove the redundancy of channels and filter the image. Next, a chi-squared distance based gradient is performed on the filtered image, then watershed segmentation is computed. This approach works well and proves that an adapted data reduction is necessary for multivariate gradient segmentation.

3.3.3.2.   *Hierarchical segmentation*

In 1989, Beaulieu and Goldberg [71] proposed a hierarchical process to segment images based on hierarchical step-wise optimization. Hierarchical segmentation is defined as a set of

segmentations of the same image at different levels of detail in which the segmentations at coarser levels can be produced from a simple merging of regions at finer levels [71]. First, each pixel is assigned to a region label. Then, spatially adjacent regions with small dissimilarity value are merged. The dissimilarity between new spatially adjacent regions are calculated and the pairs with smallest value are merged. The process is repeated until the number of regions needed is obtained or all values of dissimilarity are below a predefined threshold. The drawback of this method is the long computational time while dealing with large data.

Tilton in 1998 [72] proposed a new hierarchical segmentation method called HSEG. The main improvement of this method is that non-adjacent regions could be merged together and the dissimilarity function is selectable. Another recursive version of this algorithm called RHEG was proposed in [73] to overcome the problem of long computational time of HSEG. These algorithms are registered patents for US government.

3.3.4. Feature extraction

Feature extraction consists in transforming the data from a high dimensional space to a lower dimensional space chosen in such a way as to conserve as much as possible the information of interest in the data. Feature extraction is used in hyperspectral image analysis to overcome the problem of a low number of data training samples in comparison to the high spectral resolution of the image and to reduce the computational time. There are many feature extraction algorithms that are introduced; some are linear while others are nonlinear. While working on landmine or target detection, not all feature extraction algorithms are useful, because the targets of interest are generally sparse and the feature extraction may remove the key features of the target. In the following, we are going to list some of these algorithms, their implementation and their advantages.

3.3.4.1. *Principal Component Transformation (PCT)*

Principal Component Transformation, also called principal component analysis, Hotelling transformation or Karhunen-Loeve transformation is a dimensionality reduction method based on the minimization of the representation error. The idea is to choose the most representing bands with the help of the eigenvalue decomposition of the covariance matrix of the hyperspectral image [74]. The first step of PCT is the calculation of the covariance matrix of the image matrix. Then, the eigenvalues of the covariance matrix are calculated and the eigenvectors are extracted. Finally, the image matrix is projected onto the new subspace formed by the k orthogonal eigenvectors corresponding to the highest eigenvalues. $Y=W^T x$ where $\mathbf{x}$ is a d x1 -dimensional vector representing one image pixel, y is the transformed $\mathbf{k}$ x1-dimensional sample in the new subspace and W is the transformation matrix of k orthogonal eigenvectors.

Note that while computing the PCT algorithm, the variance of the projections along the principal components is equal to the eigenvalues of the principal components. In theory, PCT transformation affects the classification of hyperspectral images. However, the overall effect on classification does not change the general class patterns and, therefore, the dominating classification result remains correct.

3.3.4.2. *Linear Discriminant Analysis (LDA)*

Linear discriminant analysis is a statistical based method often used for feature extraction and dimensionality reduction. It is also named Discriminant Analysis Feature Extraction (DAFE). It is an extension of the well-known Fisher discriminant analysis, which is limited to binary class decomposition. LDA computes an optimal transformation by minimizing the within-class distance and maximizing the between-class distance simultaneously, thus achieving maximum class discrimination [75]. Therefore, the first step is to calculate the within-class, between-class and total scatter matrices. A transformation matrix is then defined and computed by applying the eigenvector decomposition on the scatter matrix [76]. The main disadvantage of this method is that it requires that the scatter matrix of the data be nonsingular. This method has also other drawbacks: the maximum number of features extracted is equal to the number of classes minus one. The number of training samples should be large enough to estimate the between-class and within-class scatter matrix reliably. The between-class will be biased toward the class that has very different mean value. Also, it is very time consuming compared to other methods. In addition, it requires more training samples for hyperspectral images to calculate the class statistical parameters at full dimension [77]. Many LDA extensions have been proposed to deal with the singularity problem like PCA+LDA, regularized LDA (RLDA) , null space LDA (NLDA) , orthogonal centroid method (OCM) , uncorrelated LDA (ULDA) , orthogonal LDA (OLDA), LDA/GSVD, etc. [78].

In addition to the main methods we described above for feature extraction of hyperspectral images, many other techniques exist like matched pursuit [77], dimensionality reduction with rare event preserving [79], hybrid methods [80] and nonparametric methods [81].

3.3.5. Classification

It is the most important step in landmine and target detection. The performance of the algorithms used in each of the previous steps and in the classification phase are evaluated by the study of the classification results. The classification phase in an image based target detection process could be defined as the step in which the pixels are discerned between target and non-target. Globally, the classification algorithms are divided into two main classes: Supervised and unsupervised. Supervised classification methods are based on the knowledge of the target and the use of training samples. Unsupervised classification methods consist of grouping pixels that have similar properties without the knowledge of target properties. Considering the way the classifier computes the information in the pixels, classification algorithms are divided into per pixel classifiers, subpixel classifiers, per-field classifiers, knowledge based classifiers, contextual and multiple classifiers [82]. In landmine detection, unsupervised classification techniques are used when there is no information on the type of mine present in the field or when there is the possibility that a particular type of mine is deployed but its reflectance spectrum is not in the library of known spectra. However,

unsupervised classification methods do not work well in every possible condition and suffer from high false alarm rate due to the generally low number of target pixels compared to background pixels. While the use of unsupervised methods could help in detecting unknown types of landmines, the use of supervised classification methods is necessary for the identification of mines. In the following, we are going to mention the major classification methods used in landmine detection:

3.3.5.1.   *Support vector machine (SVM)*

Support vector machine is a powerful non-parametrical supervised classification method. Firstly, it was proposed for binary classification and regression [83]. Then, it has been used in the classification of hyperspectral images [84]. SVM consists in finding the best separation between two classes based on the separation of representative training samples called support vectors. In addition, SVM does not suffer from Hughes effect and may perform separation of classes having very close means even with a very small number of training samples [85]. First, we start with a couple of training samples (x_i, y_i) where y_i is a class label equal to ± 1 which indicates the class of the pixel and x_i is a d-dimensional vector which represents the spectrum of the pixel in d wavelengths in the case of hyperspectral images. If the classes are linearly separable by a hyperplane, the SVM classifier is represented by the function f(x)=w.x+b where w is a vector $\in R^d$ and b is a real bias $\in R$ that could separate the classes without errors. The decision is made according to the sign of f. The SVM approach consists in finding the separating hyperplane that has the largest distance from the closest training samples. This distance is expressed as $1/\|w\|$. The margin is defined as $2/\|w\|$. So to calculate W and b, the following optimization must be calculated: $\min\{1/2\ \|w\|^2\}$ with $y_i(w.x+b) \geq 1$, for all samples. By introducing the Lagrangian formalism, the problem is transformed to the dual problem:

Max of: $\sum_{i=1}^{N} \alpha_i - \frac{1}{2}\sum_{i=1}^{N}\sum_{j=1}^{N} \alpha_i \alpha_j y_i y_j (x_i . x_j)$ with the condition $\sum_{i=1}^{N} \alpha_i y_i = 0$ $and\ \alpha_i \geq 0$. Where α_i are Lagrange multiplier that can be estimated using quadratic programming.

If the samples are not linearly separable, suitable kernel functions are used to project the data into a higher dimensional feature space in which the data could be linearly classified. Profiting from this transformation, the inner product in the maximization $(x_i . x_j)$ is replaced with the function $k(x_i . x_j)$.

There are many types of kernel functions, including: polynomial: K(xi, xj) = (1 + xi.xj)^q ;Gaussian radial basis K(xi, xj) = exp(−‖xi−xj‖^2/(2σ^2)) ; Laplacian radial basis K(xi, xj) = exp(−‖xi−xj‖/(2σ^2)) ; Sigmoidal K(xi, xj) = tanh(α$_0$(xi.xj) + σ^2). In the case of multiclass classification, two approaches could be used: One against all, where each class is discriminated using the samples of all classes. One against one, where a larger number of classifiers are computed using each time the training samples of two different classes.

3.3.5.2.   K means clustering

K means clustering is one of the most used clustering methods for hyperspectral images. In k means clustering, the pixels of the image are grouped into classes based on spectral similarity. First, k random centroids are assigned. Then each pixel is assigned to the closest centroid. The norm used to calculate the distance between the pixel and the centroid could be the Euclidian distance, Manhattan distance, max distance, or linear combination of the above distances. After that, new centroids are found by calculating the mean value of each cluster. Then, the clusters are reformulated. This process is repeated until the total number of iterations is achieved or the total distance between classes is minimized [86].

3.3.5.3.   Orthogonal subspace projection (OSP)

Orthogonal subspace projection is a supervised classification method used to detect targets in hyperspectral images at subpixel level. This method is based on the theory of spectral unmixing which consists in subdividing the reflectance spectra of each pixel into endmembers spectra. This method was proposed by Harsanyi and Chang in 1994 [87] in order to exploit a priori knowledge of the target and facilitate the target detection. Suppose the image pixel is modeled by the equation: **x=ta +Bα+ξ** where:

x = spectral vector characterizing the pixel

t = spectral vector associated with the target

a = unknown fractional abundance of the target within the pixel

B = matrix of vectors of the scene endmembers (materials found in the scene background)

α = unknown fractional abundance of each basis vector

ξ = residual error associated with this model.

After the background suppression, OSP uses the matched filter to determine if the target spectrum is a part of the pixel spectra by calculating its abundance. This is done using the OSP operator $\delta_{OSP}(x)= t^T P_B^\perp x$ where $P_B^\perp = I\text{-}BB^\#$ is the orthogonal background operator, and I is the identity matrix. The fractional abundance of the target within the pixel can be computed as follows: $\hat{a} = T_{osp}(x)= (t^T P_B^\perp t)^{-1} \delta_{OSP}(x)$ [87].

3.3.5.4.   Matched Filter (MF)

This technique is based on the statistical approach. The problem is posed as a hypothesis testing problem between the two hypotheses:

H_0: Mine absent (Background material)

H_1: Mine present

In the statistical model, the background and the target mine are usually considered to be following a Multivariate normal distribution (MVN) as follows [88]:

$$H_0: x \sim N(\mu_b, \sigma^2 \Sigma_b)$$

$$H_1: x \sim N(aS_t, \sigma^2 \Sigma_t)$$

Where μ_b is the background mean vector, S_t is the target spectrum, Σ_b and Σ_t are the variance-covariance matrices of background and target respectively, a and σ are scaling factors.

The detectors should satisfy the Generalized Likelihood Ratio Test (GLRT)

$$L(x) = \frac{f(x/H_1)}{f(x/H_0)}$$

where $f(x/H_i)$, $i = 0,1$ is the conditional probability density function (PDF) of the input x given hypothesis H_i. The unknown parameters of the PDFs are replaced with their maximum likelihood estimates.

In order to simplify the model, we consider that the target and the background have the same covariance matrix. In addition, we remove the mean of the background from all pixels and from the target. The new hypotheses are as follows [89]:

$$H_0: x \sim N(0, \sigma^2 \Sigma_b)$$

$$H_1: x \sim N(aS, \sigma^2 \Sigma_b)$$

Where S=S$_t$-μ_b.

The conditional density functions are:

$$f(x/H_0) = \frac{1}{(2\pi)^{\frac{p}{2}}|\Sigma_b|^{\frac{1}{2}}(\sigma^2)^{\frac{p}{2}}} \exp\left(-\frac{1}{2\sigma^2} x^T \Sigma_b^{-1} x\right)$$

$$f(x/H_1) = \frac{1}{(2\pi)^{\frac{p}{2}}|\Sigma_b|^{\frac{1}{2}}(\sigma^2)^{\frac{p}{2}}} \exp\left(-\frac{1}{2\sigma^2} (x - aS)^T \Sigma_b^{-1} (x - aS)\right)$$

To simplify the calculation of the maximum likelihood ratio, a monotonic function (usually logarithmic) is applied without affecting the performance of the matched filter [90]. The derivative of the logarithmic of the likelihood ratio is equal to

$$L'(x) = -\frac{1}{2\sigma^2} (x - aS)^T \Sigma_b^{-1} (x - aS) + \frac{1}{2\sigma^2} x^T \Sigma_b^{-1} x$$

expanding L'(x) we will arrive to the MF detector

$$y_{MF} = \frac{S^T \Sigma_b^{-1} x}{\sqrt{S^T \Sigma_b^{-1} S}}$$

In the literature, we may find the MF defined as a finite impulse response (FIR) filter y=h^{T}x where

$$h^T = \frac{S^T \Sigma_b^{-1}}{\sqrt{S^T \Sigma_b^{-1} S}}$$

3.3.5.5. *Constrained energy minimization (CEM)*

This algorithm is derived from a different point of view than the MF but in the end, it provides a very similar solution. The main difference is that CEM uses the correlation matrix instead of the covariance matrix. Therefore, there is no need in CEM to subtract the mean of image scene from all pixels.

The objective of CEM is to design a FIR linear filter W=$(w_1,w_2...,w_L)^T$ that maximizes the response for a given target d while minimizing the output power [91].

$$d^T w = 1$$

The output of the filter is given by:

$$y = w^T x = \sum_{i=1}^{L} w_i x_i$$

The average output power is equal to:

$$\frac{1}{N}\sum_{i=1}^{L} y_i^2 = \frac{1}{N}\sum_{i=1}^{L} (r_i^T w)^T r_i^T w = w^T (\frac{1}{N}\sum_{i=1}^{L} r_i r_i^T)w = w^T R_{LxL} w$$

where R_{LxL} is the autocorrelation matrix of the samples.

The solution is found using the Lagrange multipliers methods as shown in [92].

The optimal filter coefficients are:

$$w_{opt} = \frac{R_{LxL}^{-1} d}{d^T R_{LxL}^{-1} d}$$

3.3.5.6. *Multiple Target CEM (MTCEM)*

This is an extended version of the CEM algorithm that supports the detection of multiple targets. Suppose we have a matrix D=$[S_1,S_2,...S_p]$ that contains the signature of p targets. The objective now is to minimize the output energy with the constraint $D^T. w=1$. Where 1 is a px1 column vector of ones.

The solution is given in [93]by:

$$y_{MTCEM} = (R_{LxL}^{-1} D(D^T R_{LxL}^{-1} D)^{-1} \mathbf{1})^T . x$$

3.3.5.7. *Winner take all CEM (WTACEM) and Sum CEM (SCEM)*

Another two techniques for multitarget detection based on CEM are Winner take all CEM and Sum CEM [93]. These algorithms necessitate running the CEM algorithm each time for each target. Then the results of the detectors are summed up in SCEM or we take the maximum among other detectors in case of WTACEM. One advantage of WTACEM over SCEM is that if the results are noisy, the noise is not summed up in the final detector.

3.3.5.8. *Adaptive Coherent/Cosine estimator (ACE)*

In the derivation of the Adaptive Coherence Estimator, we will use the same procedure we used in the case of MF. However, in deriving the ACE we will assume that the covariance matrix in the two hypotheses is scaled by different factors $\sigma_0^2 \ and \ \sigma_1^2$. Therefore, the hypotheses are drawn as follows [88]:

$$H_0 : x \sim N(0, \sigma_0^2 \Sigma_b)$$

$$H_1 : x \sim N(aS, \sigma_1^2 \Sigma_b)$$

The likelihood ratio will be:

$$L(x) = \left(\frac{\sigma_1^2}{\sigma_0^2}\right)^{-p/2} exp\left\{ -\frac{1}{2\sigma_1^2}(x - aS)^T \Sigma_b^{-1}(x - aS) + \frac{1}{2\sigma_0^2} x^T \Sigma_b^{-1} x \right\}$$

The MLE of the scaling factors $\sigma_0^2 \ and \ \sigma_1^2$ are obtained by differentiating $f(\mathbf{x}|H_0)$ and $f(\mathbf{x}|H_1)$ with respect to σ^2.

The results are:

$$\sigma_1^2 = \frac{1}{p}(x - aS)^T \Sigma_b^{-1}(x - aS)$$

$$\sigma_0^2 = \frac{1}{p} x^T \Sigma_b^{-1} x$$

The MLE of *a* is given by:

$$a = \frac{x^T \Sigma_b^{-1} S}{S^T \Sigma_b^{-1} S}$$

By replacing these estimates in the likelihood ratio equation, we can arrive to the ACE detector given by the equation:

$$y_{ACE} = \frac{x^T \Sigma_b^{-1} S (S^T \Sigma_b^{-1} S)^{-1} S^T \Sigma_b^{-1} x}{x^T \Sigma_b^{-1} x}$$

ACE could be considered as a little extension of the MF algorithm where the result is normalized by the length of the whitened input pixel $\sqrt{x^T \Sigma_b^{-1} x}$ [133].

3.3.5.9. *Fully constrained least square (FCLS)*

This is another method based on the linear mixing approach. As its name suggests, the abundances in this method are calculated so as to respect all abundances' constraints: the non-

negativity and the sum-to-one constraints. This makes the method useful for material quantification in hyperspectral imagery [94].

Returning to the linear mixing model, each pixel is written as:

$$r = M\alpha + n$$

Where r represents the spectrum of the pixel, M is a concatenation of target and backgrounds signatures, α is the abundance factor and n represents the noise.

The least square cost function is given by:

$$J = \frac{1}{2}(r - M\alpha)(r - M\alpha)^T - \lambda(\sum_{j=1}^{p} \alpha_j - 1)$$

λ is Lagrange multiplier. Differentiating the cost function with respect to α and making it equal to zero we obtain: $(M^T M)^{-1} M^T r - \lambda = 0$

We obtain $\lambda = (1 - \mathbf{1}^T \hat{\alpha})/(\mathbf{1}^T s)$ with s=$(M^T M)^{-1}\mathbf{1}$ and $\hat{\alpha} = (M^T M)^{-1} M^T r$. The solution of FCLS is found using the following procedure [94]:

- Calculate $\hat{\alpha}$

- Compute λ and set $\widehat{\alpha_{FCLS}} = \hat{\alpha} - \lambda s$

- If all components of $\hat{\alpha}_{FCLS}$ are positive, the algorithm stops.

- If not, divide each negative value of $\hat{\alpha}_{FCLS}$ by its corresponding component in the vector s, set the maximum absolute fraction to zero and remove its corresponding endmember signature. Return to step 1.

3.3.5.10.   *Adaptive Matched Subspace Detector (AMSD)*

This technique is based on Generalized Likelihood Ratio Test between the two hypotheses. The noise is supposed to be a zero-mean normal distribution with covariance matrix $\sigma^2 I$ [88].

$$H_0: x \sim N(U\alpha_U, \sigma_0^2 \mathbf{I})$$

$$H_1: x \sim N(S\alpha_S + U\alpha_U, \sigma_1^2 \mathbf{I})$$

By replacing the unknown with their MLE in the likelihood ratio we arrive to the AMSD detector given by:

$$D_{AMSD}(x) = \frac{x^T (P_U^\perp - P_Z^\perp)x}{x^T P_Z^\perp x}$$

$$P_U^\perp = I - U(U^T U)^{-1}U^T \text{ and } P_Z^\perp = I - E(E^T E)^{-1}E^T$$

E is defined as the concatenation of the background and target signatures.

3.3.5.11. *Hybrid Unstructured Detector (HUD)*

HUD is based on mixing both statistical and physical models. The first step is to calculate the abundances using non-negative least square or FCLS. By this, we use the physical model information. The obtained abundances are then used as inputs of statistical based detector like ACE. The detector is written as follows [88]:

$$D_{HUD}(x) = \frac{x^T \Sigma_b^{-1} S \hat{\alpha}}{S^T \Sigma_b^{-1} S}$$

Where $\hat{\alpha}$ is the abundance estimate obtained using constrained least squares.

3.3.5.12. *Spectral Angular Mapper (SAM)*

Like Euclidian distance, spectral angular mapper is a measure of similarity between two vectors. For hyperspectral target detection, SAM is used to calculate the angle between the target reflectance spectra and pixel reflectance spectra treated as vectors. The smaller the angle, the more similar the pixel is to the target. The angle is calculated using the following equation [93]:

$$D_{SAM} = \cos^{-1}\left(\frac{\vec{P}.\vec{T}}{\|\vec{P}\|\|\vec{T}\|}\right)$$

where $\vec{P}$ is the pixel vector and $\vec{T}$ is the target vector.

3.3.5.13. *Spectral Information divergence (SID)*

Another way to detect the presence of a target in the hyperspectral image is to calculate the similarity between each pixel and the target using spectral information divergence. This technique is inspired from information theory where the degree of similarity is calculated using the entropy formula [95]:

$$SID(x, y) = D(x||y) + D(y||x)$$

Where $D(x||y) = \sum_{l=1}^{L} p_l \log(\frac{p_l}{q_l})$ and $p_l = \frac{x_l}{\sum_{l=1}^{L} x_l}$

As in the SAM case, the result of the detection depends on the precision of the target reflectance spectra and is sensitive to the spectral variability.

3.4. Recent developments in target detection using hyperspectral images.

In recent years, researchers proposed various new algorithms to detect targets in a hyperspectral image. Although the different approaches are devoted to generic target detection, they represent promising candidates for improving the performance of current landmine detection techniques. As a matter of fact, landmines constitute a special type of targets, since they are usually rare and sparse in the scene, and they have different shapes, colors and reflectance spectra. For example, various approaches to model a hyperspectral image, in addition to a comparison between supervised Matched filter and unsupervised Reed-Xioli target detection algorithms, are presented in [89]. A nonlinear version of the algorithm *Target Constrained Interference Minimized Filter* based on kernels is recently proposed in [96]. In [97], the authors propose a new endmember extraction process to detect anomalies in a hyperspectral image. Some researchers proposed new models to interpret the hyperspectral data in order to simplify the target detection process. Here we mention: Forward modelling working in radiance space [98], Sparse Representation Based Binary Hypothesis Model (SRBBH) [99], Sparsity and Compressed sensing based models [100] and spatio-spectral Gaussian random field modeling [101].

Chapter Four

4.Experiments and Results

4.1.　Preliminary test of applicability of hyperspectral images for landmine detection

In this chapter, we will show the first tests done in order to verify the applicability of hyperspectral imaging for the detection of landmines. Here we did a test on simulated data in order to precise the spectral information in the hypercube that helps in distinguishing landmines from background materials. In addition, we tested both Supervised and unsupervised classifiers in order to highlight the pros and cons of each type of approach. The results were mainly presented in [102].

4.1.1. Detection Using VNIR, SWIR AND TIR

Even if sometimes mines are just laid on the surface or very close to it, they are still hard to be detected. New mine casings are made similar to the background and hard to be visible by naked eye at visible wavelengths. Because of that, visible wavelengths are not sufficient to detect landmines, especially the buried ones, so we will use infrared bands. While camouflage matches mine coating reflectivity to that of the background in an average sense, exact matches only occur at a few points across the visible and near infrared spectrum (Fig.10)[103][32] . It is difficult to match a coating to a background over a wide range of the spectrum. Quite narrow bands may have large differences in reflectivity between mines and background. Such subtle mismatches between mine and background spectra in VNIR range can be discerned if the spectral range is finely divided [104].
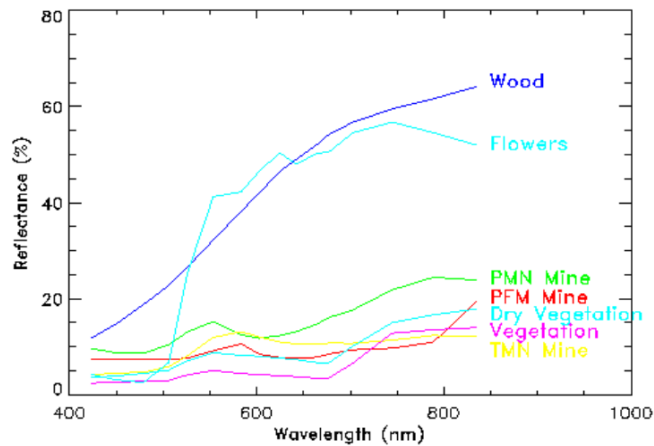
figure 10: VNIR reflectance spectra of mines and background materials [32].

The differences between surface-laid mines and background are more important in the SWIR spectral region. Earlier studies have shown that the reflectivity of many mine coatings and background materials is significantly lower in the VNIR than in the SWIR region (Fig.11) [26]. For example, the reflectivity of the AP landmine is very close to that of a healthy leaf in the visible spectrum, but different in most of the infrared region. In order to achieve better detection, we may focus on the SWIR spectrum as in this range the contrast between background materials and man-made objects is much larger. Plastic mines and painted unexploded ordnance have special pigments in their reflectance spectrum that allow simple classifiers to distinguish synthetic objects from natural features such as vegetation and soil.
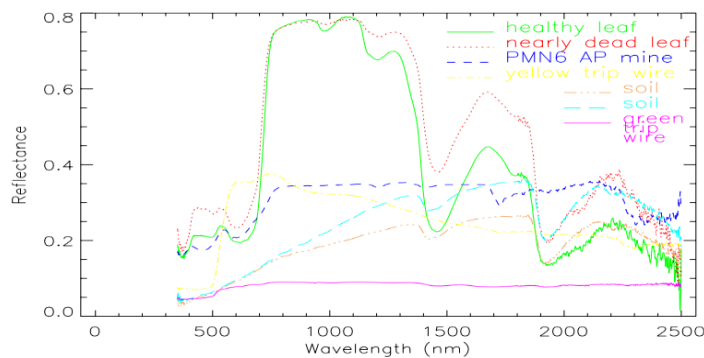
Figure 11: VNIR and SWIR reflectance spectra of mines and background materials [26]

Thermal infrared hyperspectral (TIR, 8000 to 12000 nm wavelength) have the potential to detect buried mines in certain types of recently disturbed soils. The most common mineral constituent of sand in the Earth's continental crust is quartz (SiO_4 silicon–oxygen tetrahedra); Soil disturbance has measurable impact on the quartz reflectance spectrum, presumably due to mixing of different soil particle sizes [103]. The presence of other materials, such as carbonates, may also cause similar reflectivity changes in the TIR region, which also may be suitable for

detection of soil disturbance. However, the use of TIR images for the detection of disturbance depends on results of other unfinished researches that should precise the effect of weather changes and time on the disturbance detection in different types of soil.

4.1.2. Supervised and unsupervised classification

An approach to analyze a hyperspectral image is to attempt to match each pixel spectrum individually to one of the reference reflectance spectra in a spectral library. This is the supervised classification method. Correlation-based classifiers work well with multipixel-sized mines, whereas spectral unmixing methods can detect subpixel-sized mines [105]. Some supervised algorithms are shown in section 3.3.5.

Unsupervised classification, or learning, is a term for grouping objects with similar properties together, without any foreknowledge of those properties. Clustering can be used for classification on multi-dimensional images. The image clustering result is an assignment of each spatial position to a spectral class based on the values of the different points in the image bands. The results of clustering can be used to determine the location and number of classes present. A supervised connection can later be applied to the results with available spectral reference data.

4.1.3. Experiments

To compare between the two types of algorithms we did a test in order to detect the spectrum of landmine in a hyperspectral scene. The experiments were done on the image SalinasA (which could be found on the website [106]. This scene has 224-band over Salinas Valley, California, and is characterized by high spatial resolution. It includes vegetables and bare soils. It comprises 50*50 pixels and includes six classes. In this preliminary experiment, we substitute the spectrum of one pixel with the spectrum of the landmine. The reflectance spectra of the landmines inserted and bare soil are shown in figure 12:
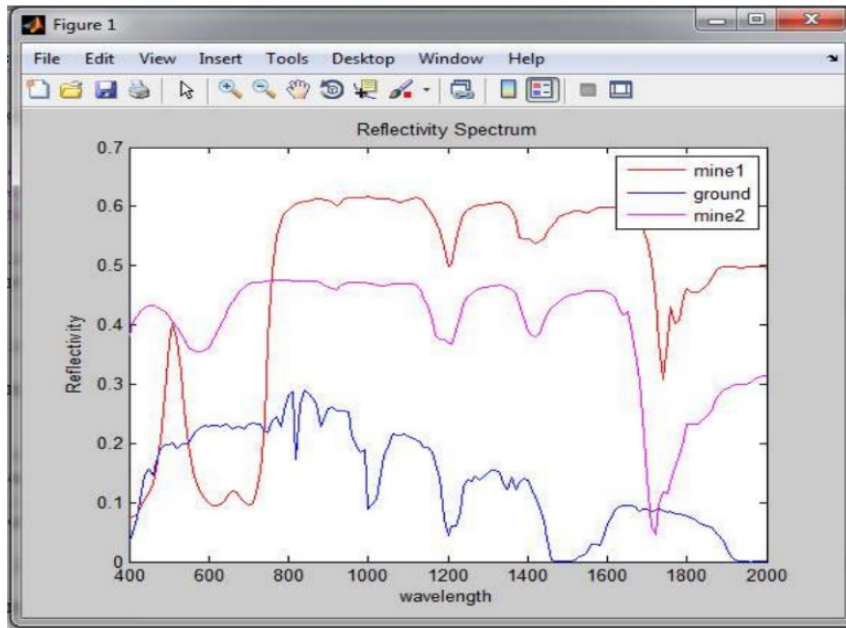
Figure 12: The reflectivity spectrum of one pixel of Salinas ground, mine1, mine2.

The application of two supervised classification methods Normalized Cross correlation and orthogonal subspace projection are shown in fig 13. Note that Red circles designate pixels classified as mine type1 and magenta stars are mine type2.
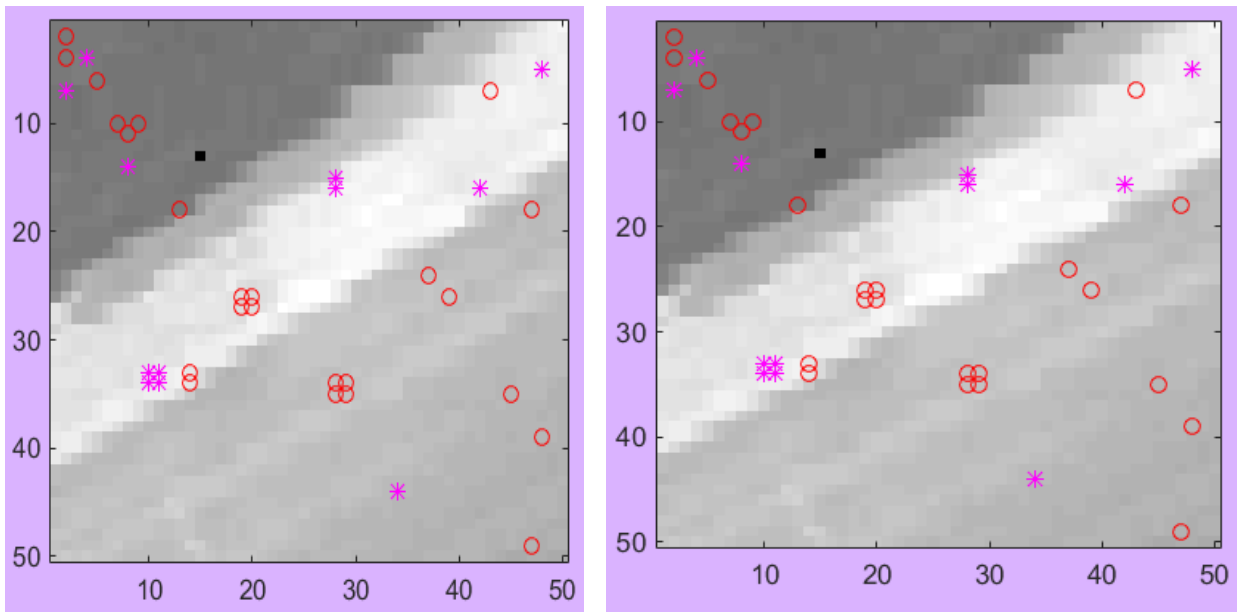
Figure 13: Detection performance of supervised methods: Normalized Cross Correlation (left) and Orthogonal Subspace projection (right)

56

Same procedure is done but using the Kmeans and Fuzzy Cmeans unsupervised classification techniques and the results are shown in the fig.12. Red circles are for pixels classified as mine type1 and mine type2. A supervised connection can later be applied to the results with available spectral reference data to discriminate between type1 and type2.
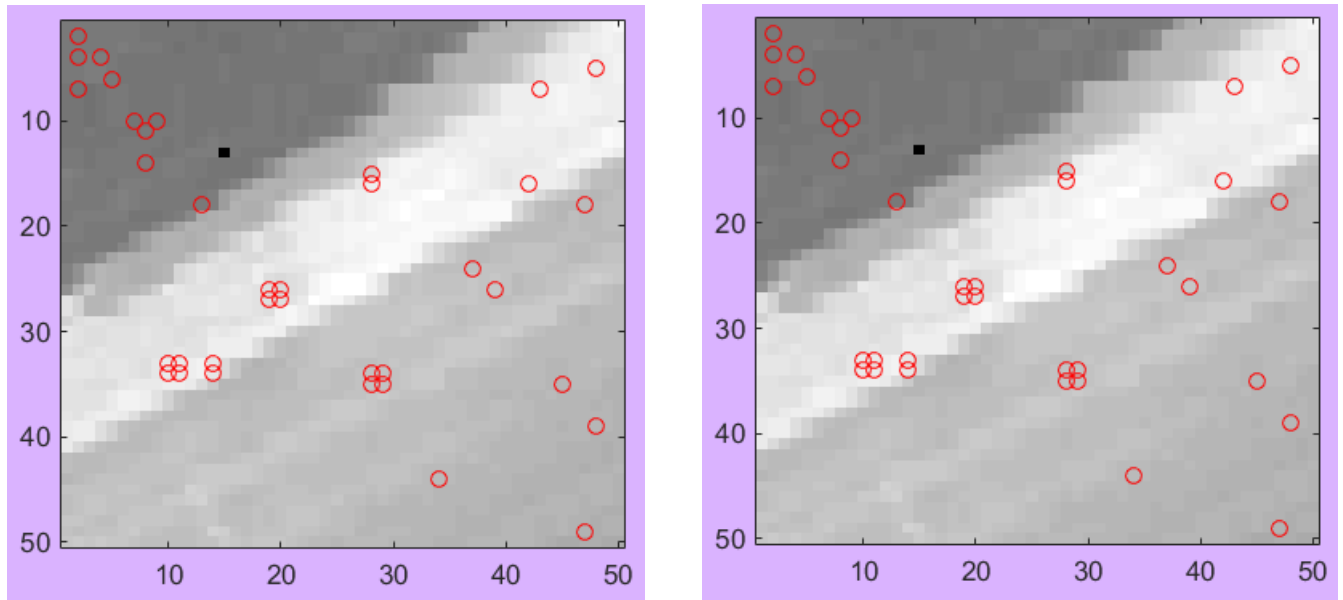
Figure 14: Detection performance of unsupervised methods: Kmeans (left) and Fuzzy Cmeans (right)

All the mines are detected with a 100% probability of detection and no false alarm rate. The discrimination is accomplished easily in our work because the spectral data of the implemented mines are spectral data of two types of plastic mines. Also the implemented spectra are not covered with any ambiguities as for the real case where mines are covered with dirt or vegetation or even camouflaged to match surrounding.

So the pixels that contain the reflectance of the mines show great difference in the reflectivity spectrum than the surrounding (Fig. 12).

There is a need for real images of minefields to investigate accurately the classification and clustering methods.

The tested processing methods showed the potential for a high probability of detection, although further investigation is required for detection in more difficult scenarios. The performed experiment shows that mines possess spectral features that allow them to be distinguished from other materials. Successful surface landmine detection in the VNIR has been shown using spectral signatures. However, the graphs showed that there is more distinguishing spectral characteristics in the SWIR than in the VNIR. More spectral characteristics may increase the detection and identification rates and lower the false alarms. Although reliable detection is not obtained yet, TIR HS imagers suggests promise for buried landmine detection.

In another scenario, the planted spectrum was mixed with the reflectance spectrum of background material. We mixed the reflectance spectrum of landmines by a portion of 0.3 background and 0.7 mine. We applied the two supervised method (NCC and OSP) and the two unsupervised clustering methods (Kmeans and Fuzzy Cmeans) on the new scene. Using the two supervised methods, we were still able to detect landmines with 0 FAR. However, using

the unsupervised method, many FA showed up (see Fig.15). In case of k means, if we run it several times, few false alarms at the borders shows up (Fig. 15 left). But if we run the FCM several times, same large number of false alarms will show up every time. A possible explanation is that by implanting the mixed spectrum (landmine + background), the contrast between the implanted target and surrounding background is reduced in such a way that the implanted spectrum could not be distinguished in a specific cluster. In addition, other rare events that exist in the scene and were not planted are marked as targets.
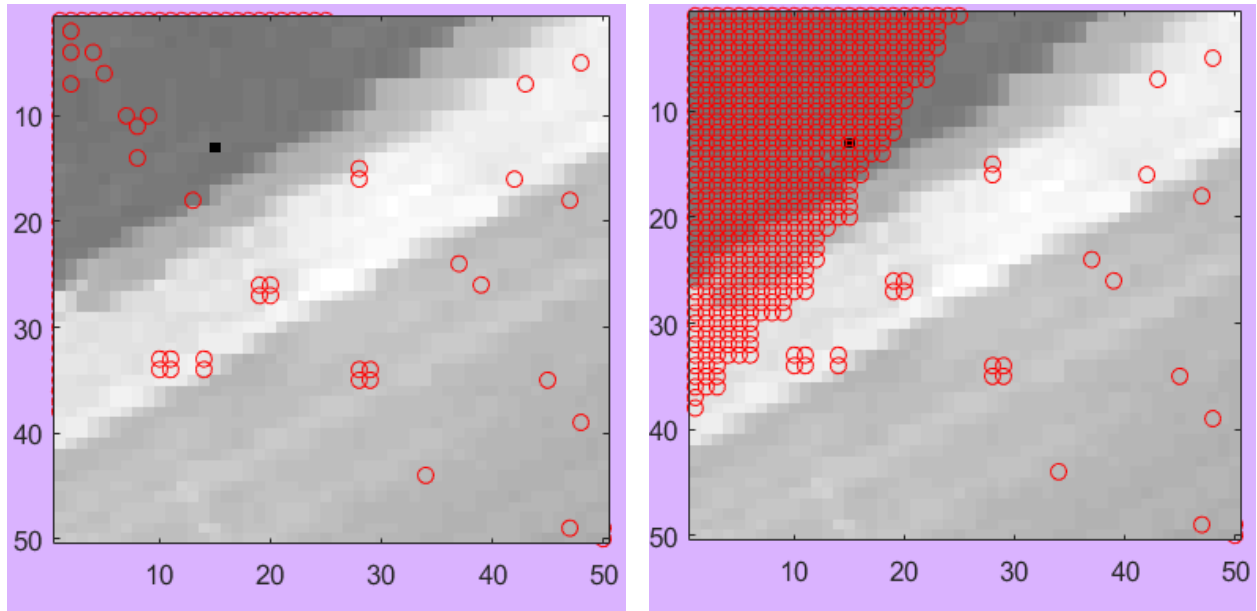
Figure 15: Kmeans clustering after several run (left) and FCM clustering (right) in case of subpixel target

4.2. Full pixel and subpixel mine detection

In this section, we describe the simulation tests done in order to emulate a hyperspectral scene of a minefield and evaluate the performance of different types of supervised detection algorithms. In the first part, we present the image used in addition to the methodology that we followed to simulate a minefield. In the second section, we present the results of this simulation followed by a discussion and conclusions deducted out of this experiment.

4.2.1. Data description

In this experiment, we use a part of an AVIRIS image scene named f100902t01p00r03 available on the following website (http://aviris.jpl.nasa.gov). This image was acquired by the airborne AVIRIS sensor that acquire hyperspectral images in 224 bands ranged between 395 nm and 2500nm with 10nm spectral resolution. The spatial resolution of the image is 0.8m. The original size of the image was 995 samples and 8716 lines. A part of the original scene containing grass and sand in the background was taken. The size of the chosen area is 148x123 pixels (118.4 x 98.4m= 11651 m^2). In order to emulate a minefield, the spectrum of a landmine is inserted in different locations of the hyperspectral image scene.

In the first step, as the image is given in radiance unit, it is converted to reflectance domain. This process is called atmospheric correction. Usually working in the reflectance domain is preferred because the reflectance value is independent of the illumination and weather conditions. Then we spatially upsample the image to arrive to a pixel size equal to the size of the landmine to be inserted. For this, we use the bicubic interpolation. By upsampling the image, we increase the number of pixels per unit area and the spectrum of the added pixels are interpolated according to the spectra of the surrounding pixels. So we obtain an image with lower Ground Sample Distance (GSD) where each pixel represents smaller area but have the same characteristics of the original one (same components).

On the other hand, the information acquired in some bands are too noisy as these bands correspond to the water absorption bands. We may remove these bands in order to reduce the noise and reduce the size of the image at the same time.

After that, depending on the surrounding background material, we replace some pixels in the image with the reflectance of the landmine. By this, we implant the mines in the scene. Now we can apply the classification algorithms on this image to detect the full-pixel target.

In order to simulate the case of subpixel target, the same classification algorithms are applied on downsampled versions of the image. The downsampling was done by grouping the neighbor pixels using bicubic interpolation after using an anti-aliasing low pass filter. The downsampled images have the same area size of the original one but the pixel size is larger. Therefore, the reflectance spectrum of the mined area now is the reflectance of the mine mixed with surrounding background spectra.

Finally, to study the effect of downsampling, we apply the same algorithms on images that have the same size of downsampled images but have pixel size equal to the size of the mine. In this case, we try to detect full-pixel targets in smaller images. However, the area covered by these images is smaller.

Each time we apply a classification algorithm, we obtain a metric for each pixel that represents the degree of similarity between the pixel and the target that we are searching for. After that, we choose a threshold to classify the suspected regions from clean ones. Changing this threshold will change the probability of detection and the False Alarm Rate (FAR). In this study, we chose the threshold in a way to detect all targets and then we registered the FAR obtained when using each algorithm. To note that by FAR here we mean the number of wrongly detected landmines per square meter.

The following chart resumes the characteristics of the images on which we tested the classification algorithms:

```
┌─────────────────────────────────┐
│  Original image (809340 pixels,  │
│  GSD=12cm, Total area=11654      │
│             m²)                  │
└─────────────────────────────────┘
```

| Downsampled image 2 times (202540 pixels, GSD=24cm, Area=11654 m²) | Downsampled image 4 times (50635 pixels, GSD=48cm, Area=11654 m²) | 2 times smaller image(202540pixels, GSD=12cm, area= 2916.6m²) | 4 times smaller image (50635pixels, GSD=12cm, area= 1458 m²) |
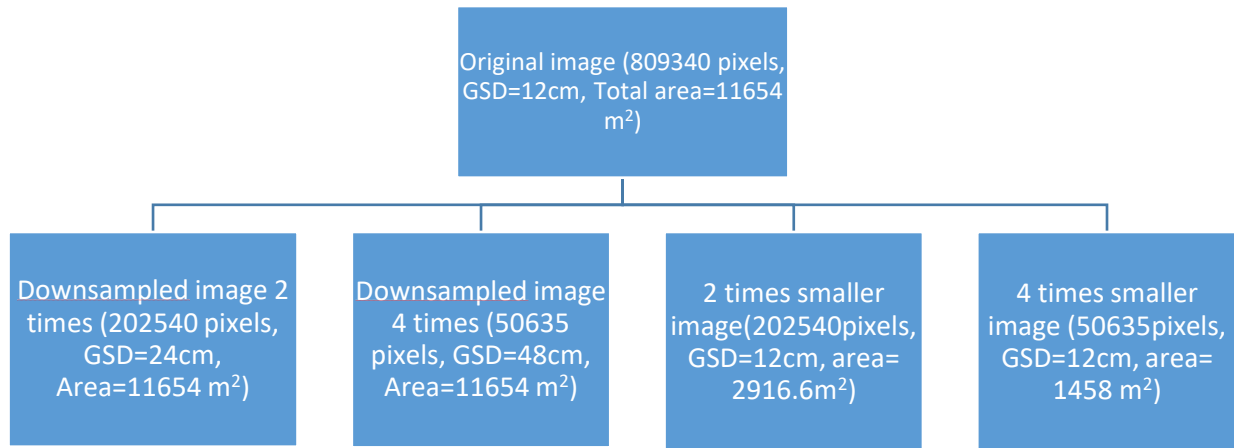
Due to water absorption, here we use 189 of 224 bands. The deleted bands are between 1353 nm & 1443nm and between 1812 & 1958 nm.

4.2.2. Classification Results

In this section, we show the results obtained after we applied the following classification algorithms:

- SAM: Spectral Angular Mapper
- OSP: Orthogonal Subspace Projection
- ACE: Adaptive Coherence Estimation
- CEM: Constrained Energy Minimization
- SID: Spectral Information Divergence
- FCLS: Fully Constrained Least Square
- AMSD: Adaptive Matched Subspace Detector
- MF: Matched Filter
- HUD: Hybrid Unstructured Detector

Table 2 contains the FAR obtained after applying different algorithms on the 5 images. The computation times in each case are registered in Table 3.

Table 3: FAR (nb of false alarms/m2)

	Original	*D2*	*D4*	*S1*	*S2*
CEM	0	0	0.0049	0	0
MF	0	0	0.0058	0	0
ACE	0	0	0.0003	0	0.0048
OSP	0.001	2.3236	2.4261	0.0014	0
SID	0	3.6867	2.7836	0	0
AMSD	0	16.5982	4.151	0	0
FCLS	0.443	12.0172	3.6171	0.2859	0.6076
HUD	0.3782	0.9234	3.738	0.5119	0.4786
SAM	0	4.8432	3.1551	0	0

Table 4: Computation time in seconds

	Original	*D2*	*D4*	*S1*	*S2*
CEM	19.8	4.62	2.22	4.8	2.17
MF	23	5.12	2.37	5.7	2.1
ACE	28.8	6.63	2.65	7	2.5
OSP	19	4.54	2.1	5	2
SID	27.2	6.5	2.9	7	2.5
AMSD	27.3	6.83	2.72	6.8	2.4
FCLS	177	19.66	6.43	42	11.2
HUD	152	38	11.6	39	10.4
SAM	23	5.15	2.3	5	1.68

   As we can notice from the tables, ACE, MF and CEM show the best performance for detecting the landmines in the hyperspectral images because even when the image was spatially downsampled by a factor of 2, the FAR remained zero at full detection. When the image was downsampled by a factor of 4, few false alarms appeared whereas for the other algorithms the FAR is too high to consider the detection as useful. Moreover, the computation times of these algorithms are acceptable and are lower than other algorithms.

As we have seen in section 2, the coefficients of the filter in CEM and MF methods are very similar. They differ in using the correlation matrix or the covariance matrix. This explains why the computation time and the FAR obtained when applying CEM and MF algorithms are very close.

In addition, we can see that the OSP algorithm, which is based on linear unmixing model, is sensitive to the target abundance. The detection was good in case of full-pixel target but the FAR increased significantly in case of subpixel target in D2 and D4 images. AMSD performance shows the same behavior, but in addition to its sensitivity to target abundance, the computation time is a bit higher.

Spectral information divergence (SID) and spectral angular mapper (SAM) belongs to the same family of detectors as both measure the difference between the target and the pixel. Globally, SAM has higher FAR than SID but has a lower computation time. A comparison between both techniques could be found in [95].

Fully constrained least square (FCLS) algorithm is used to calculate the abundances of the background and the target at each pixel. Therefore, it takes the reflectance spectra of the background materials and of the target as input and calculates the abundance of each component in every pixel of the image taking into consideration the non-negative and sum-to-one constraints of the abundances. It is a complex process, which explains the long computation time. The high FAR obtained using this method demonstrates that the estimated abundance of the target could not be used alone as a decision metric of the presence of the target. As the background and target spectra are used in FCLS processing, the detection results depend on the quality of the input spectra and the number of background materials used in the input.

Finally, The two-step detection process of the hybrid unstructured detector (HUD) explains the high computation time. The high false alarm rates may be due to errors in estimating the abundances as in the case of FCLS.

4.2.3. Discussion

Several approaches have been proposed for target detection using hyperspectral imaging. Some of these approaches are based on linear mixing model where the reflectance of each pixel is made of mixing the endmembers' reflectance spectra in different abundances with additional white noise. OSP, FCLS are algorithms based on this approach. However, the detection performance of these algorithms is too sensitive to the choice of the endmembers. If the number or the type of the endmembers was wrongly chosen, the detection will be difficult.

Another approach simulates the spectral variability of the targets and background materials using statistical models like MF and ACE. This approach proves its efficiency in detecting the mines at subpixel level in an acceptable computation time.

MF and CEM methods do not require other information than the reflectance spectrum of the target. This makes the detection of the target faster and simpler but makes it dependent on the precision of the spectrum used in the search. When the spectrum of the target in the acquired scene is different from the spectrum that we are looking for, the detection performance get worse. This may occur due to differences in weather and illumination conditions at the moment

of registering the spectral response of the landmine (maybe taken in lab conditions) and at the moment of image acquisition.

4.2.4. Conclusions

In this study, we arrived to the preliminary result that the CEM, MF and ACE algorithms are three of the best algorithms to be used when trying to detect landmines using hyperspectral imagery. This result is in agreement with the results obtained in the hyperspectral target detection tests [107] that proofs the effectiveness of ACE in target detection. Linear mixing model based algorithms depend on the definition of the endmembers and the fill fraction of the target. The definition of the endmember may differ between images and between users changing the detection results. In the future, we will try to improve the detection of the algorithms in the case of a multi-target scenario as we will see in chapter 4.6.

4.3.   Effect of PCA Feature Selection Prior To Detection

In another experiment, we tested the effect of dimensionality reduction prior to detection on the classification performance. Here we used the Principal component analysis (PCA) to choose the most representative bands out the 224 bands of the image and then we applied different detection methods. Our goal is to evaluate the consistency of the detection algorithms if less information is used in the detection.

4.3.1. Data Description

Here we use a part of the same AVIRIS image scene named f100902t01p00r03 used in the previous test. However, in this experiment we chose another part of the scene where the main background material is sand. The size of the chosen part is 588 samples and 1430 lines (238.4x262.4 m). Here we chose a larger area in order the see the effect in computation time. As in the previous test, the image is pretreated before implanting the mines. First, atmospheric correction is applied to transform it from radiance into reflectance domain. Then, the image is upsampled in order to obtain pixel size equal to the size of landmine. After that, the bands corresponding to water absorption bands are discarded. In the resultant image composed of 189 bands, we implant the spectral reflectance of landmines. Then, we made another copy of the image reduced to 100 bands with the use of Principal Component Analysis algorithm. By applying the PCA algorithm, we are taking the bands that have the largest variability. Thus, these bands contains most of the information in the hypercube.

The same algorithms used in the previous chapter were applied in this test. We applied them on the reduced and normal image. Also in this test, we chose the threshold to discriminate between target ad background so as to detect all planted mines, and then we registered the False alarms and computation time. The results are shown in the next section.

4.3.2. Results

In this section we present the results obtained when the classification algorithms are applied on the original and reduced image using PCA. the tests were done on Windows server with the following characteristics: CPU quad Core 2.9 GHz, 32 GB RAM and 1TB Memory.

The variation of FAR when using each algorithm is shown in fig 14 and the Computation time in Fig 16:
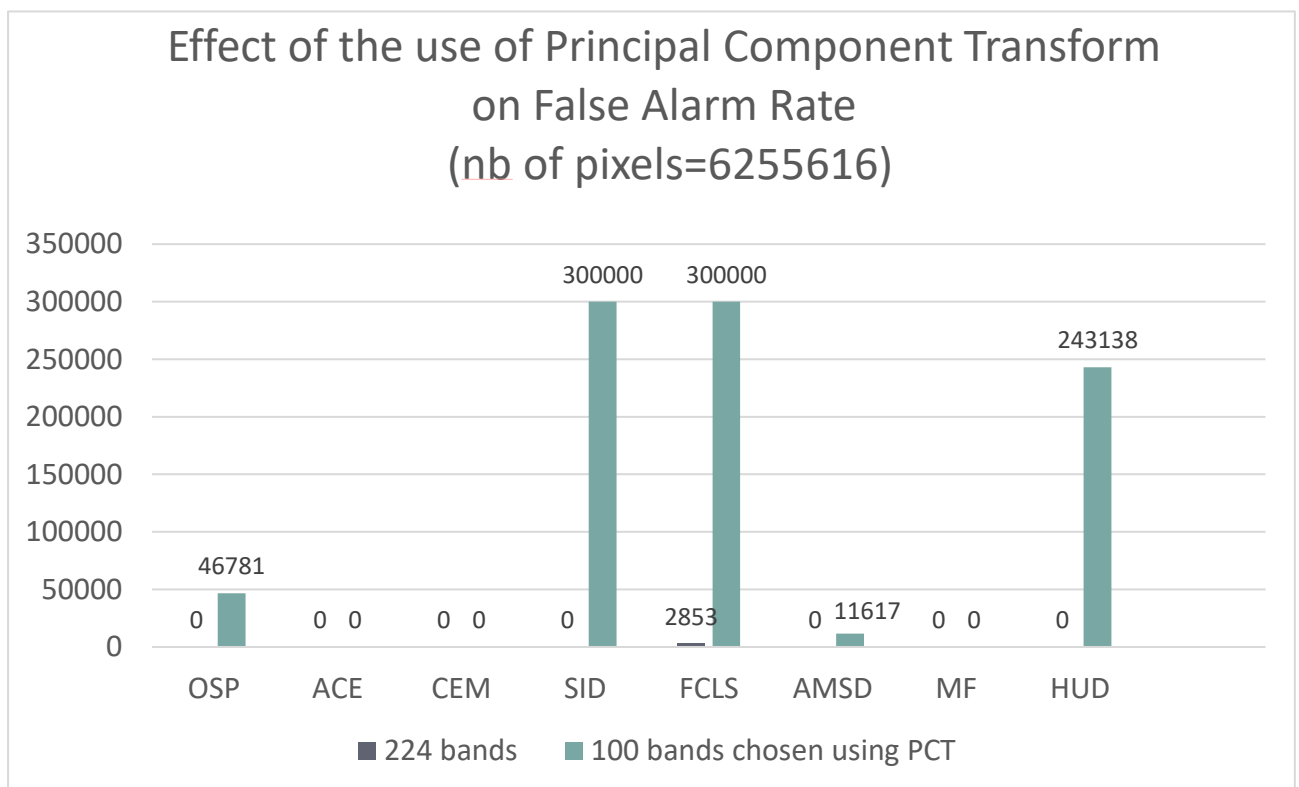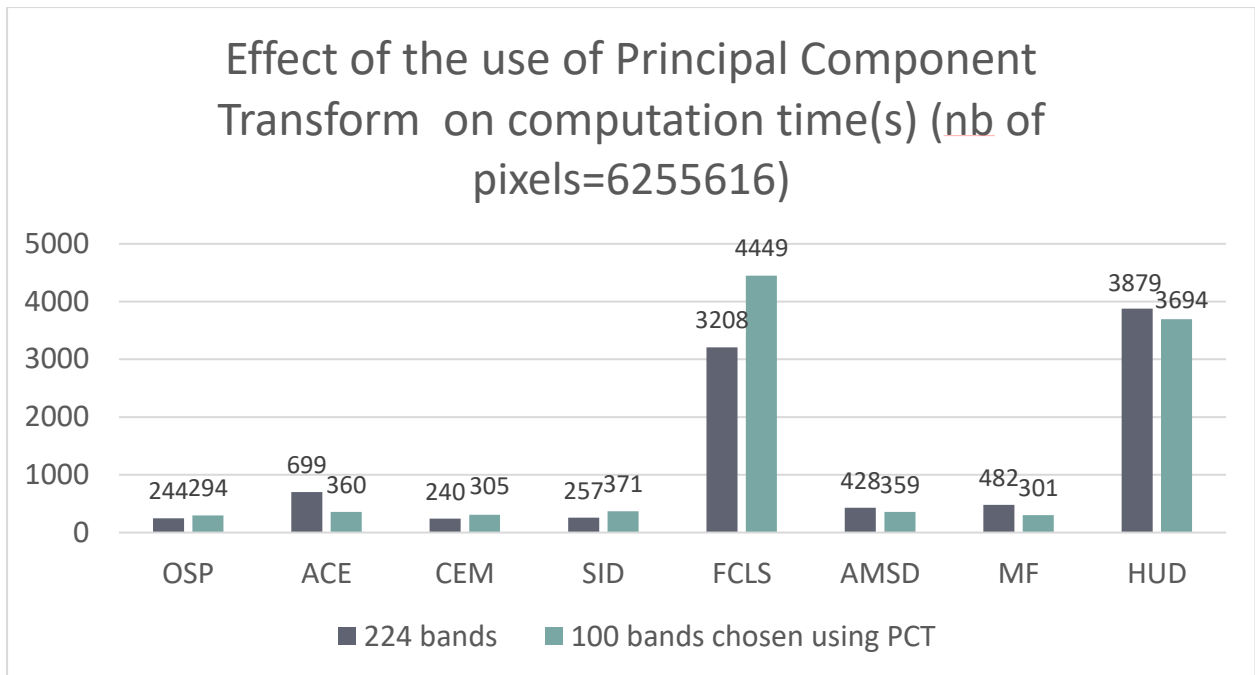

Figure 16: Effect of PCA on FAR

Figure 17: Effect of PCA on computation time

As we see in the charts, after dimensionality reduction using PCA, the performance of ACE, MF and CEM did not change in terms of FAR. Zero FAR rate is obtained in both cases. However, in case of OSP, AMSD and HUD too many false alarms show up after the size of the image is reduced. In case of SID and FCLS, the number of false alarms became too high to consider the detection as effective. So in these algorithms, we lost the information useful to distinguish the targets from background. To note that the false alarm here is higher than the 300000 limit that we considered as maximum value to consider the detection as useful. 300000 is almost half of number of pixels of the image. An algorithm is not effective if half of the field is considered as landmine, because it is not a realistic result. Usually landmines are rare in the scene. In addition, in the case of landmine detection, each false alarm will require about one hour of work to take the necessary precautions before starting the deactivation process. Therefore, if we have a high FAR, the wasted time is too long making the detection using other preliminary techniques more effective.

Talking about the computation time, here we register the computation time needed to perform both the dimensionality reduction and the classification. We see that the computation time is reduced about 48.5% in case of ACE and is reduced about 37.5% in case of MF. In both cases, the FAR remained zero after the use of PCA. However, in case of CEM, the total time to perform PCA and apply CEM on reduced image is higher than the time needed to compute the detection on the original image. This phenomena is repeated with OSP, SID and FCLS however using these algorithms, the FAR became higher after using PCA. So reducing the size of the data prior to use these algorithms is not beneficial in terms of both FAR and computation time.

4.3.3. Conclusions

As in the previous test, ACE and MF showed the best performance. Even if the image was reduced to 100 bands we were still able to detect all landmines with 0 FAR. In addition we gained some time in the computation time. This performance improvement do not apply to CEM: even though the FAR obtained is zero in case of reduced image, the computation time in the two steps (reduction+classification) algorithm is higher than when applying the detection on all image.

Spectral unmixing based methods are too sensitive to the dimension of data used. As we see here, when we applied the OSP AMSD and HUD on reduced image, the FAR obtained was too high. So the use of these algorithms on reduced images won't be effective.

If we would like to use a dimensionality reduction method prior to classification in a real target detection scenario, as on board of a quadrotor while acquiring the hyperspectral image, we should verify if the use of reduction method is useful. Because using some methods, we may have increased computational time as in case of OSP and we may have large FAR.

4.4.   Effect of spectral variability on landmine detection

In this part, we will test the same algorithms but on images in which the mines were planted with different errors. Here we would like to test the possibility to detect landmines if their spectral signature in the hyperspectral image is not exactly the same signature that we have in a library. This very usual case occurs when the mine is covered by another background material like sand, soil or vegetation, or happens in the case of low spatial resolution image. So the reflectance spectrum in the pixel where the mine exists is a mixture of the signature spectrum of landmine and other background material.

4.4.1. Data description

In this test, we use a small part of AVIRIS image named f100902t01p00r03. The chosen part contains mainly vegetation and soil. The size of the chosen area is 494x410 pixels (59.28 x 49.2 m). In different locations of the image, we planted the spectrum of the PMN landmine mixed the spectrum of green leaf (vegetation) that is the background material most dominant in the scene. We mixed the target and the background material in different proportions: 0.5 PMN+0.5 leaf; 0.6 PMN+0.4 leaf; 0.8 PMN+0.2 leaf. In the following section we show the results.

4.4.2. Results

In this paragraph, we will show the results obtained when we tried to detect the PMN signature in the hyperspectral image in which the PMN was planted in different proportions. As in the previous tests, the threshold was set in such a way as to detect all landmines and then we registered the number of false alarms and the computation time.
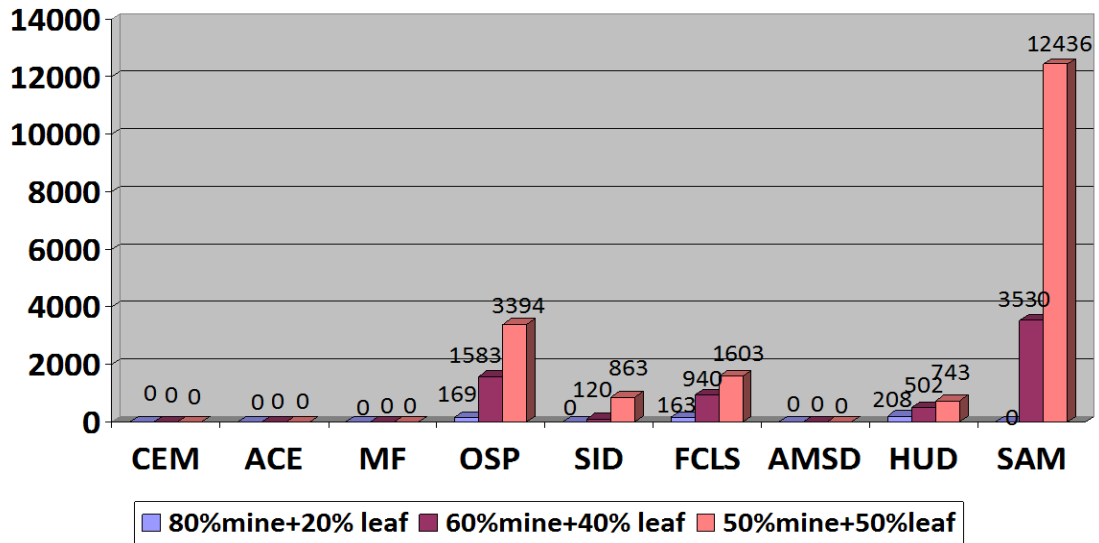
False Alarm Rate of different classification algorithms applied
on various image with different errors
(IMAGE size=494*410=202540 pixels)
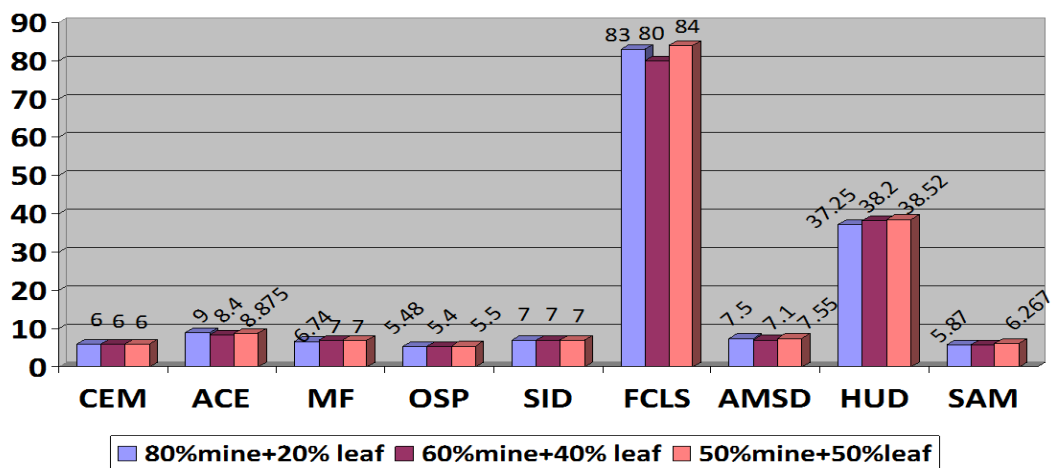
Computation time of different classification algorithms applied
on various image with different errors
(IMAGE size=494*410=202540 pixels)

In this test, the graph of computation time do not have any differences between images of different abundance factor because the images have the same number of pixels. But it helps to compare between different detection algorithms.

In consistency with previous tests, even in this test, CEM ACE and MF show the best performance as using these algorithms, we are still able to detect landmines with 0 FAR even when the abundance factor of target is 0.5. In addition, AMSD show the same performance in this test.

In OSP case, even when the abundance factor of landmine is 0.8, we did not detect the landmine without false alarms. The number of false alarms increases if we are searching for mines with

lower abundance. The same could be deduced in case of HUD algorithm. This may be due to linear unmixing step in which the abundance of targets was wrongly estimated.

By using the FCLS, the computation time is too high by comparison with other algorithms. In addition the FAR is high. Therefore this method is not preferred for landmine detection case.

SID and SAM methods are similar as they both compare between target signature and pixel signature based on similarity measure. SAM uses the angular distance between the spectra while SID measures the mutual entropy between them. However, these methods are sensitive to target abundance. Because of that, we see 0 FAR in case of pure target or target with abundance factor of 0.8, but the detection become harder and too many false alarms will show up in case we try to detect the landmine with abundance factor of 0.6 or 0.5.

4.4.3. Conclusions

In this test, we arrived to almost same result of previous tests that ACE CEM and MF are some of the best algorithms to detect landmines with different abundance factors.

The linear unmixing based methods like OSP do detect the landmines but a right definition of background endmembers is necessary to reduce the false alarm rate or to detect landmines with low abundance factor. We can say the same conclusion for the hybrid detector (HUD) where the first step of its computation is based on linear unmixing model.

SAM, SID or other similarity or distance calculation methods are not reliable for landmine detection, because if the abundance of target is 0.6 or less, the detection of targets is possible but we will have several false alarms. This is not practical especially in case of landmines where each false alarm will take at least one hour of precautions and land preparations.

4.5. MLP Neural network for landmine detection using hyperspectral imaging

In this chapter, we present the tests done in order to detect landmines in hyperspectral images using MLP neural networks. In order to have good performance (reduce the FAR at full detection), we did several tests. In each test, we change some factors that affects the results. These factors are:

➢ Training data set

➢ Number of neurons in the hidden layer

➢ activation function of the neurons

➢ Error minimization strategy used in the training phase.

In the following, we will present a brief introduction about the multi-layer perceptron used in this experiment. Next to it, we will show the results when applied on 17 images and finally the conclusions are provided.

4.5.1. Multi-Layer Perceptron (MLP) Neural networks

The general structure of MLP NN is presented in section 11.1. It is a kind of feed-forward neural networks constituted of at least three layers: Input layer, Hidden layer and output layer. Feed-forward neural networks provide a general framework for representing non-linear functional mappings between a set of input variables and a set of output variables [126]. The network may have an arbitrary number of hidden layers, which in turn may have an arbitrary number of perceptrons [127].
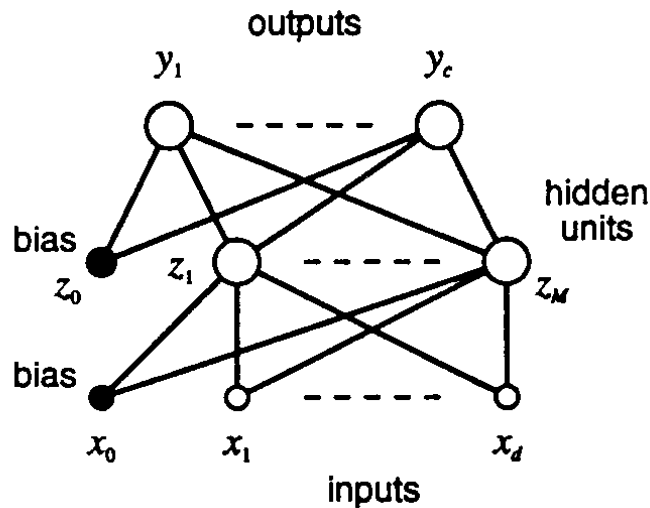

Figure 18: Example of multilayer perceptron NN

The activation function of the hidden layer could be linear, hyperbolic tangent, sigmoid or other. Usually sigmoid activation function is preferred as the output of the perceptron are limited between zero and one so they can be considered as probabilistic values. To train a MLP NN, usually supervised learning is used. The error function to be minimized by backpropagation in the learning process tested here are the sum-of-square errors and cross-entropy. In general, we got a better performance in case we used cross entropy error function.

4.5.2. MLP training and application

In order to train the MLP NN, we used a part of AVIRIS hyperspectral image composed of 280 rows, 150 columns that contain green leaf and sand in the scene. We use the most useful 189 bands out of 224 bands after excluding the water absorption bands. In addition, we test the trained NN on the same 17 images used in chapter 4 section 6.

Here in follow, to give a nomenclature of the results, the training image used in this test will be named TI. The 17 images on which the resultant neural networks are tested are named according to the number of the field number in our data set. The 17 images are named respectively: field2, field3, field4, field51, field52, field53, field54, field55, field56, field61, field62, field63, field64, field71, field72, field73, field10. We used 17 images that have different background materials in order to test the performance of the neural networks in different case studies.

In this experiment, the simulation are performed using MATLAB simulation tool. I referred to NETLAB toolbox [128]. It contains a group of functions prepared to simplify setting up the network parameters.

In the first test, we trained a NN using data from TI. The input is composed of 189 neurons corresponding to the reflectance bands. The size of the output is 3: 100 for PMN, 010 for M20 and 001 for background. The hidden layer is composed of 115 neurons. The training dataset is composed of 200 entry referring to PMN reflectance spectrum, 100 entry referring to M20 and 200 background pixels from TI. The network is composed of 2 hidden layers. This NN is named "netTI". When applied on TI, all mines in the training image are detected with 0 FAR. When we used this network to detect landmines in the 17 images, all mines in all images were detected. However, in some images some FA appeared. The average FAR obtained is $0.121/m^2$ the detection was done in 3.64seconds.

In the second test, I used the data from images field3 field4 field51. The dataset were composed of all pixels of these images including the pixels were the landmines are inserted. This NN is named "netfield3451". When applied on all fields, the obtained Pd was 0.85 with FAR $1.385/m^2$. the computational time is on average 6.5 s.

In the third test, in an attempt to increase the Pd and decrease the FAR, I used for training the images field2 field3 field4 field51. The input for training was the reflectance spectrum of each pixel in these images. This NN is named "netfield23451". By comparison with the previous test, the probability of detection has increased to 0.94, the FAR has also increased to $7.3074/m^2$. the computation time was 6.65s.

In a fourth test, I trained a NN using the data of images field4 field71 field72 field73 field9 field10. The number of neurons in the hidden layer is fixed to 115. This network is named "net4717273910withoutpmn". When this NN is applied on all fields, the average Pd obtained is near 1 (0.99) but the FAR was High ($29.31 / m^2$).

Then I build another NN in an attempt to reduce the FAR using the pixels of field4 field71 field72 field73 field9 field10 in the training phase. In addition, I introduced in the training phase 500 replica of the spectrum of PMN. The number of neurons in the hidden layer is 115. The trained NN is named "net4717273910". This strategy didn't work well. The probability of detection was near zero and the FAR so. So introducing the spectra of the targets several times will not improve the detection. After that, I trained another NN with the same data of the same fields with addition replica of PMN landmines spectra with abundance factor 0.9 mixed with other background material. This NN is named "net4717273910with9". The results are similar to the results of previous neural networks where the Pd and FAR obtained is near zero.

In another test, I trained the data of the fields that usually had high Pd and low FAR in other tests. So in this test I trained a NN using the data of field2 field51 field52 field53 field56 field62. The NN is named "net25152535662". When applied on all fields, the average Pd and FAR were close to zero.

As I found that training data of TI give better results than training few images from the test images, I choose to use it in the training. This time I trained a NN named "n1" using 20 spectra of PMN mine, 10 spectra of M20 mine, and 20000 spectra of background from TI image. The number of hidden neurons was 2. Using this NN, we were able to detect all landmines in all

fields. But in some images we got some false alarms. the average FAR obtained is 0.464. The detection is done in an average of 3.8 seconds.

To reduce the FAR obtained when using "n1" NN, I used the same data used in the previous test. The training set is composed of 20 spectra of PMN mine, 10 spectra of M20 mine, 20000 spectra of background materials in addition to 150 pixel spectra of background road from image field3 usually marked as FA this time is included in the training. To note that the new samples included in the training of "n2" and successive NN are not used for testing the NN performance. When "n2" is used to detect the landmines in all fields, we detected them all landmines. The FAR is reduced to $0.142/m^2$. The average computational time is 3.36. So including some FA in training may help to reduce the FAR. The same NN named "n2" was applied on all images but this time the fields contains mines with different abundances. The results are showed under name n2_2. We got the same FAR as in case of n2 but the Pd dropped to 0.35.

To improve the results of "n2", I took the pixels that were marked as false alarms using n2 and add them to the training sample. So the training set of "n3" is composed of 20 spectra of PMN, 10 spectra of m20, 20000 background spectra from TI and pixels marked as FA when using "n2". When I applied this NN on all fields, all mines are detected in 4.18 seconds. The average FAR obtained is 0.609. So the FAR did not decrease as expected.

After that, instead of using all false alarms found in case of n2, I used in the training of "n4" the data used to train "n2" in addition to FA obtained with fields4 52 53 54 and 55. In this case, I got Pd=1with FAR=$0.397/m^2$ in 3.673s. So in this case, the FA is reduced by comparison with the results of "n2".

Finally, I used in the training of new NN named "n5" the same data used to train "n2" in addition to pixels marked as FA in case of when "n2" was applied of field54 field55 field72 field9. when "n5" is applied on all fields, all mines are detected in 3.68s with slightly high FAR of 3.797/ m^2.

In a new series of experiments, we first applied a feature extraction method to reduce the size of the image prior to train the MLP NN. Here I used the Net analyte signal presented in section 11.1 to choose the best bands that represent the landmines. In the first test, I chose 20 bands using this method. then I trained a MLP NN names "net_nas20" using the data in the image field3. This NN when applied on all fields we got low Pd=0.12 with FAR of 0.209 in 0.58 seconds. So using this method, the computational time is reduced but the detection performance has decreased.

Then I trained another NN this time using 50 bands chosen using Net analyte signal. I used the data in field2 in the training. The resultant NN is named "net_nas50_f2". This network when applied on all fields, we detected all mines but with very high FAR of 65.74. To decrease the FAR, I used the same 50 bandswidth a training data set composed of the pixels of the fields field2 field3 field4. When I applied this NN named "net_nas50_f234" on all fields, all mines were detected with FAR of 6.214.

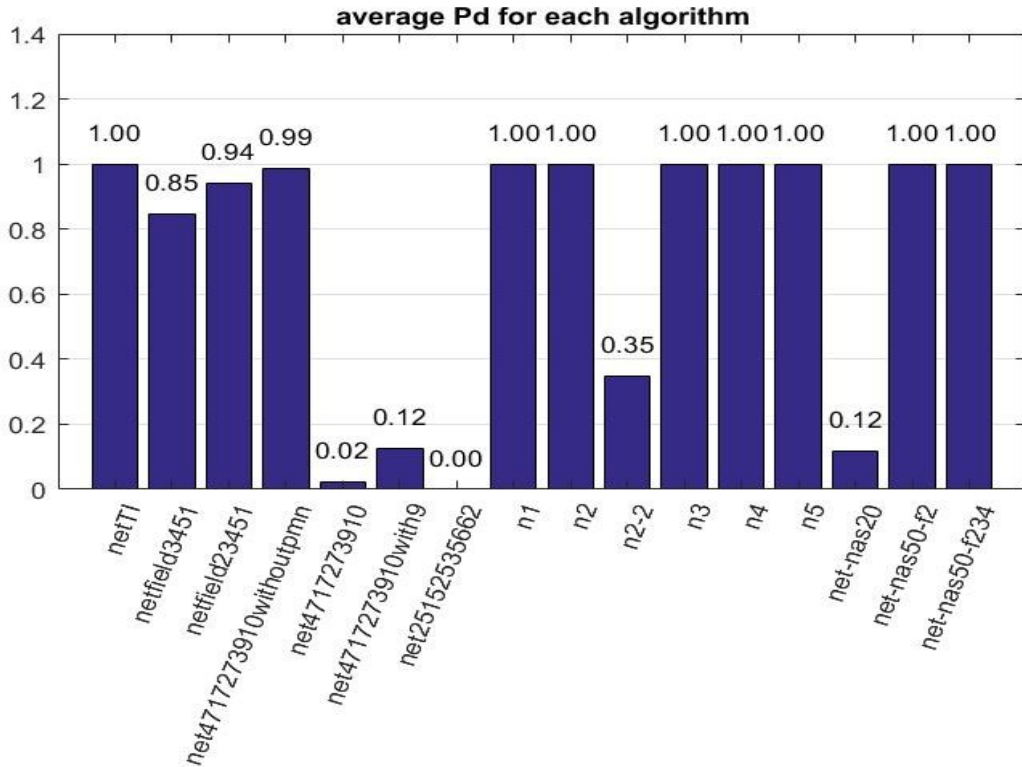The charts that resume all results obtained are shown in the following figures:
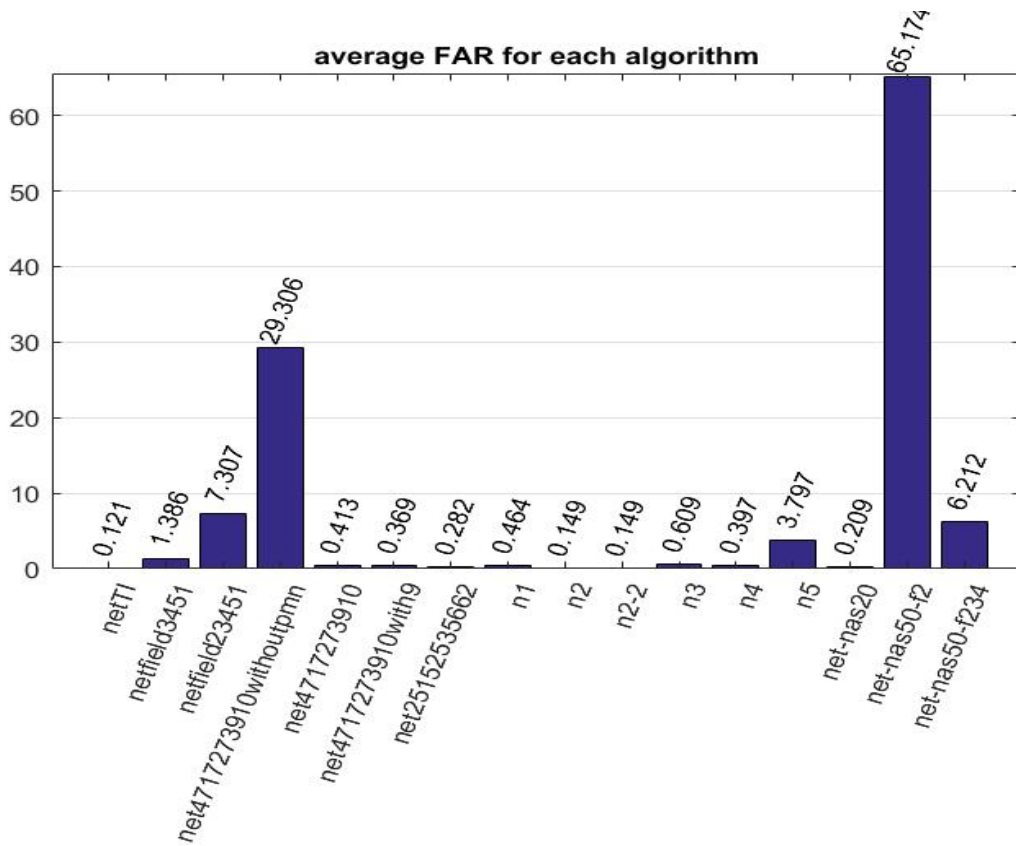
Figure 19: Average Probability of detection

Figure 20: Average False Alarm Rate
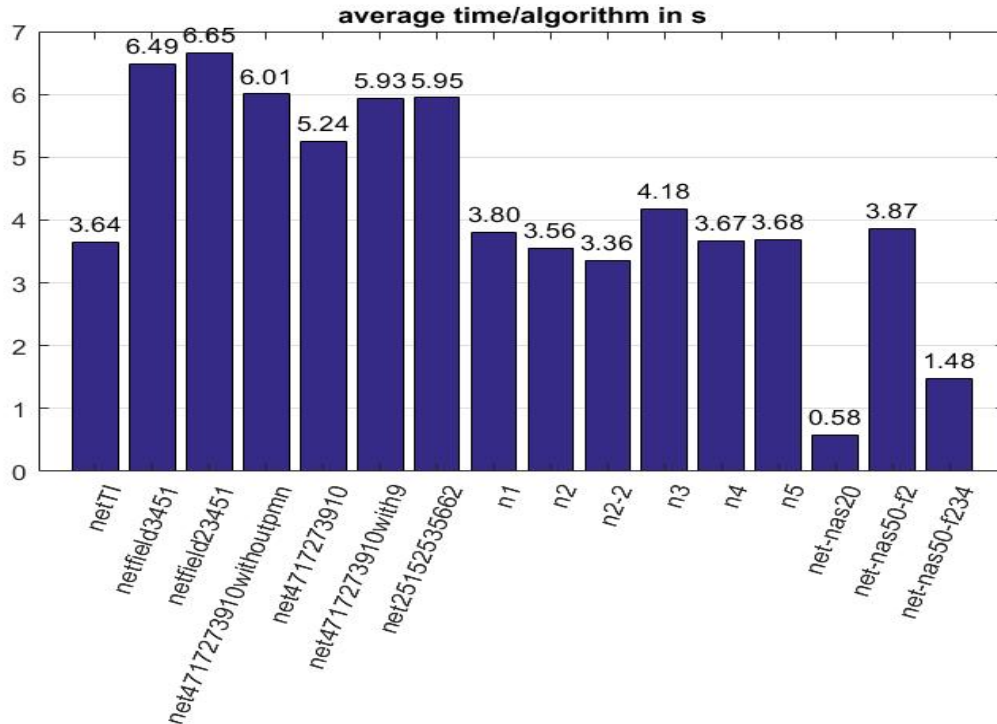
Figure 21: Average computational time

4.5.3. Conclusions

Referring to all tests done in this experiment, we can deduce the following:

➢ Repeating the spectra of the targets in the training sample is not necessary as we obtained similar performance when using n2 and netTI.

➢ The training should be rich and included almost all cases in which a landmine could be in the hyperspectral scenes in order to be detected using MLPNN.

➢ The use of few neurons in the hidden layer with more representative data is more effective than using too many neurons with intensive Training samples. this is concluded when comparing between 'net4717273910withoutpmn' that have 115 neurons and 'n2'.

➢ When the landmines in the image have different abundance factors, the training sample used to train the MLP NN must include several samples of targets with low abundance factor. Without this, the Probability of detection won't be sufficient as happened in case of n2_2.

4.6. Multi Target Detection Using Neural Networks

In this chapter, we evaluate different classification algorithms used for multitarget detection using hyperspectral imaging. We take into consideration different scenarios of landmine detection in which we compare the performance of each method in various cases. In addition,

we introduce the detection of targets using artificial intelligence based methods in order to increase the probability of detection, to reduce the false alarm rate and to foster the detection. These algorithms were tested on simulated data where the spectra of landmines is planted in different proportions with respect to the pixel size in a hyperspectral image scene. We retested these algorithms on real image with real targets. The results show that we can use a well-trained radial basis function (RBF) neural network in order to detect targets using hyperspectral imagery.

Several algorithms have been proposed for target detection in hyperspectral imagery. Some of them are mentioned in the fifth section of chapter 5. Most of them do not support multitarget detection unless we run them several times each run for a specific target. However, this will be a time-consuming process especially if the number of targets is high. Some algorithms were extended for multitarget case e.g the Constrained Energy minimization (CEM) algorithm originally made to give an estimation of the abundance of the target, has several extension to fit the multi target detection: multiCEM, SumCEM, Winner-take-all CEM (WTACEM) and others [108]. Other unsupervised algorithms may be used to detect targets without referring to their reflectance spectrum [109]. But it has been proved that this type of algorithms usually have high False alarm rates as some inert low frequency pixels may be marked as targets while they are not.

In this chapter, we test different supervised classification algorithms used for multitarget detection in a landmine detection scenario and show the possibility of detecting targets using artificial intelligence based techniques. A comparison of the results will be discussed. The types of tests will be carried out: the first one uses images where the targets have been spectrally added to an AVIRIS image while the second one uses real images containing manmade targets.

4.6.1. Neural Networks based Target detection

In this section, we will introduce the use of artificial intelligence in order to detect targets in hyperspectral imagery. Specifically, we will work on neural networks (NN). This approach is adopted due to several reasons:

First, to construct a neural network classifier, two phases are needed: training and classification. The training phase could be done offline and then the detection is achieved online during image acquisition. Therefore, this method may be optimized for real time detection as most of the workload is done offline in the training phase. Secondly, we can customize the detector to detect a large number of targets in one scan, which means that the detection of several targets is fast and requires only one scan. In addition, the network could be customized for different types of backgrounds i.e. we could have several trained neural networks, each for different types of scenes (background, water, sand or forest); therefore, we reduce the FAR by taking the combination of results of several NN.

Artificial Neural Network (ANN) is a computational model used for various machine learning and computer vision tasks. It is designed to work in the same way as the neural networks of the human brain work [110]. It is composed of a network of connected units called "neurons" where each connection has a weight. The neurons are grouped into layers. In addition to the weights, each layer has a bias that plays a crucial role in the detection [111]. A basic NN is composed of two layers: input layer and output layer. This type of NN is called Single layer

NN. Other type of NN may have additional hidden layers between the input and output layers. In this category, we can find the Multi Layer Perceptron. This kind of ANN has the ability to solve nonlinear complex problems that the single layer NN will not be able to solve [111].

Another type of neural networks is the Radial basis functions neural networks. It has the same structure of layers as the MLP. However, in the hidden layer, the activation function is a kernel function (usually Gaussian) [112]. Usually, MLP NN are faster than RBF NN as their computation do not necessitate the use of kernels and therefore is simpler. However, in case of high dimensional data, as in our case where the pixel is of 189 band dimensions, the RBF performs better. RBF showed better performance in our case and thus we will adopt this method in the comparison.

Here, we used two-layers RBF neural networks. The activation function of the first layer (hidden layer) is Gaussian. The activation function of the output layer is linear. The number of neurons is empirically estimated to minimize the global problem.
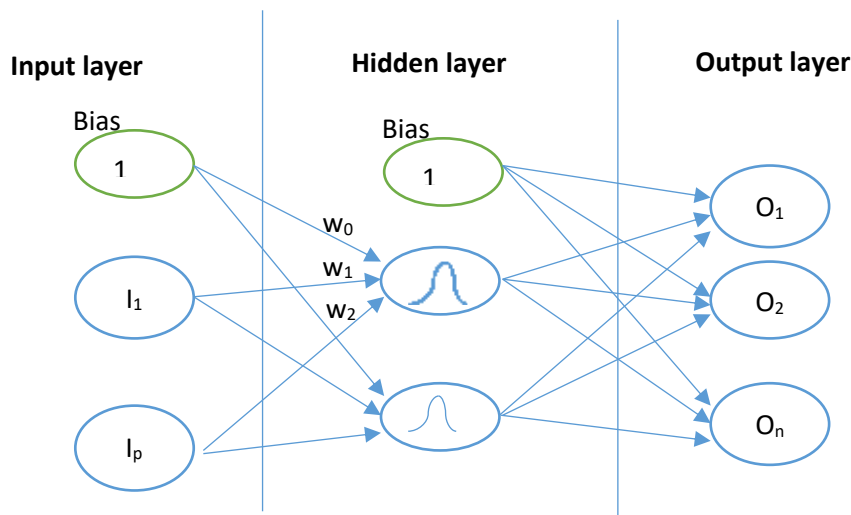

Figure 22: Multi-layer RBF Neural network

Several studies introduced the use of deep learning neural networks for target detection using hyperspectral imaging [113]. However, this will not be our work in this study. Here we focus on ordinary neural networks due to several reasons: First, the main objective of our test is the detection of landmines at subpixel level, therefore extracting some features from a window of pixels as in the preliminary step of convolutional neural networks will make the detection harder. Secondly, we are dealing in this paper with hyperspectral images where each pixel is composed of hundreds of bands. So by mixing several bands we loose some spectral information that are necessary in the detection. In addition we are searching for a simple solution to make the detection faster.

In order to reduce the size of the neural network, our first step will be the feature mapping. In this stage, some key features of the hypercube will be chosen in such a way to reduce the size of the input image and rely on useful information. For this objective, there are several methods that could be used: Principal Component Analysis (PCA), matched pursuit [114], neighborhood

embedding [115], Sammon's mapping [116], multicriteria method [117], nonparametric weighted feature extraction [118] linear discriminant analysis (LDA) and others [119]. In this experiment, we use the concept of Net analyte signal introduced by Lorber 1986 in order to specify the unique part of an analyte signal in chemical spectrum analysis. The idea is to find the part of the signal that belongs to the orthogonal plane of all materials other than the target. By this, we choose the most representative bands of the target. These bands will be used as input to the neural networks in order to detect the targets instead of detecting the complete signal spectrum.

The chosen bands are calculated as follows [120]

$$\mathbf{n}_j = (\ \mathbf{I} - \mathbf{S}_{-j}\ (\mathbf{S}^T_{-j}\ \mathbf{S}_{-j})^{-1}\ \mathbf{S}^T_{-j}\ )\ \mathbf{s}_j$$

where $\mathbf{s}_j$ is the target spectrum, $\mathbf{S}_{-j}$ is a matrix of background analyte spectra and n_j is the portion of $\mathbf{s}_j$ that is orthogonal to $\mathbf{S}_{-j}$. First we estimate all endmembers spectra of the image using Automatic Target Generation Process (ATGP) algorithm [121], $\mathbf{S}_{-j}$ is obtained after removing the endmembers corresponding to the targets.

4.6.2. Experiment on simulated data

4.6.2.1.   Data description

In the first scenario, we tested the target detection algorithms on 17 hyperspectral images taken using Airborne Visible/Infrared Imaging Spectrometer (AVIRIS) of JPL NASA Laboratory. These scenes are available online on the site [122]. The spatial resolution of the images depends on the altitude of the airplane during image acquisition. We can find different scenes of different spatial resolutions. In the chosen scenes, we introduced in different locations the spectrum of manmade targets that will be PMN landmine (Fig.24) and VS-2.2 mine (Fig.25). The reflectance spectra of the landmines were taken in our Lab using Field Spec 4 Hi-Res spectroradiometer. This device is able to acquire the reflectance spectrum between 350 and 2500 nm with spectral resolution of 1nm. We took the spectral signature in different conditions: in lab where specific source of light is used, in grass field and in soil field during a sunny day. Here we plant the spectral reflectance taken when thin layer of grass covered the landmine in the AVIRIS scenes. The insertion was done after several image-preprocessing steps: firstly, atmospheric correction is done to convert the image from radiance domain that depends on the illumination and weather conditions into unified reflectance domain scaled between 0 and 1.

Some bands characterized by low SNR due to vapor absorption are discarded. Then the image is up sampled in order to increase the spatial resolution of the image to arrive to pixel size equivalent to the size of the mine.
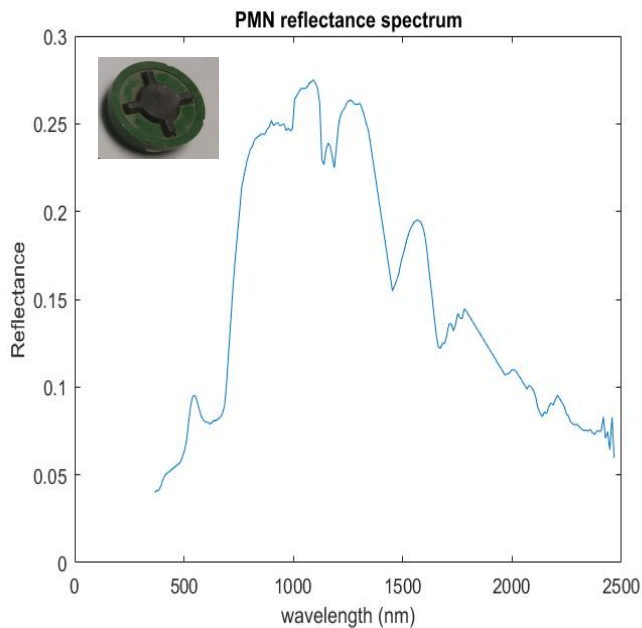

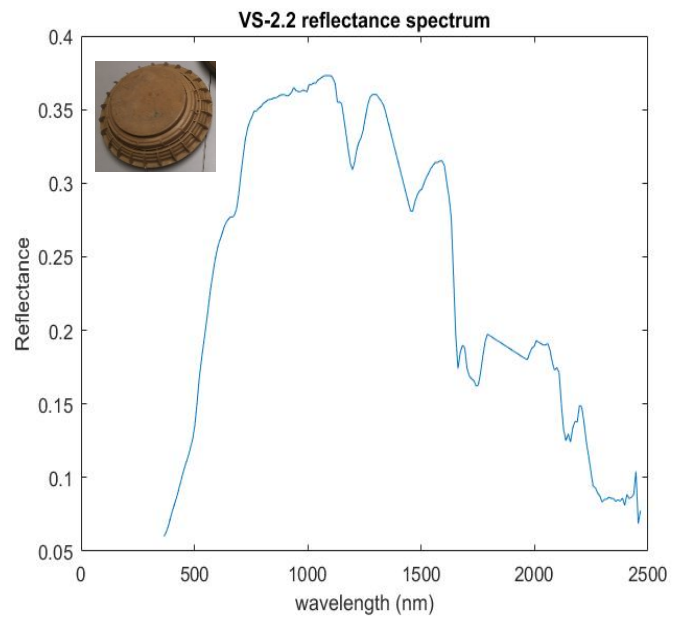*Figure 24: Reflectance spectrum of the pmn mine (target) inserted in the image*

Figure 23: Reflectance spectrum of the vs-2.2 mine (target) inserted in the image

In order to test the full pixel and subpixel cases, the targets were planted in different proportions in the images. The signatures of the targets were mixed with the neighbor pixel signatures in different fill fractions: $PS = \alpha * T + (1 - \alpha)B$ where PS represents the planted spectrum in the image, T is a vector containing the target reflectance spectrum, B the background reflectance spectrum and α the target fill fraction varying between 0.6 and 0.9. In the 17 images, the total number of pixels with landmine abundance factor of $\alpha = 0.6$ (PMN& VS-2.2) is 136, 170 have landmine abundance factor $\alpha = 0.7$, 102 have landmine abundance factor $\alpha = 0.8$ and 110 pixels have landmine abundance factor $\alpha = 0.9$. By this, we evaluate the ability of a target detection technique to detect subpixel targets.

As the target in this scenario is a landmine, the risk of missing a target is much dangerous than having a FAR. Therefore, the decision threshold to discriminate between target and background material is set such a way to detect all targets (Pd=1) and then the FAR is registered. Therefore, a technique is said to be more efficient if it has lower FAR giving that all targets have been detected.

4.6.2.2. Results

In this part, we show the results obtained when applying the detection techniques on all images that contain targets in different abundances. We show the average false alarm rate and computation time at full target detection. The tests where done on Dell server with 64 cores, 128 GB RAM and 1TB Memory.

The tested algorithms are the following:

➢ SAM: Spectral Angular Mapper

77

- OSP: Orthogonal Subspace Projection
- ACE: Adaptive Coherence Estimation
- CEM: Constrained Energy Minimization
- MTCEM: Multiple target CEM
- WTACEM & SCEM:Winner take all CEM and Sum CEM
- SID: Spectral Information Divergence
- MF: Matched Filter
- RBF NN: Radial basis function Neural Network

In case of neural networks, the best NN in terms of false alarm rate was individuated after several tests where we took into consideration different training samples and spread values. First, we randomly divided the 17 images between training and testing data where we used some images in order to train the NN and the other images to evaluate the performance. Using this strategy, the training was very intensive process, took a long time, necessitates large number of neurons to consider all possible cases and we did not arrive to zero FAR. To make sure that we are training the useful data without repetition, we decided to use another strategy. We found that training few pixels that represent the image endmembers is sufficient to obtain a NN able to estimate the abundance of targets and background in each pixel. The input training dataset is the background reflectance spectra automatically estimated using Automatic Target Generation Process (ATGP) algorithm [121]. The PMN reflectance spectra and the VS-2.2 reflectance spectra. The training data is composed as follows: 377 spectra represents various background materials, 5 spectra of PMN landmine and 5 spectra of VS-2.2 landmine. The corresponding output are respectively: 001,100 & 010. To note that the reflectance spectrum of the targets exist with different fill fraction in the scene (0.6 0.7 0.8 &0.9). However, in the training phase, the pure reflectance spectrum of the target is introduced. Using this training strategy, the output for each pixel will be abundance fraction of PMN, VS-2.2 or general background.

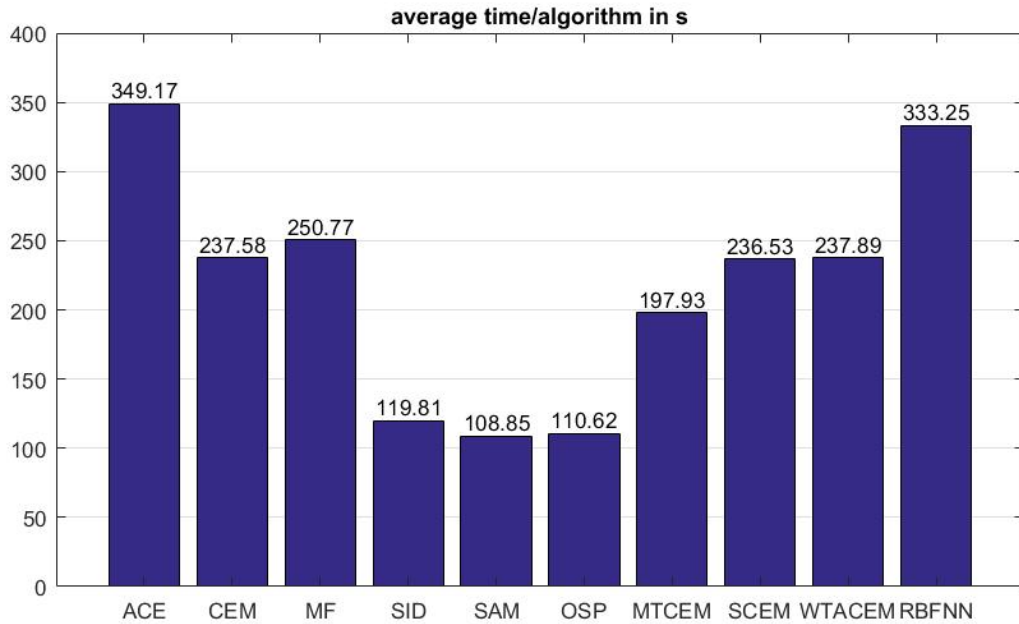The following charts represent the results of the adopted methods:

Figure 25: Average computational time /algorithm
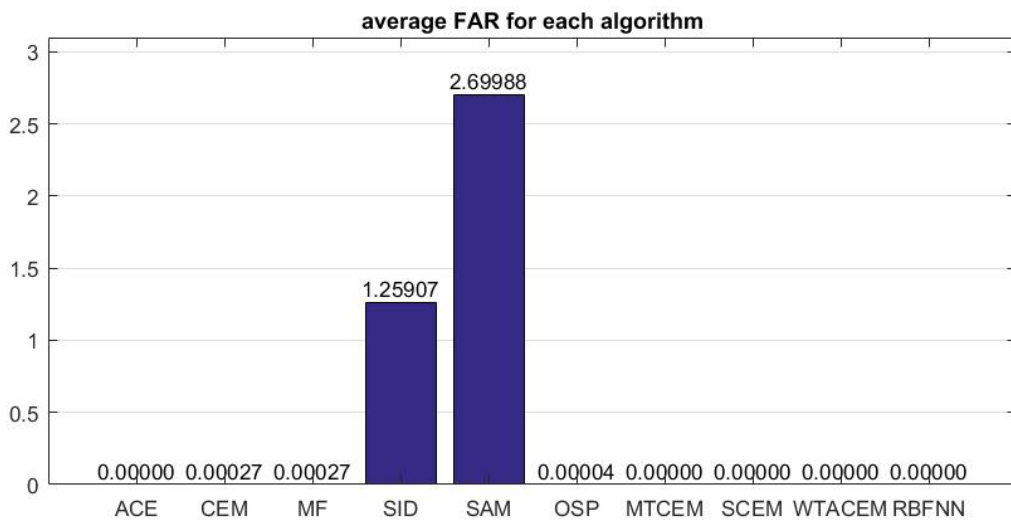
Figure 26: average FAR/ algorithm

In figure 25, we see the average time needed for each algorithm to detect all the targets in the 17 images. As we see in the figure, to detect both types of targets using ACE we needed about 349 seconds while the computation time of MF is 250.77 s and is 238 s for CEM. About the same time is needed using SCEM and WTACEM as these algorithms are based on running the same detector 2 times each run to detect one target. They differ in the decision making step as follows: in case of CEM we set a threshold for each target; in case of SCEM, we add the outputs of the detectors and set one threshold for the sum; or we take the maximum of the outputs and set the threshold accordingly as in WTACEM. SAM and SID are faster than other algorithms but they have very high FAR as we see in Fig 26.

Talking about the FAR, we see that almost all algorithms could detect the targets with very low FAR except for SID and SAM that have high FAR. Both algorithms are based on comparing the spectrum of pixels with the target's spectrum both treated as vectors. Thus, they depend on how similar the pixel is to the target. In case of target with abundance 0.6, they are too much different causing this high false alarm rate.

The other algorithms show very good performance even in case of small abundance factor where few FA shows up when trying to detect low abundance targets using MF and CEM. ACE algorithm gives the ability to detect all targets with 0 FAR. This confirms the previous tests used for target detection [107],[123].

It is worth to note that when applying CEM 2 times and setting a threshold for each target, we got false alarm of 0.00027. Most of the false alarms refer to VS-2.2 targets. However, when we took the sum of the results or their maximum as in SCEM and WTACEM, no more false alarms are obtained. This is due to the increased contrast between targets and background in case of Sum CEM or by ignoring noise effect while taking most valuable results in case of WTACEM.

On the other hand, MTCEM has better performance as all targets are detected without any false alarms with lower computation time. It should be pointed out that, using ACE MF CEM SID SAM and OSP, we have an additional advantage when identifying the targets since using these algorithms we are able to distinguish between PMN and VS-2.2 targets. While using the other algorithms, we can know the presence of a target without knowing its type. This type of information is crucial in some target detection tasks, especially in case of landmine detection in order to determine the best strategy to isolate the landmine according to its blast and fuse type. However, this ability comes at an additional cost in terms of time and/or computational resources.

As we see in the charts, using the adopted training strategy, we got an RBF NN able to detect the landmines without any false alarm. By setting a large value of spread while training the NN, the output was less sensitive to the spectral variability of the input pixel and able to distinguish the presence of target even with low abundance factor.

On the other side, the computation time needed to get this result is lower than ACE that has also 0 FAR, but is higher than other multitarget detection algorithms MTCEM, SCEM and WTACEM. However, using RBFNN, we are able to distinguish between targets whereas in these algorithms we are not.

4.6.3. Real target experiment

In this section, we show the results obtained when we applied previously mentioned algorithms in order to detect targets in real hyperspectral images. This is done in order to prove the applicability of these algorithms in real case scenarios. Even if it has been proven in [124]that the target implant method does provide accurate relative predictions in terms of both target difficulty and detector performance, but reliably predicting the actual number of false alarms for a given target at a given fill fraction is difficult or impossible [124].

4.6.3.1. Test Image

Target detection algorithms tested in previous sections will be applied on the hyperspectral data collected over Viareggio city, Tuscany, Italy by Centro Interforze Studi e Applicazioni Military (CISAM) in collaboration with university of Pisa [125]. The image that we worked on is named D1_F12_H1 and contains 5 different targets (2 panels and 3 vehicles). The data has spectral resolution of about 1.2 nm between 400 nm and 1000 nm with 0.6 m spatial resolution. The targets are as follows: two green colored panels made of carton named P1 and P2, Ford fiesta car named V1, a FIAT DUCATO mini commercial vehicle named V3 and a Ford Focus car named V4. These targets are located in different positions of the image scene. The positons are given in a ROI file for performance evaluation. The spectra of the targets are also given. The first step we did is to convert the image from radiance into reflectance. Then, some bands are chosen to reduce the error. In case of RBF NN, we used in the training phase, the endmembers of the image automatically extracted through the ATGP algorithm, knowing that the spectra of the targets are given in the file. The total training sample is composed of 396 background pixels and 5 spectra corresponding to the targets.

In the next paragraph, we will show the results of FAR and the computation time.

4.6.3.2. Results

Here we will show the results obtained when we applied the previously mentioned algorithms on the image containing real targets. Note that as in the previous case, the threshold for classifying targets is chosen in such a way in order to detect all the targets and then we compare the false alarms obtained in each method.

Table 5: Nb of false alarms and computation time obtained when applying each algorithm

Algorithm/Target	P1	P2	V1	V3	V4	Total	Time (s)
ACE	0	0	0	3	0	3	63.7
MF	6	3	3	7	0	19	35.8
CEM	8	3	3	7	0	21	28
OSP	544	0	0	24	0	568	25.8
SID	43608	11309	10	12	30	54969	27
SAM	19498	111	1	46	0	19656	5.37
MTCEM	NA	NA	NA	NA	NA	44	29
SumCEM	NA	NA	NA	NA	NA	24	28
WTACEM	NA	NA	NA	NA	NA	40	28
RBFNN	0	0	0	0	0	0	37

As we see in Table 5, similarly to the previous section, SID and SAM have a high false alarm rate in comparison with other techniques. These algorithms are too sensitive to the spectral signature of the targets and; therefore, will not be able to distinguish it in case of mixture with other spectra. Thought the computation time of SAM is minimal; the high false alarm rate makes this algorithm useless for this task.

ACE algorithm is one of the best algorithms to use in order to detect the targets because it shows very low FAR (just 3 pixels marked as V3), but its computation time is high (63.7s) in comparison with other techniques. The performance of CEM and MF in terms of FAR and computation time is similar. Both have an acceptable false alarm rate with a small advantage for CEM over MF in terms of computation time and vice versa (for MF over CEM) in terms of FA. This is due to the similarity in the model in which they only differ in using the correlation matrix in case of CEM, while the covariance matrix is used in case of MF.

In addition, in case of OSP, we found out that several FA appeared especially while searching for P1 target. This is because there are three panels in the scene, so we lowered the threshold in order to detect the third panel that exists in the scene with low abundance fraction. This caused this high number of false alarms; however, we didn't notice this huge change when using other algorithms.

When using the multi target versions of CEM MTCEM, SCEM and WTACEM, we couldn't identify the target using this type of algorithms because we were setting one threshold for the mixture of all detectors. For this reason, the false alarms under these algorithms are marked as Non Available (NA) in the table. However, an additional similarity test may help us in identifying their type. In comparison with the results obtained in the simulated image test, we were setting one threshold to discriminate the two types of landmines from background. Here in this image we have 5 different types of targets so we are setting the same threshold for the 5 detectors corresponding to each target. This causes the appearance of more FA as the number of targets is higher.

When applying the proposed type of NN, we were able to detect all targets without any false alarm for all of them. Even though the computation time is a bit high (37 s) in comparison with other multitarget detection algorithms, however detecting all targets without false alarms is more important for this kind of application. It is worth noting that when training the RBFNN to detect the targets in this image, we used Gaussian activation function in the hidden layer with high spread value to overcome the spectral variability of the targets in the scene. The results prove the advantage of using RBFNN with the above-mentioned training strategy in order to detect several targets using hyperspectral imagery in one scan.

4.6.4. Conclusions

In this experiment, we tested some supervised multitarget detection algorithms using hyperspectral imagery. We tested simulated data where the reflectance spectrum of the target was planted in the scene in different proportions and, at the same time, when applied on real hyperspectral image with real targets.

Some of the tested algorithms (ACE, MF, CEM, OSP, SAM, SID) are designed for the detection of one target. They were applied several times each run for each target. This may be a time consuming process, especially if the number of targets is high. This is why we addressed the multitarget detection in this paper. When using some of the multitarget detection process, we lose the privilege of identifying the type of the target. However, this can be recovered by an additional similarity test to classify each target.

SAM and SID are similarity measures between pixel signatures and target reflectance spectrum. The former calculates the angle between the target spectrum and the pixel spectrum, while the latter calculates the entropy between them. When the pixel spectrum is a linear mixture of target and other background material, the similarity measure will differ according to the abundance fraction of the target making the detection process harder. This is the reason of the high false alarm rate that appeared in the simulated data and real image tests.

ACE is one of the best algorithms for target detection. It showed few false alarms by comparison with other algorithms in this test and previously done tests [[107],[123]]. However, its computation time is high. This limits the use of this algorithm in such situation where the detection should be fast like the case of real-time detection.

Using RBFNN, we are able to detect, identify the targets and to estimate the abundance fraction without any problem. The proposed strategy for training an RBF NN has reduced the size of the used NN making also possible to estimate the abundance fraction of the targets. In both tests shown in this test, we got a full detection rate without any false alarm rate. This was not achieved by any of other algorithms, which proves the advantage of using NN for target detection in the proposed. On the other hand, the computation time is a bit higher than other techniques, but it can be reduced if the size of the NN is reduced.

4.7.   Created Spectra method

In this test, we propose a new algorithm for multi target detection using hyperspectral imaging. The objective is to detect the presence of two signatures referring to 2 types of landmines in one scan. The idea here is instead of running the classification algorithm to detect the spectrum of the target two times each run for each target, we run the algorithm one time for both. In this only one run, we search for a synthetic new spectrum that represents both targets. The details about how this spectrum is created in addition to results of tests are shown in the next paragraph.

4.7.1. Spectrum creation

As said in the introduction of this section, in this experiment we create a new spectrum out of the reflectance spectrum of the landmines that we are searching for in order to detect several targets in one scan. Our goal in this step is to foster the detection process to arrive in the future to real target detection at the same time during image acquisition.

In the same AVIRIS scene used in the previous simulated data tests, here we implanted the spectrum of 2 types of landmines: PMN anti-personnel mine and M20 anti-tank mine. The scene is composed of 987x 820 pixels with 0.12 m spatial resolution. The total number of planted mines 30: 15 PMN mines and 15 M20 mines.

In this experiment, we will test the difference in probability of detection, false alarm rate and computation time when applying the CEM, ACE and MF algorithms 2 times each time for each target and when applying the detection algorithms once searching for the created spectra.

Having the image and the reflectance spectrum of landmines in 189 bands between 395 and 2500nm, to create the representative spectrum of the two target, firstly we calculate the distance between the two vectors PMN-M20 and we sort it in increasing order. We take 5 bands where the distance is maximum to represent the PMN mine, we take the 5 bands where the distance is minimum to represent the m20 and we take 70 bands where the distance in near zero. The new spectrum is composed of 80 bands. An image of the created spectra is shown in the next figure:
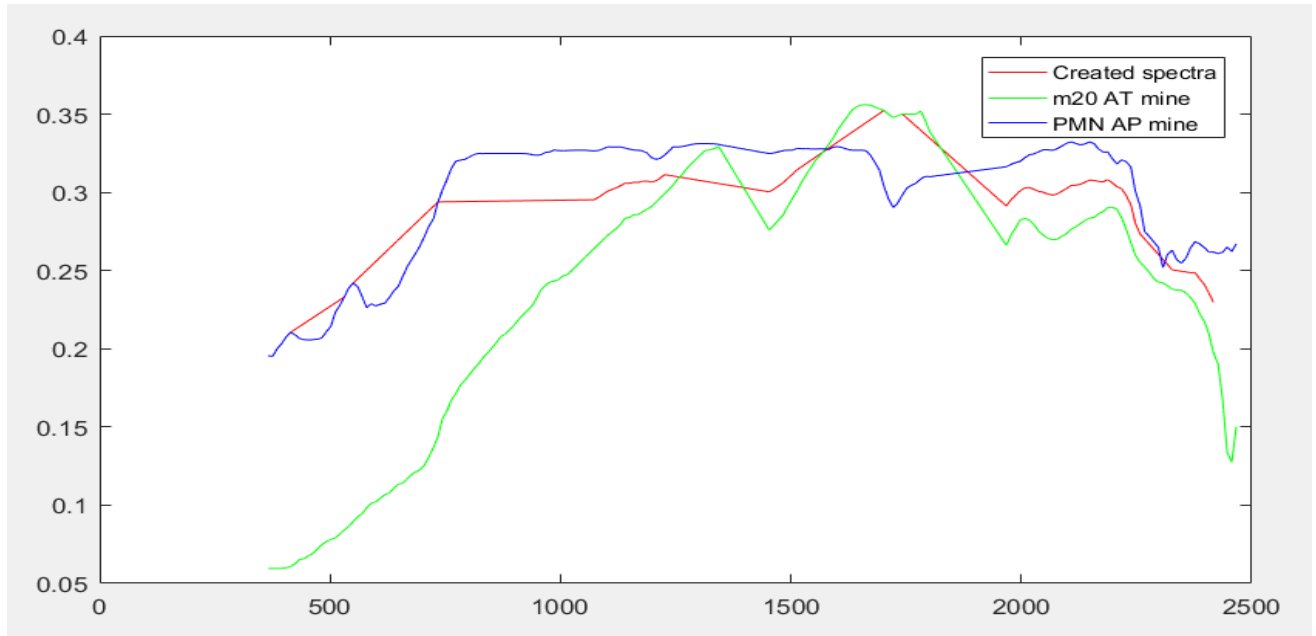

Figure 27: Created reflectance spectrum

Then we applied the classification algorithm ACE, CEM and MF in addition to MultiCEM on reduced image to 80 bands. The results are shown in the following chart:
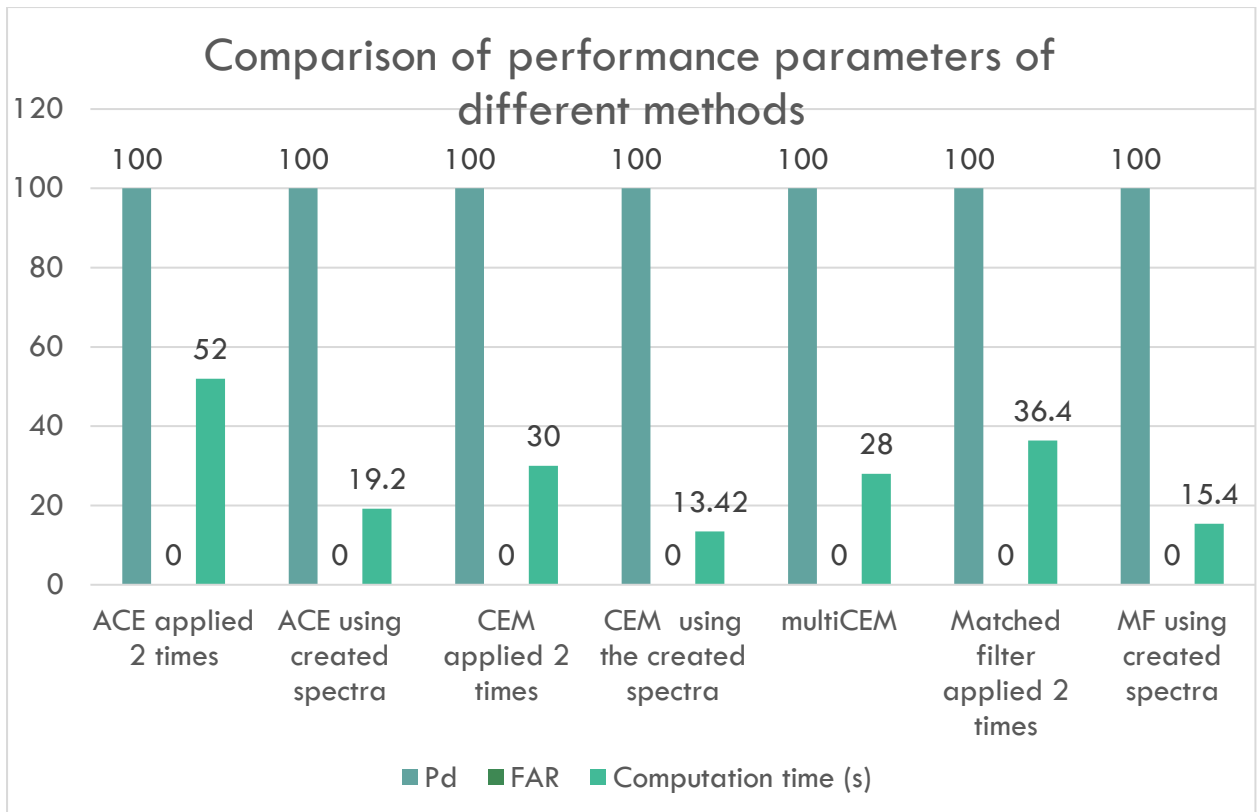
Figure 28: Created spectrum performance

As we see in the chart, in the three algorithms, the created spectra method has the same performance in terms of Pd and FAR as if we applied the algorithms two times. However, we have a gain of more than 57% in computation time. Using this method, we would be able to detect both landmines in less time. To note that in case of CEM, the method of created spectrum is even faster than the MultiCEM that is specified to detect multiple targets.

We applied the same procedure on another image 870x1330 pixel that have different background materials. We got similar results:
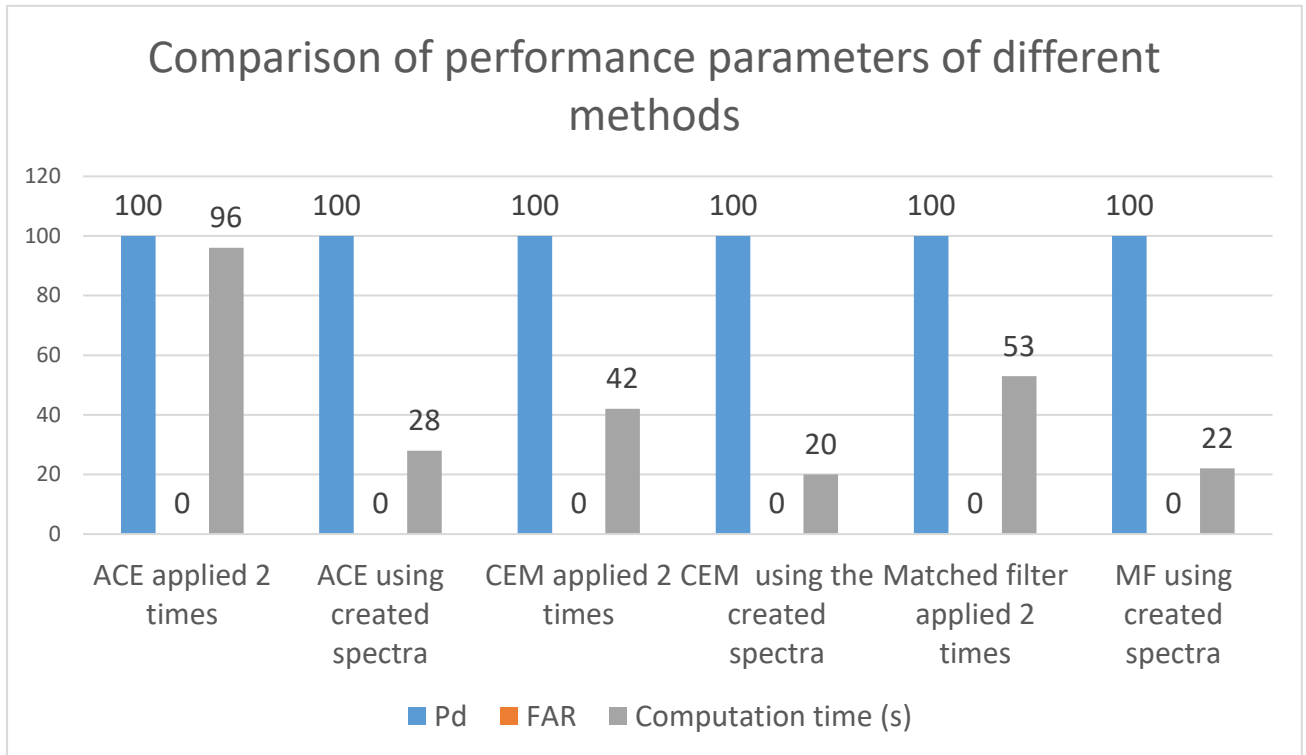
Figure 29: Performance of created spectrum method when applied on another image

However, when we applied these algorithms on downsampled images by a factor of two, so the spectrum of landmines in the image is corrupted by neighbor pixels, the detection of landmines became harder. Too many false alarms show up making the use of this method in case of subpixel targets inefficient.

4.7.2. Conclusions

Using the new method, the computational time has decreased up to 60% while conserving 100% Pd and FAR=0 when applied on original image with full pixel targets. This method does not perform well when applied on downsampled image or on in case of subpixel targets because we are taking part of the information to distinguish the landmines and this part is corrupted while downsampling.

The number of bands taken to represent each mine affect the Probability of detection. So we may take more bands to represent each landmine in the resultant spectrum. The number of common bands also affects the detection probability. If we use more bands to produce the created spectrum, we may have better detection but with lower false alarms. This depends on the type of the spectra that we are trying to mix and how much they are similar.

A study to apply this method in case of three or more targets and different types of targets must be conducted in order to optimize the bands selection and spectra creation.

4.8.   Field Experiment

In order to study the spectral characteristics of landmines and how they may change according to the environment conditions and the type of background where they are planted, it was necessary to collect mines, plant them and acquire their reflectance spectra using a spectrometer in different conditions. For this purpose, we contacted the Lebanese army to get some samples of landmines already found in the Lebanese territory that have been deactivated. After we got the necessary permissions, the Lebanese army gave us 6 samples of 6 types of landmines. 4 are anti-personnel mines and 2 are anti-tank mines. (see Fig. 30)

Figure 30: Samples of landmines used for acquiring their reflectance spectra

To collect the reflectance spectra, we used a high-resolution spectroradiometer named FieldSpec 4 HI-RES. This device is made by ASD Inc. Company. It has the capability to detect the spectrum in the range between 350 and 2500 nm. The specifications of the spectroradiometer are given in table 5.

The device is composed of several components:

➢ The main radiometer in which is connected the probe via 1.5m fiber connected wire.

➢ Power bank battery to supply the radiometer and very useful in case of field experiment where no power source is near.

➢ Computer with specialized software to control the instrument and register the data

➢ White board used to calibrate the device before registering the data.

There are other optional accessories. To note that the connection between the computer and the spectrometer is wireless. This made simpler the data collection in the field.

Table 6: FieldSpec 4 Hi-res spectroradiometer specifications

Spectral Range	350-2500 nm
Spectral Resolution	3 nm @ 700 nm 8 nm @ 1400/2100 nm
Spectral sampling (bandwidth)	1.4 nm @ 350-1000 nm 1.1 nm @ 1001-2500 nm
Scanning Time	100 milliseconds
Stray light specification	VNIR 0.02%, SWIR 1 & 2 0.01%
Wavelength reproducibility	0.1 nm
Wavelength accuracy	0.5 nm
Maximum radiance	VNIR 2X Solar, SWIR 10X Solar
Channels	2151
Detectors	VNIR detector (350-1000 nm): 512 element silicon array SWIR 1 detector (1001-1800 nm): Graded Index InGaAs Photodiode, Two Stage TE Cooled SWIR 2 detector (1801-2500 nm): Graded Index InGaAs Photodiode, Two Stage TE Cooled
Input	1.5 m fiber optic (25° field of view). Optional narrower field of view fiber optics available.
Noise Equivalent Radiance (NEdL)	VNIR 1.0 X10^{-9} W/cm^2/nm/sr @700 nm SWIR 1 1.4 X10^{-9} W/cm^2/nm/sr @ 1400 nm SWIR 2 2.2 X10^{-9} W/cm^2/nm/sr @ 2100 nm
Weight	5.44 kg (12 lbs)
Calibrations	Wavelength, absolute reflectance, radiance*, irradiance*. All calibrations are NIST traceable. (*radiometric calibrations are optional)
Computer	Windows® 7 64-bit laptop (instrument controller)

The Remote Sensing department of the National Research Council in Lebanon owns this device. They helped us in the acquisition of the spectra of landmines.

To test the variation of the reflectance spectra in different conditions, we acquired the reflectance spectra in Lab, in grass field and in soil field as we will show in the next sections.

4.8.1. Reflectance spectra of landmines acquired in the lab

In a first step, in order to register the reflectance spectrum of the landmines that we have, we acquired the spectrum in Lab conditions. By this, we mean that in a lab room, we used a specific source of light that produces light of different wavelengths between 350 and 2500nm of the same intensity. It is designed to produce stable output with a smooth spectral curve into the

SWIR range and to minimize backscatter and any change of lamp energy output over time [131]. The lamp produces a well-defined beam to maximize the amount of light energy on a sample area while minimizing stray light from surrounding surfaces [131].

The Illuminator benefits as stated by the manufacturer are [131]:

- The 70 watt quartz-tungsten-halogen light source with integrated reflector produces stable illumination over the 350 to 2500 nm range

- Stable output yields accurate and dependable reflectance measurements

- Well-defined beam maximizes light energy on sample area

- Precise voltage regulation for high stability light output

- Multiple mount options for lab stands or tripods

The source of light is used in order to avoid the noise and other artifacts that we may face in the field. In addition, the sunlight when reaches the soil, it will not have the same intensity at all wavelengths due to CO_2 ,water vapor and other pollutants that absorb radiations of specific wavelengths.

This experiment was done in Scientic research center in Engineering at Lebanese University faculty of Engineering.

Figure 31: Acquisition of the reflectance spectrum of TM-46 landmine

Figure 32: trying different incident angle

As we see in the image, to acquire the reflectance spectrum of the landmines, we used the source of light shown in the figures. First, the detector is calibrated on the white board. The calibration is necessary so after it is achieved, the registered spectra are automatically converted from radiance into reflectance value according to the reflection of light on the white board.

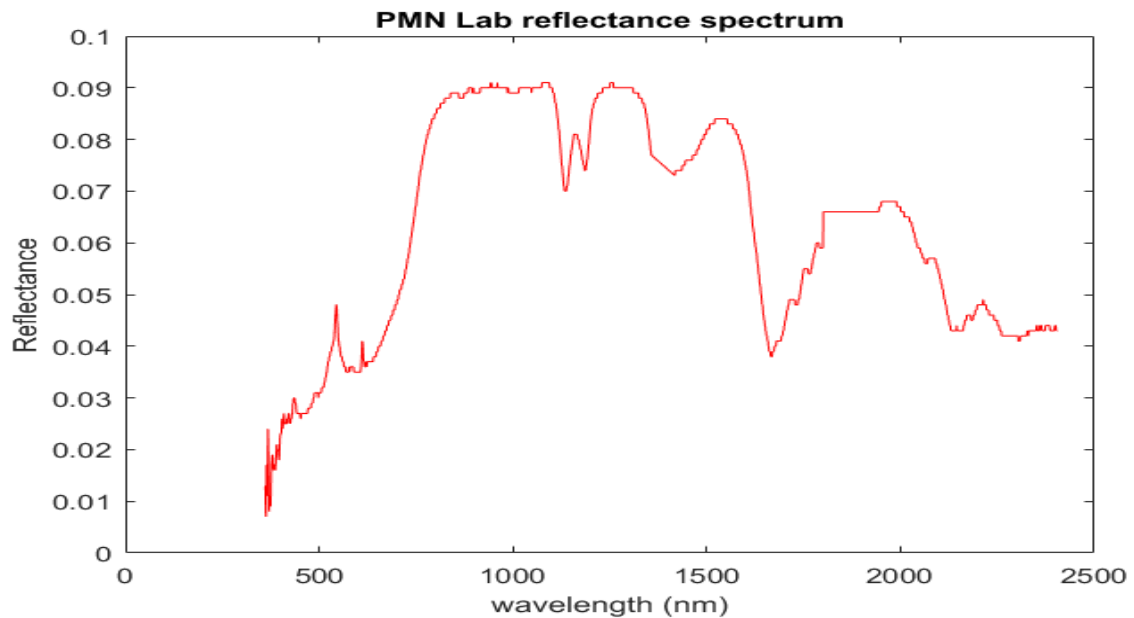We registered the reflectance spectra of the 6 mines. The results are as follows:

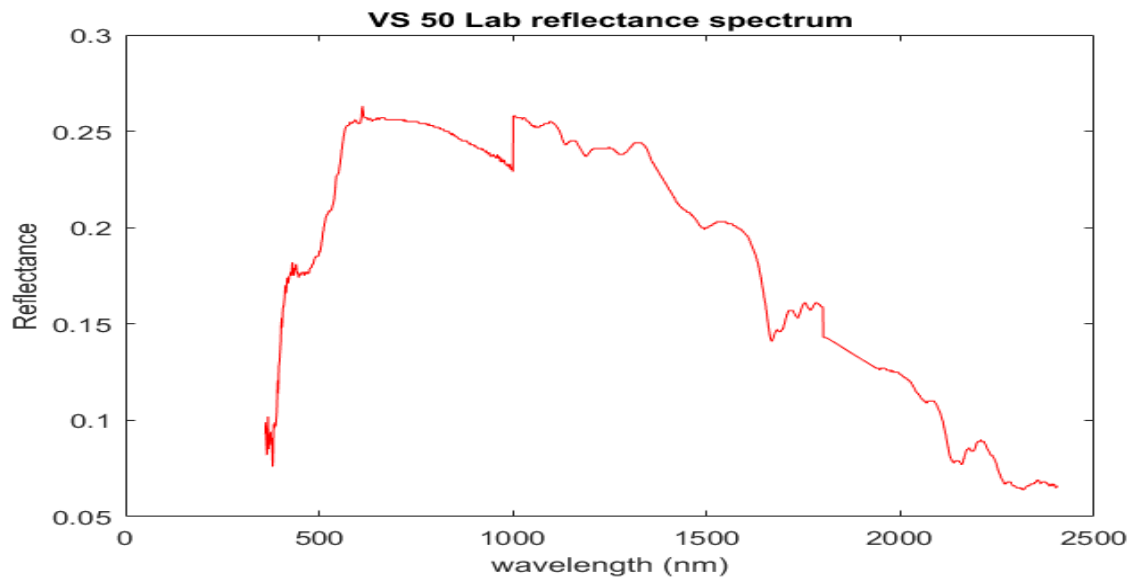*Figure 33: PMN reflectance spectrum taken in LAB*

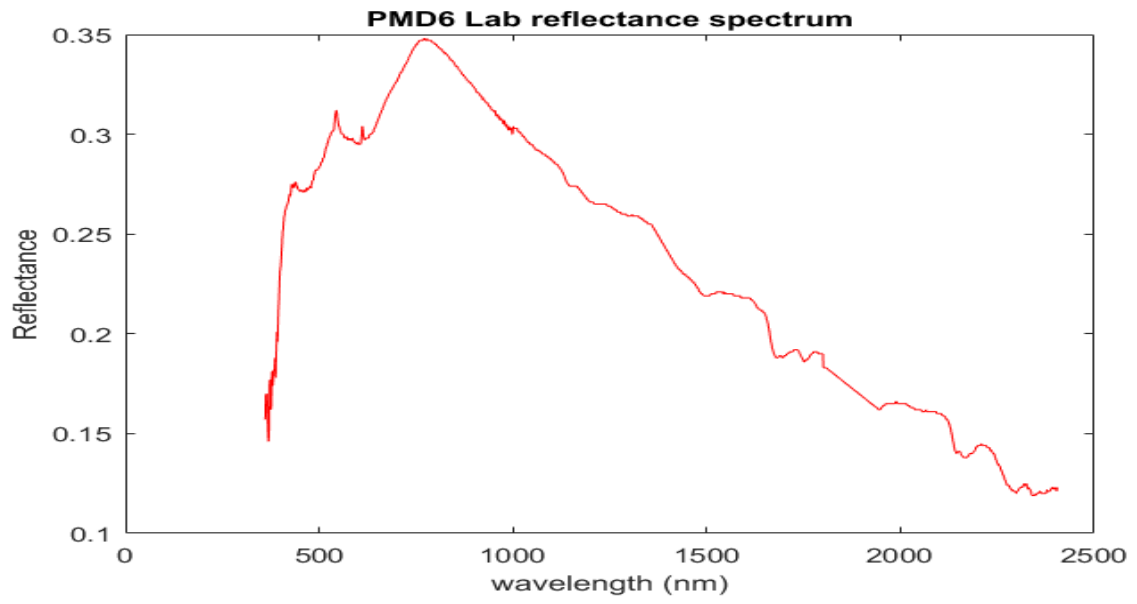*Figure 34: VS-50 reflectance spectrum taken in lab*

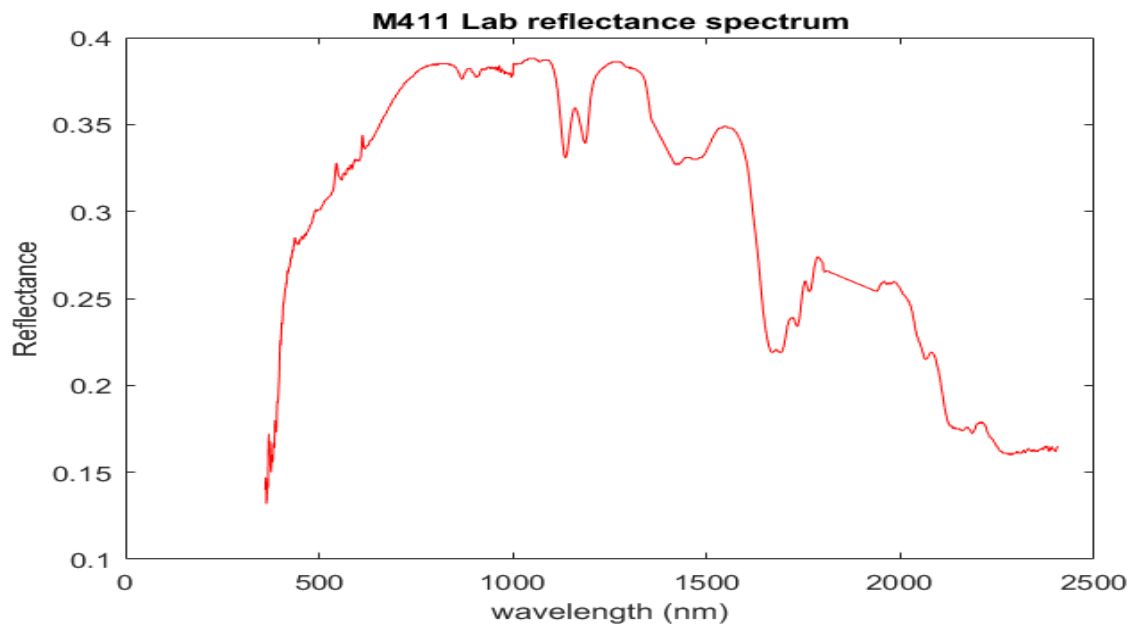*Figure 35: PMD-6 reflectance spectrum taken in lab*

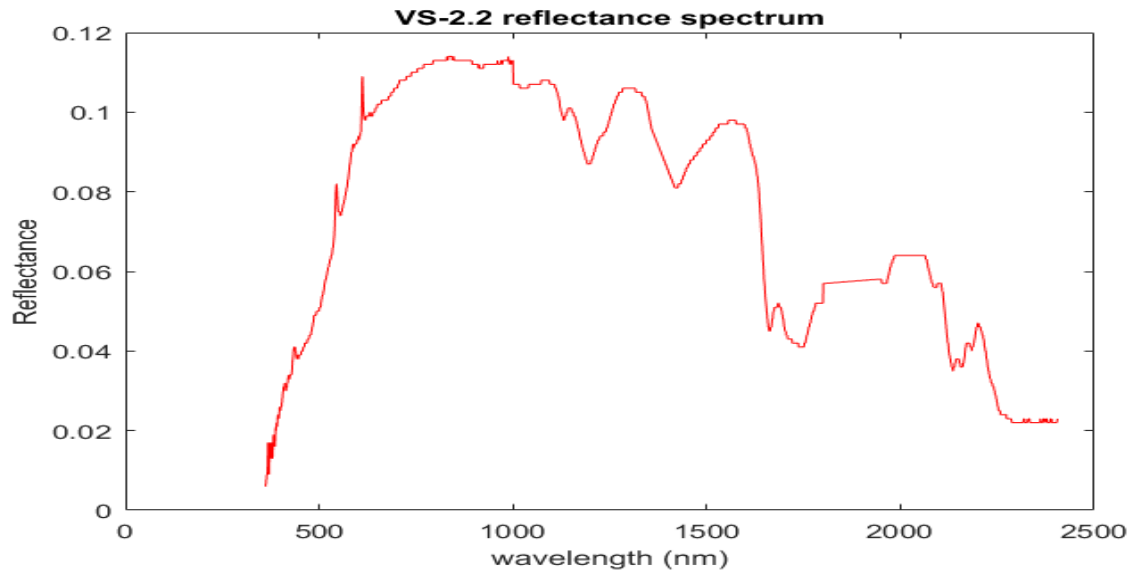*figure 36: M411 reflectance spectrum taken in lab*

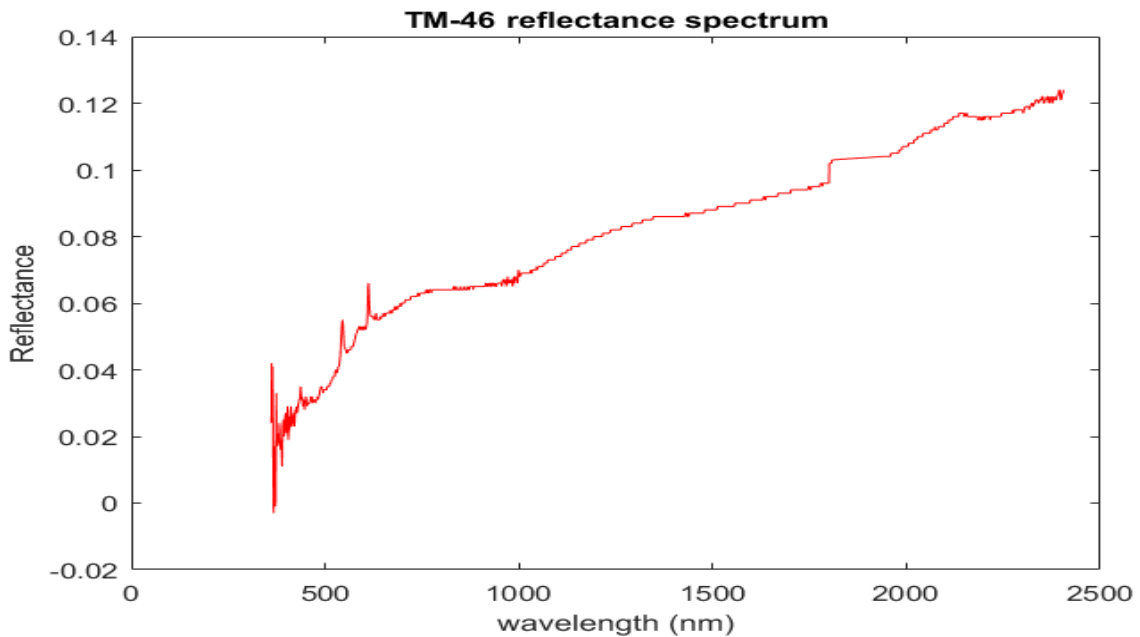*Figure 37: VS 2.2 reflectance spectrum taken in lab*

Figure 38: TM 46-reflectance spectrum taken in lab

As we can see in the images, each landmine has a specific reflectance spectrum. This proves the utility of hyperspectral imaging technique in landmine detection because by profiting from the spectral information in the hyperspectral images, we are able to detect the landmines and in addition to distinguish their type.

Another thing we can notice is that metal cased landmines like the TM46 antitank mine have an increasing reflectance value as the wavelength increases in the VNIR and SWIR domains. However, other plastic cased mines, like VS50 M411 and PMD6 have a decreasing value in the VNIR and SWIR ranges. In the next section, we will see how these reflectance spectra will change when landmines are planted in grass.

4.8.2. Reflectance spectra of landmines acquired in grass Field

In this part, we show the spectra of reflectance of the landmines when they were planted in grass field. This experiment was done at Lebanese university campus-Hadath in a sunny day. The weather was clear and sunny without clouds in the sky. Here we planted all mines in the field. In addition, we acquired the reflectance spectrum of the grass just to compare the signature with and without landmines.

Figure 39: AP mines planted in grass

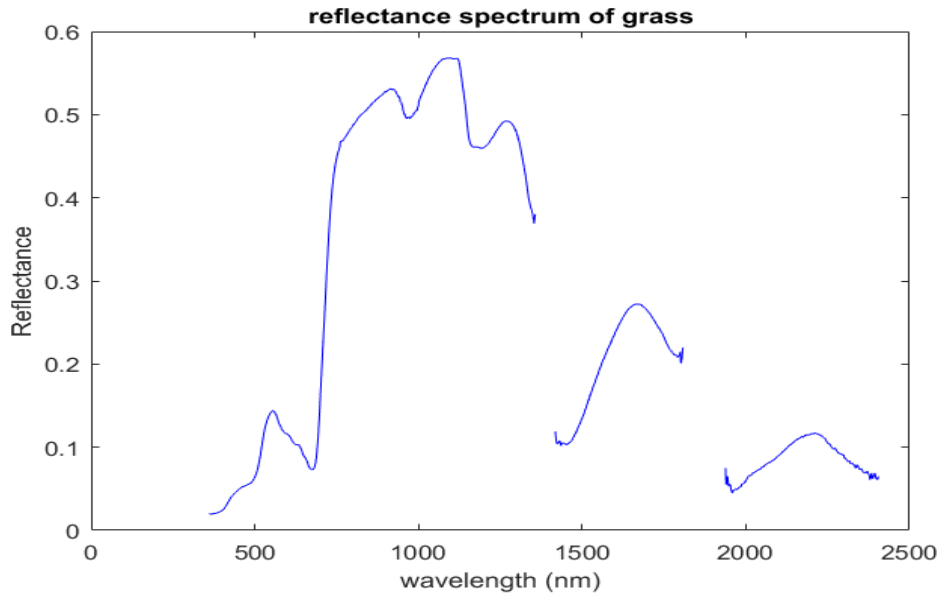The reflectance spectrum of the grass is as follows:

Figure 40: Grass reflectance spectrum

In this test, we removed the bands that corresponds to water absorption bands. In these bands, the data collected is too noisy. Just for example, the complete reflectance spectrum of the grass including the water absorption bands is as follows:
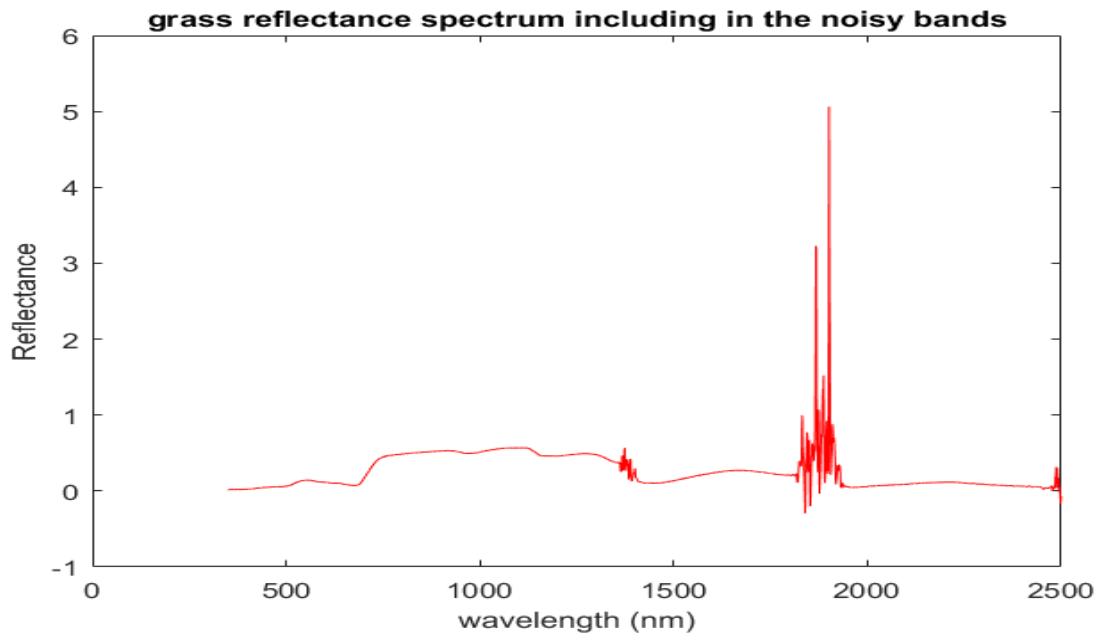

Figure 41: Grass reflectance spectrum including water absorption bands

It is clear that the reflectance spectrum contains some erroneous registrations as we see that the reflectance value in some bands is higher than one. This is not possible as at maximum an object can reflect the entire incident light (reflectance value =1). These erroneous values are registered in the wavelengths that correspond to water absorption bands. So the humidity in the air causes this error.

The reflectance spectrum of the landmines in the grass field is as follows:

Figure 42: PMN reflectance spectrum when covered by grass

Figure 43: VS50 reflectance spectrum when covered by grass

Figure 44: PMD 6 reflectance spectrum when covered by grass
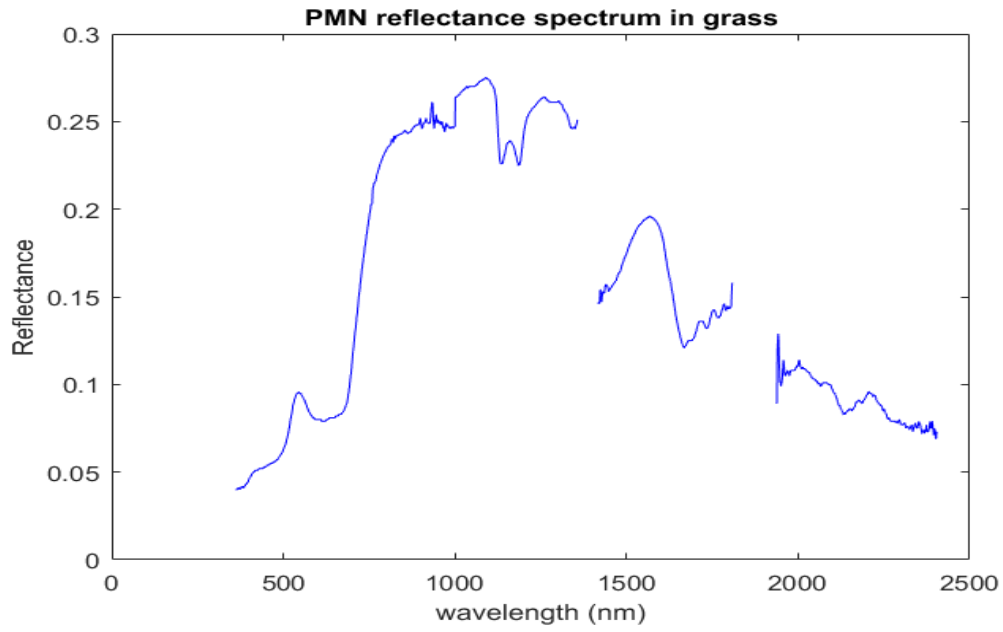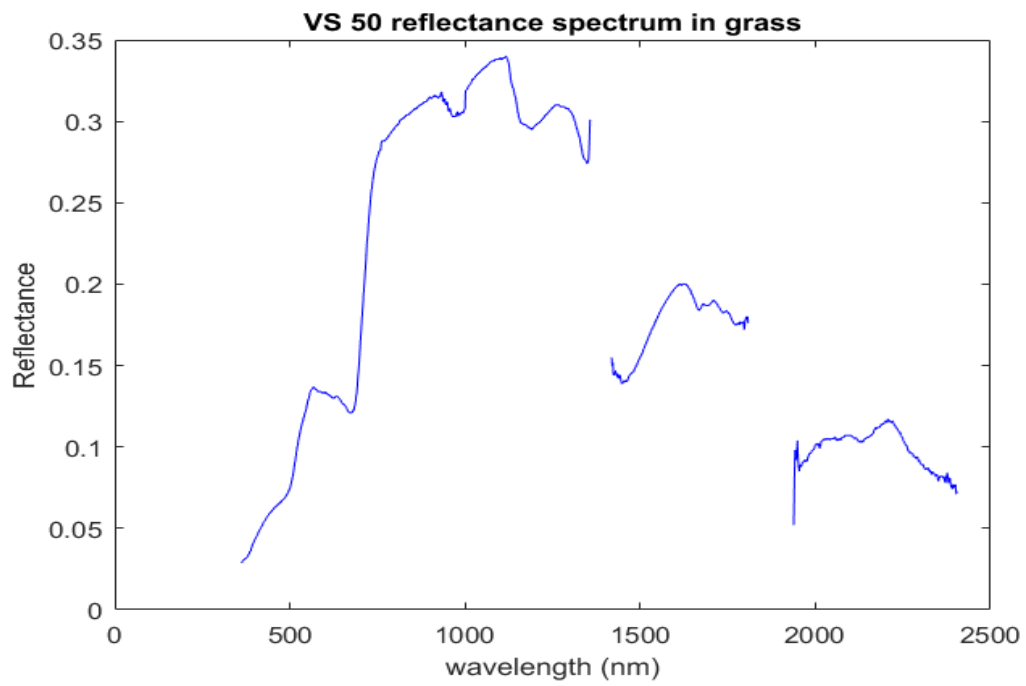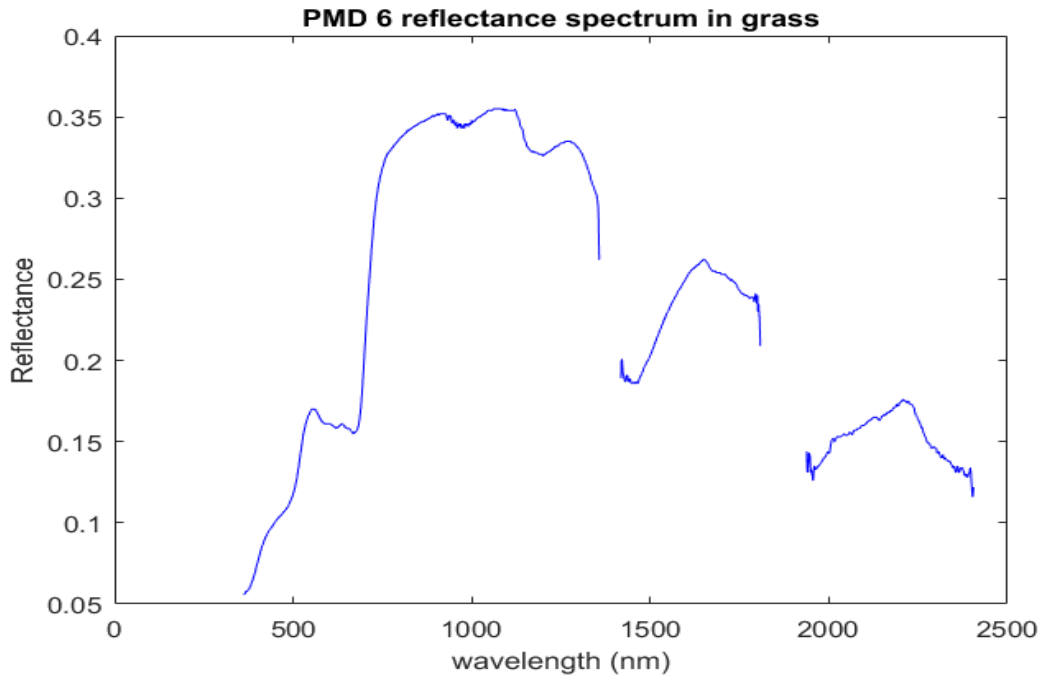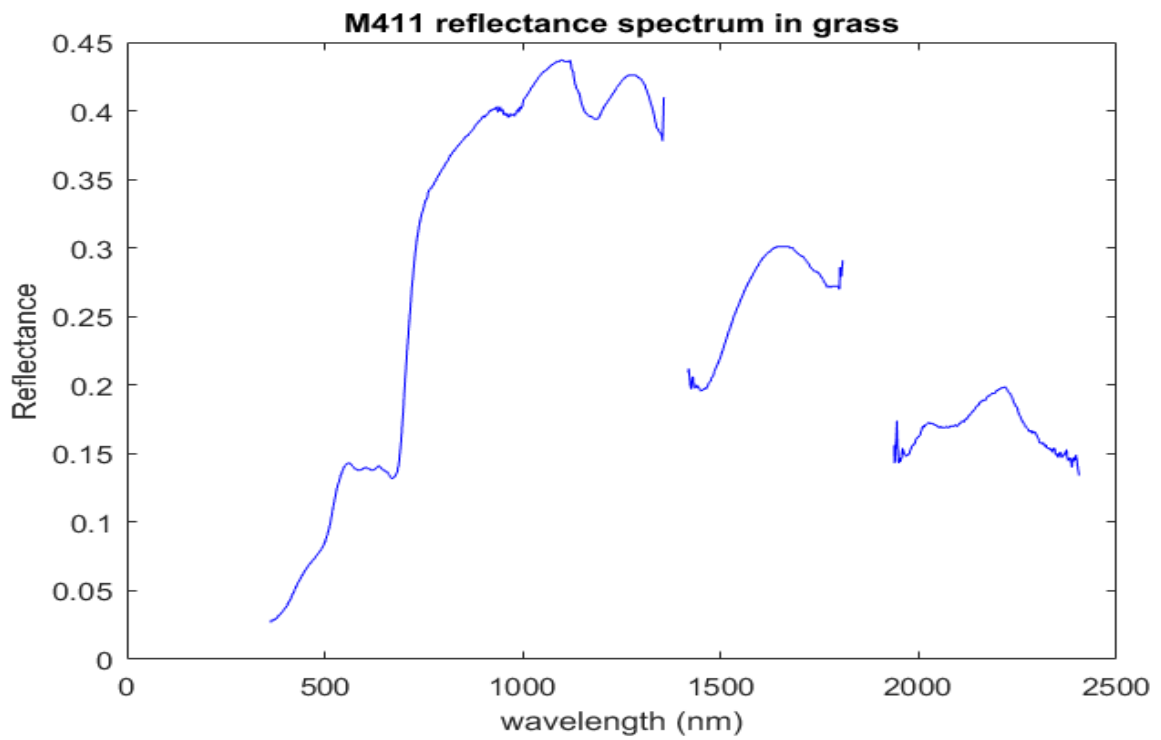

Figure 45: M411 reflectance spectrum when covered by grass
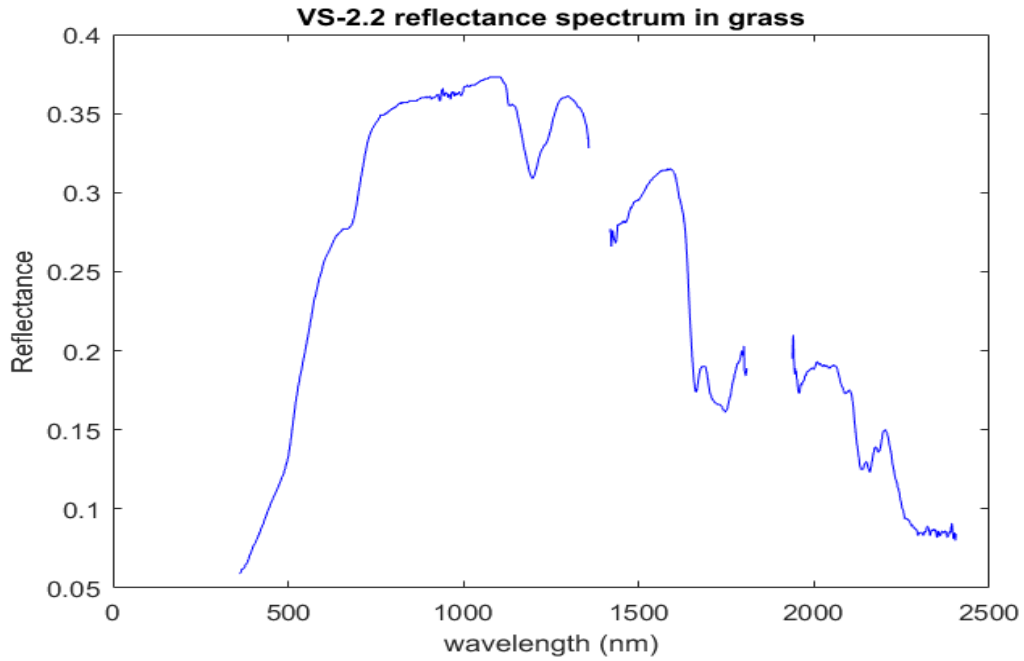
Figure 46: VS 2.2 reflectance spectrum when covered by grass
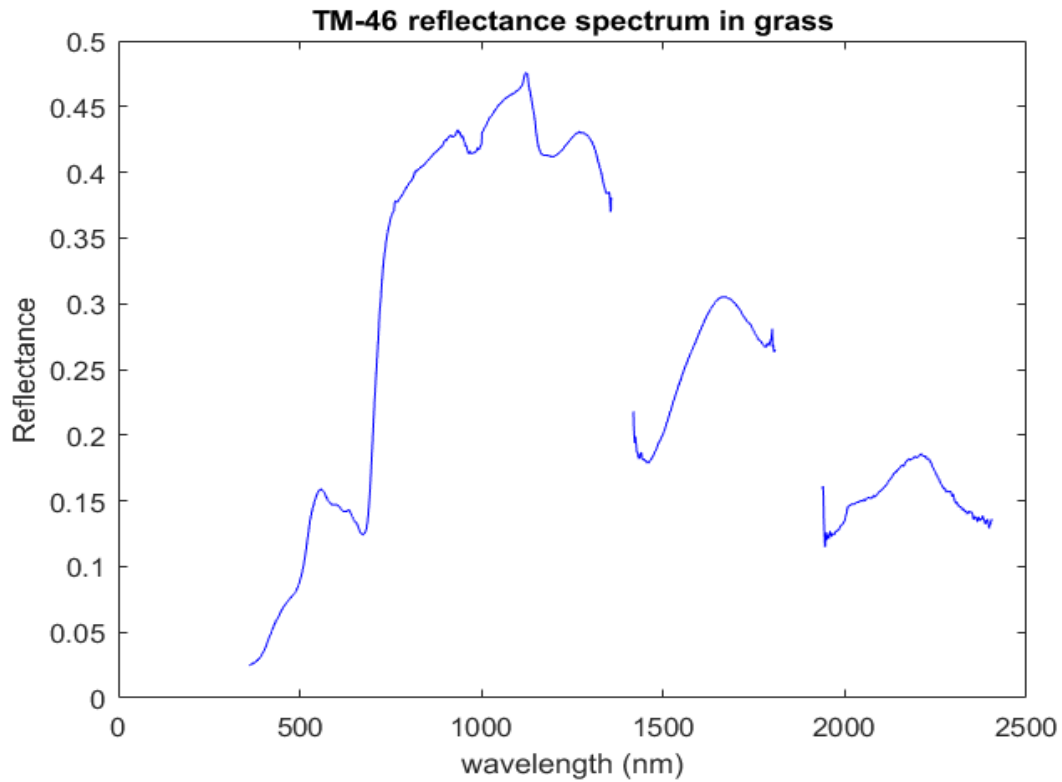
Figure 47: TM-46 reflectance spectrum when covered by grass

As we notice in the figures, when landmines are covered with grass, the reflectance spectrum changes and became more similar to grass. The maximum reflectance value sensed in case of

pure grass is 0.58. However, in case of landmine presence, the maximum achieved is lower than 0.5.

In the case of plastic mines, we notice that the reflectance values at high wavelength value (1500 nm- 2500 nm) are lower than the case of grass material and have similar shape to landmine (especially in case of PMN). However, in case of metallic antitank mine (TM-46), the reflectance values are a bit higher.

These are some key points that we noticed in this test. Many other details would help us to estimate the abundance of landmine in the sensed pixel.

Figure 48: Four AP mines exist in this scene. Could you localize them all?

4.8.3. Reflectance spectra of landmines acquired in soil Field

During the same day when we acquired the reflectance spectra in the grass field, we acquired the reflectance spectra of landmines in another field made of soil only and surrounded by trees of pines. Also this test was done at Lebanese University Campus in the same weather conditions.

Figure 49: Holding the device on my back, we acquired the spectra of the landmines after burying them in the soil

In this test, we acquired the reflectance spectrum of four anti-personnel mines. In the following some figure of the landmines buried in the soil:

Figure 50: Landmines buried in soil

The spectrum of soil without landmines is as follows:
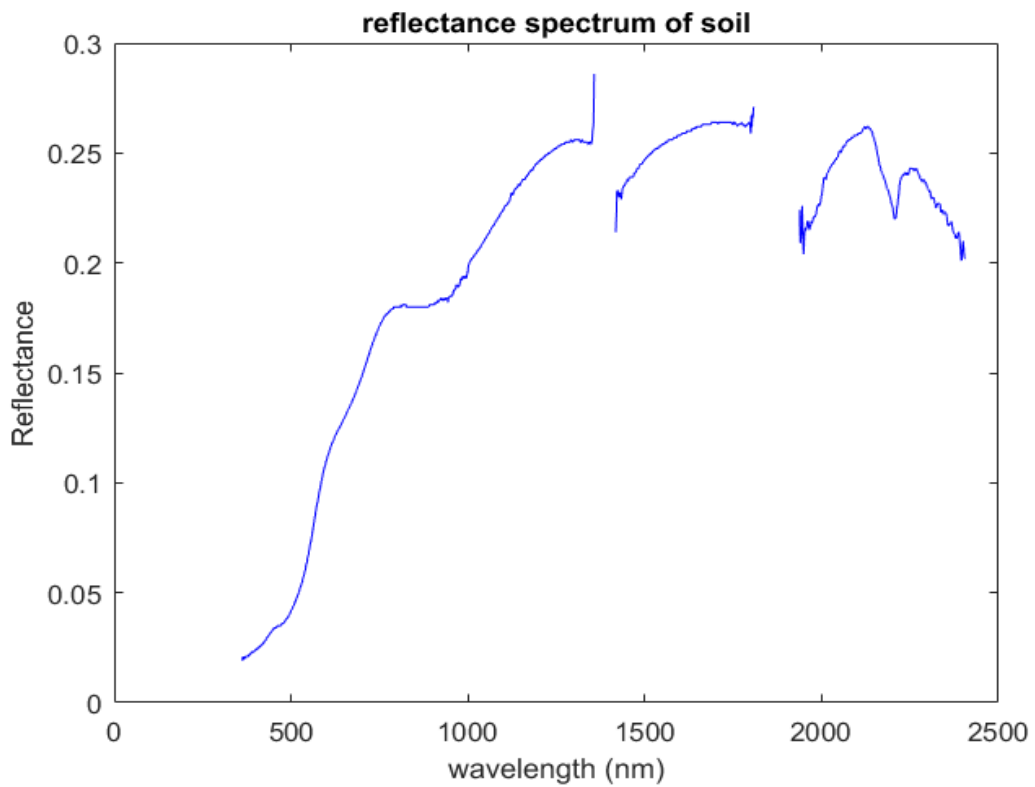
Figure 51: Untouched soil reflectance spectrum

The reflectance spectra of the landmines buried in soil are as follows:
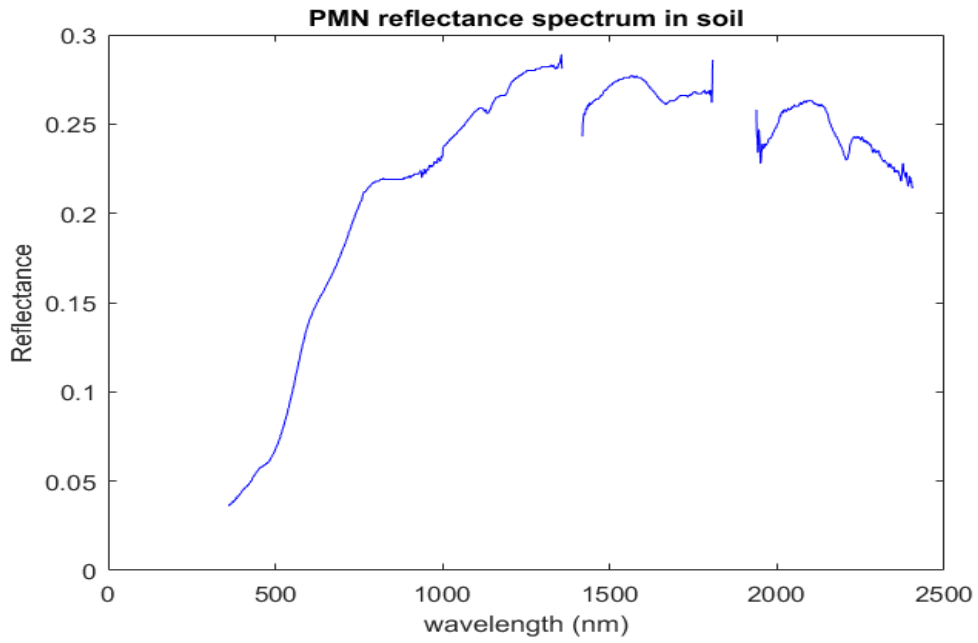
Figure 52: PMN reflectance spectrum when buried in soil
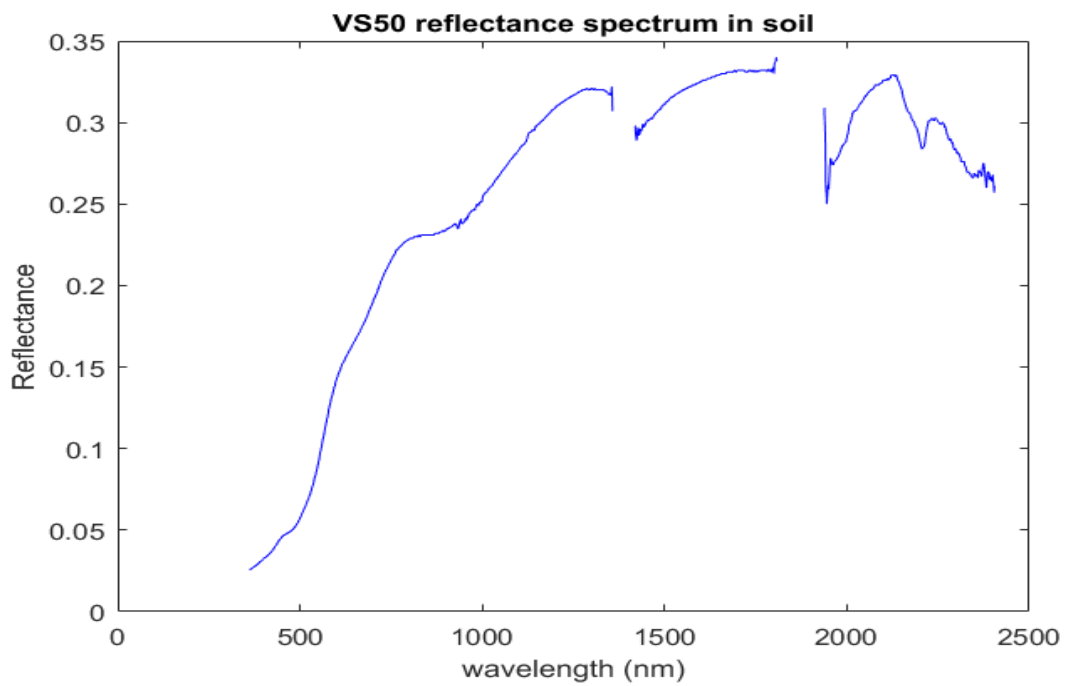
Figure 53: VS 50 reflectance spectrum when buried in soil
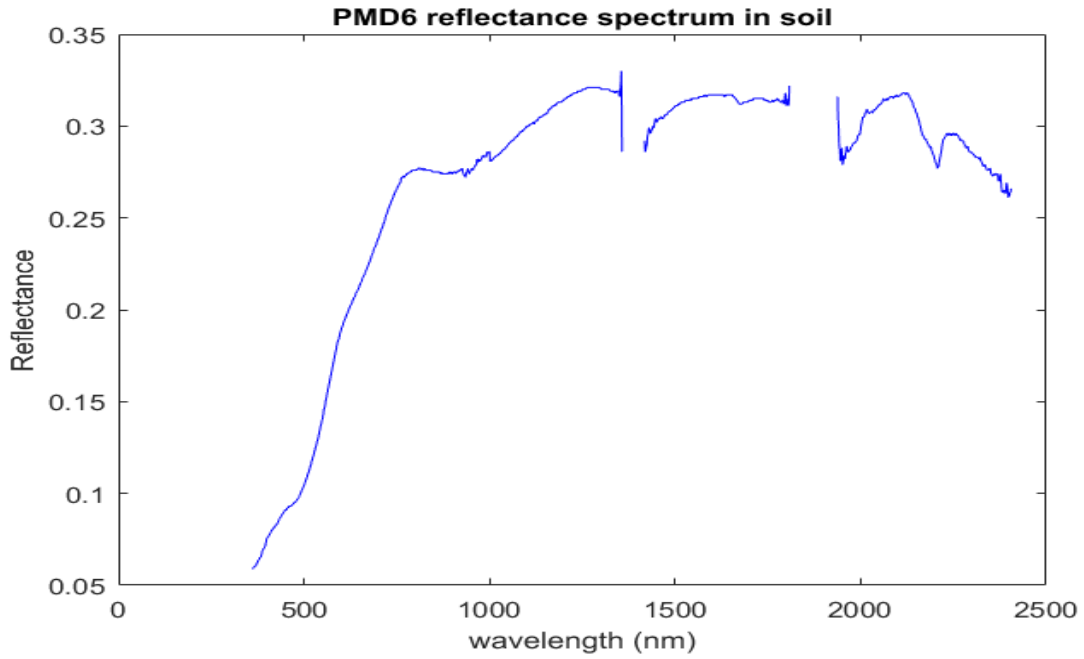
Figure 54: PMD 6 reflectance spectrum when buried in soil
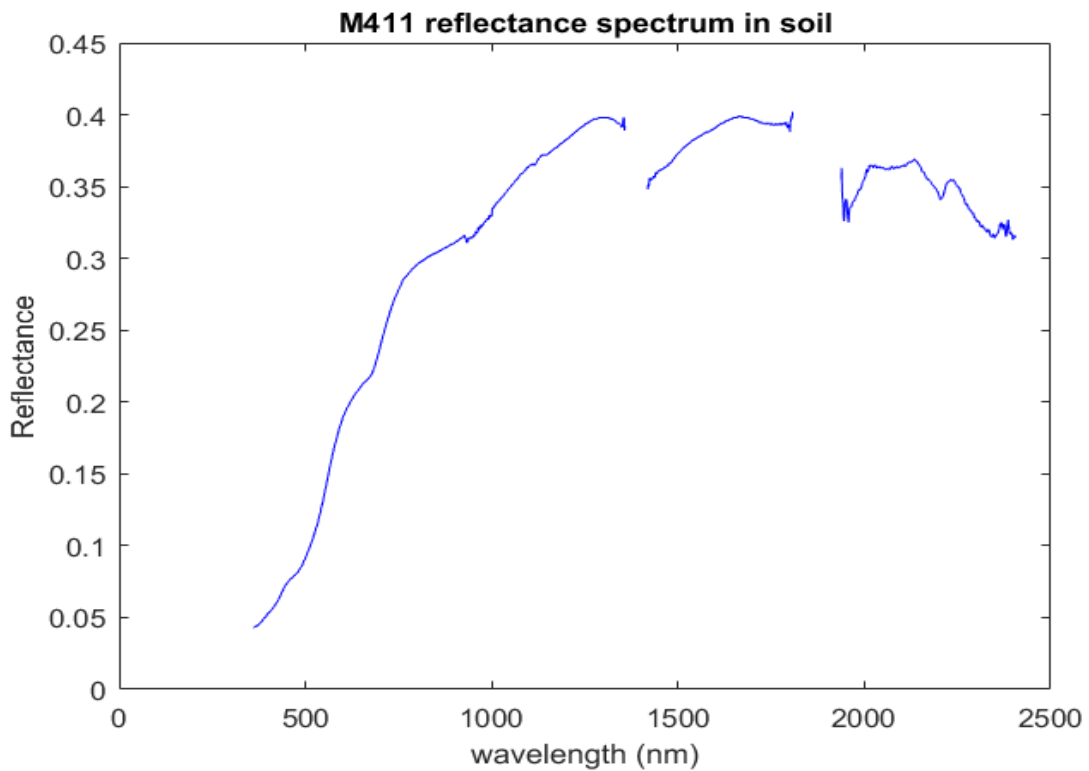
Figure 55: M411 reflectance spectrum when buried in soil

We see in these spectra, that once the mines are covered by soil, the reflectance spectrum will have an aspect very similar to the spectrum of inert soil without landmine. Just the small details

in the spectrum will help to distinguish the presence of landmine as untouched soil will have a spectral response different than returned or excavated soil.

In the visible domain, the spectral response is almost identical for all types of mines and is similar to the response of the soil. That is expected, as all mines look like soil to naked eye.

In case of M411, VS 50 and PMD 6 we arrived to maximum reflectance spectra of higher than 0.3 whilst in case of bare soil, the maximum is less than 0.3. This gives a sign of presence of another material other than soil and led us to suspect the presence of landmines.

4.8.4. Conclusions

In this field experiment, we collected the spectral reflectance of 6 different types of landmines in various background conditions. Some of these spectra are used in the experiment shown in chap. 4.6.

In real experiments, we are relying on the sun to acquire data. Sun do not produce light of same intensity at all wavelengths. Also, there are other artifacts that may affect the detection mainly the water absorption and CO_2 absorption bands. These artifacts cause the difference in spectral signatures of landmines when acquired in Lab or in another fields.

When the landmine is covered by another material like grass or soil, the spectral signature will change also. The changes will depend on the proportion of background material covering the mine. However, it has been shown that we still have some spectral characteristics that help in the detection of landmine.

The spectral response of landmines with plastic case have different shape than the reflectance of background material. This gives an advantage of hyperspectral imaging technique over the well-known metal detectors in the detection of plastic mines as nowadays most landmines are made of plastic that the metal detector is not able to detect.

Chapter Five

5. Conclusions and Future Work

The main contribution of this thesis is that we proved the applicability of hyperspectral imaging to detect surface laid mines. Landmines buried by soil or in grass are still detectable but proper classifiers must be used.

The problem of landmines is expanding worldwide. Although it is necessary to ban the use of landmines immediately, there is a need to find a new solution able to detect landmines of different types and shapes and is at the same time safe, fast and reliable. Hyperspectral imaging technology is a good candidate for this purpose. The mostly used technique until now is the metal detector thanks to its low cost. However, most of landmines nowadays are made of plastic, which made their detection using the metal detector harder. One of the advantage of hyperspectral imaging technique is that it detects the presence of landmines whatever the type of the case is. The hyperspectral imagers are too expensive, but when mounted on a UAV to scan minefields on large scale, its efficiency will be comparable to other techniques especially if the time of detection is considered in the comparison. It is expected that the price of hyperspectral cameras decreases as more companies fabricates this type of devices in addition to finding new technologies that makes the fabrication of optical devices cheaper.

Every material has its special spectral signature. Therefore, knowing the mine spectral curve, by comparison between the mine spectrum and the pixel spectrum, we can decide on the presence or the absence of the mine at that specific position.

It has been shown in the previous tests that using VNIR band, recently buried landmines could be detected. Also, the fusion of VNIR and SWIR could give better results. Landmine burying changes the thermal properties of the upper level of some type of soils. It also changes its surface reflectivity and stresses vegetation. Hence, buried landmines can be detected by measuring the change of reflectivity both between manipulated soil and background and between stressed and unstressed vegetation. Consequently, as anti-tank mine deployment is done by digging up a larger area of surface (soil and/or vegetation) and a larger volume of soil is disturbed, the possibility of detecting them is higher than with anti-personnel mines. MWIR and LWIR bands are also used to detect buried landmines. Even if SWIR and VNIR alone could detect soil disturbances due to buried mines, MWIR and LWIR can reduce the false alarm rate. However, the use of SWIR bands is more common since the majority of manufactured imagers operates in the VNIR and SWIR bands. After testing several hyperspectral imagers of different bands, it was found that imagers in LWIR bands have the potential to detect buried landmines with the use of proper algorithms. The algorithms could be supervised or unsupervised based on the data availability. Note that this does not eliminate the possibility to detect landmines with the use of other bands. However, proper algorithms and thresholds should be used for each case.

If we consider high spatial resolution images, which means the image has ground sample distance close to the size of landmine, the possibility to detect a landmine is higher as the reflectance spectrum of the pixel will result only from the reflectance of the mine, or at least the reflectance of the landmine will be present with a high abundance. In addition, military target detection could be achieved at subpixel level using hyperspectral images. This means that by acquiring images from high altitude, using UAV or aircrafts, fast target detection is possible even if the target constitutes a small part of the pixel.

In order to attain quasi real-time detection, all the processes involved, starting from geocorrection until classification, must be studied and organized so as to reduce the computational time. Since the detection performance will be possibly affected by some optimizations, a tradeoff between computational time and detection performance has to be achieved.

Several factors affect the reflectance signature obtained by the imager. Wind and rain are the main factors, but the effect of rain is the dominant one. In the case of buried landmines, rainfall decreases the reflected portion of the thermal energy and therefore the reflectance signal received. However, the shape of the signature remains the same. More rainfall will result in more reduction and therefore the reflected signal will be more and more similar to the background.

The use of PCA or other feature extraction method prior to classification do not always reduce the total computational time. Depending on the target detect algorithm used in the following step, reducing the dimension of the data may be effective or not. For example, the computational time have been reduced and the good detection performance have been preserved if we used PCA with ACE algorithm. However, the performance became worse when using similarity-based detection methods like SAM and SID.

The use of supervised detection methods is preferred over unsupervised detection techniques because usually higher FAR is obtained in case of unsupervised techniques as low frequency elements in the scene are marked as targets while they are not. However, supervised detection

techniques necessitates knowing the target reflectance spectra and sometimes the reflectance spectrum of the background materials prior to detection. This kind of information is not always present.

There are different types of supervised detection techniques. Some may be less tolerant to the spectral variability or the abundance fraction of the target as in case of ACE, CEM and MF. Other techniques will not be able to detect the target if the spectral signature is slightly different from the reference spectra as in the case of SAM detector.

To detect several targets in one scan, we may run single target detection algorithm several times, each run to detect one target. However, this may be time consuming and not effective for real time detection. Other target detection algorithms supports the detection of several targets simultaneously.

After several experiments, we proved the advantage of using neural networks in landmine detection using hyperspectral imaging. Even if the abundance of landmines was about 0.6, an RBF neural network trained with few background endmember data and target spectra was able to detect the landmines, identify them and estimate their abundance. Also MLP neural networks were examined to detect the spectra of landmines in hyperspectral scenes. The results are obtained in a very fast computational time using this type of NN, but we were not able to detect all landmines with 0 FAR. So MLP NN have a good potential to be used in real-time detection but proper preparation of training data and network parameters calculation must be conducted first in a future work.

In the field experiment, we collected valuable data of landmines reflectance spectrum in different environment. We acquired the reflectance spectrum of 4 types of AP mines and 2 types of AT mines. The experiment shows how much the reflectance spectrum change when taken in lab conditions and in field situation where too many factors affects the registration. The main factors that changes are the sun emission spectrum that is not uniform in all wavelengths, the water vapor and CO_2 in the air that absorb light in some specific bands, in addition to other artifacts and noise.

In a future work, a scan of real minefield using hyperspectral imager mounted on an UAV must be conducted in order to validate the algorithms proposed and developed here in real case scenario.

In addition, MLP training must be optimized to obtain 0 FAR.

Also, we would collect data in new background scenarios to study the possibility to detect landmines in situations other than we can find in Lebanon like in desert.

References

[1] Landmine monitor report 2015 http://www.the-monitor.org/media/2152583/Landmine-Monitor-2015_finalpdf.pdf

[2] UNICEF, "Children and Landmines: A Deadly Legacy", New York Sep 2013 https://www.unicef.org/french/protection/files/Landmines_Factsheet_04_LTR_HD.pdf

[3] N. Cumming-Bruce, K.Harrison, M.Loddo, L. Pinches, S. Casey-Maslen, "CLEARING CLUSTER MUNITION REMNANTS", Geneve 5-7 Septembet 2016. http://www.mineactionreview.org/assets/downloads/Clearing_Cluster_Munition_Remnants_2016_WEB.pdf

[4] B. Ghali, "The landmine crisis: a humanitarian disaster. Foreign Affairs", Oct 1994 https://www.foreignaffairs.com/articles/1994-09-01/land-mine-crisis-humanitarian-disaster

[5] Landmine Monitor Core Group," Towards a Mine Free World: Executive Summary", Feb 2016

[6] A.A Berhe, "The contribution of landmines to land degradation." *Land Degradation & Development* 18, no. 1: 1-15. California Aug 2006 http://eps.berkeley.edu/~aaberhe/Berhe%202007-%20LM%20and%20LD.pdf

[7] N. Anderson, S. Paredes, "Social cost of land mines in four countries: Afghanistan, Bosnia, Cambodia, and Mozambique", British Medical Journal ,British Sep 2016

[8] A.A. Berhe, "Landmines and land degradation: a regional political ecology perspective on the impacts of landmines on environment and development in the developing world." *Michigan State University: East Lansing, MI* (2000).

[9] M.A. Buenker, "Landmines: A threat to wildlife and sustainability", World Conservation. 1: 19–20, Jan 2000

[10] Global Security Fact Sheets, "Landmines", Jul 7, 2011

[11] R.Keeley, "Understanding Landmines and Mine Action. MIT", Massachusetts Institute of Technology (US), Feb 2003

[12] United Nations Mine Action Service (UNMAS), "Glossary of mine action terms, definitions and abbreviations ", New York Jan 2003

[13] J. MacDonald, J.R. Lockwood, J. McFee, T. ALtshuler, T. Broach, L. Carin,R. Harmon, C. Rappaport, W. Scott,R. Weaver," Alternatives for Landmine Detection", Pittsburg, RAND Science and Technology Policy Institute, Online book 2003, page:6- 47.

[14] M.G.Kale, V. R. Ratnaparkhe, A.S.Bhalchandra. "Sensors For Landmine Detection And Techniques: A Review", International Journal of Engineering Research & Technology (IJERT)Vol. 2 Issue 1, January- 2013 p:2-4.

[15] C. P. Gooneratne, S. C. Mukhopahyay and G. Sen Gupta. "A Review of Sensing Technologies for Landmine Detection: Unmanned Vehicle Based Approach" , Institute of Information Sciences and Technology, Massey University, Palmerston North, New Zealand December 2004. p:401-407

[16] M. Carrasco, D. Mery, L. Robledo. "A survey of land mine detection technology" International Journal of Remote Sensing Vol. 30, No. 9, 10 May 2009, p:2400-2404.

[17] I. Makki, R. Younes, C. Francis, T. Bianchi, & M. Zucchetti (2017). "A survey of landmine detection using hyperspectral imaging", ISPRS Journal of Photogrammetry and Remote Sensing, 124, 40-53.

[18] J. E. McFee ; K. L. Russell and M. R. Ito, "Detection of surface-laid minefields using a hierarchical image processing algorithm", Proc. SPIE 1567, Applications of Digital Image Processing XIV, 42 (December 1, 1991); doi:10.1117/12.50802

[19] J. E. McFee, H. T. Ripley, R. Buxton, A. M. Thriscutt, "Preliminary study of detection of buried landmines using a programmable hyperspectral imager", Proc. SPIE 2765, Detection and Remediation Technologies for Mines and Minelike Targets, 476 (May 31, 1996); doi:10.1117/12.241250

[20] J. E. McFee and H. T. Ripley, "Detection of buried land mines using a CASI hyperspectral imager", Proc. SPIE 3079, Detection and Remediation Technologies for Mines and Minelike Targets II, 738 (July 22, 1997)

[21] S. B. Achal ; J. E. McFee and C. D. Anger, "Identification of surface-laid mines by classification of compact airborne spectrographic imager (CASI) reflectance spectra", Proc. SPIE 2496, Detection Technologies for Mines and Minelike Targets, 324 (June 20, 1995);

[22] T. Skauli, and I. Kåsen. "The effect of spatial resolution on hyperspectral target detection performance." In European Symposium on Optics and Photonics for Defence and Security, pp. 59870V-59870V. International Society for Optics and Photonics, 2005.

[23] S. B. Achal; C. D. Anger; J. E. McFee and R. W. Herring "Detection of surface-laid mine fields in VNIR hyperspectral high-spatial-resolution data", Proc. SPIE 3710, Detection and Remediation Technologies for Mines and Minelike Targets IV, 808 (August 2, 1999)

[24] T. Ivanco, S. B. Achal, C. D. Anger, and J. E. McFee, "Casi Real-Time Surface-Laid Mine Detection System", Proc. SPIE 4394, Detection and Remediation Technologies for Mines and Minelike Targets VI, 365 (October 18, 2001)

[25] T. Ivanco, S. Achal, J. E. McFee, C. Anger, J. Young, "Real-time airborne hyperspectral imaging of landmines", Proc. SPIE 6553, Detection and Remediation Technologies for Mines and Minelike Targets XII, 655315 (April 26, 2007); doi:10.1117/12.720442

[26] J. E. McFee, S. Achal, T. Ivanco and C. Anger, "A short wave infrared hyperspectral imager for landmine detection", Proc. SPIE 5794, Detection and Remediation Technologies for Mines and Minelike Targets X, 56 (July 08, 2005);

[27] S. Achal, J. E. McFee, T. Ivanco and C. Anger, "A thermal infrared hyperspectral imager (tasi) for buried landmine detection", Proc. SPIE Conference on Detection and Remediation Technologies for Mines and Mine-like Targets XII, Vol. 6553, Orlando, FL, USA, 9-13 April, 2007, pp.655316-1-655316-11.

[28] J. E. McFee, S. B. Achal, A. U. Diaz and A. A. Faust, "Comparison of broad-band and hyperspectral thermal infrared imaging of buried threat objects", Proc. SPIE Conference on Detection and Sensing of Mines, Explosive Objects and Obscured Targets XVIII, Volume 8709, Baltimore, MD, USA, 29 April - 03 May 2013.

[29] A. A. Faust, J. E. Mcfee, R. H. Chesney, K. L. Russell, Y. Das, "Canadian Teleoperated landmine detection systems part I", International Journal Of Systems Science 36(9):511-528 · JULY 2005

[30] J. E. McFee, K.L. Russell, R. H. Chesney, A. A. Faust, Y. Das, "The Canadian forces ILDS- A military fielded multi-sensor, vehicle mounted , teleoperated landmine detection system", Detection and Remediation Technologies for Mines and Minelike Targets XI, Proceeding of Spie (2006)

[31] A.A. Faust, R.H. Chesney, Y. Das, J.E. McFee, K.l Russell, "Canadian teleoperated landmine detection systems Part II: Anti personal landmine detection", International journal of Systems Science, vol.36, no.9, 15 July 2005, p 529-543.

[32] J. E. McFee ; C. Anger ; S. Achal and T. Ivanco, "Landmine detection using passive hyperspectral imaging", Proc. SPIE 6554, Chemical and Biological Sensing VIII, 655404 (April 26, 2007)

[33] J. E. McFee and S. Achal, "Infrared and hyperspectral systems", in Subsurface Sensing, Section 7.6, Editors: A.S.Turk, A.K.Hocaoglu, A.A.Vertiy, ISBN 978-0-470-13388-0, John Wiley and Sons, Wiley Series in Microwave and Optical Engineering, New York, Series Volume 197, August 2011, pp.465-483.

[34] J. E. McFee, S. Achal, A. A. Faust, E. Puckrin, A. House, D. Reynolds, W. McDougall and A. Asquini, "Detection and dispersal of explosives by ants", Proc. SPIE Conference on Detection and Sensing of Mines, Explosive Objects and Obscured Targets XIV, Vol. 7303, Orlando, FL, USA, 13-17 April, pp.730302, 2009.

[35] S. Achal, J. E. McFee and J. Howse, "Gradual dispersal of explosives by ants and its possible implication for future landmine production", Proc. 7th International Symposium on Humanitarian Demining 2010, Croatian Mine Action Center (CROMAC), Sibenik, Croatia, 27-29 April 2010, paper available on line at http://www.ctro.hr/universalis/148/dokument/bookofpapers_373441161.pdf, page 60.

[36] J. E. McFee, A.A. Faust, Y.Das, K.L. Russell, "Final report Shield ARP 12 rl" – Optical imaging of explosive threats, August 2010.

[37] J.R. Simard, P. Mathieu, G. R. Fournier, V. Larochelle, and Stephen K. Babey. "Range-gated intensified spectrographic imager: an instrument for active hyperspectral imaging." In AeroSense 2000, pp. 180-191. International Society for Optics and Photonics, 2000.

[38] J.-P Ardouin, J. Levesque and T.A. Rea, "Demonstration of Hyperspectral Image Exploitation for Military Applications", Information Fusion, 2007 10th International Conference on 9-12 July 2007

[39] L. B. Wolff ; D. A. Socolinsky ; C. K. Eveland ; J. I. Yalcin and J. H. Holloway, Jr. "Image fusion of shortwave infrared (SWIR) and visible for detection of mines, obstacles, and camouflage", Proc. SPIE 5089, Detection and Remediation Technologies for Mines and Minelike Targets VIII, 1298 (September 15, 2003).

[40] E.M. Winter, M. J. Schlangen, A.P. Bowman, M. R. Carter, C. L. Bennett, D. J. Fields, W. D. Aimonetti et al. "Experiments to support the development of techniques for hyperspectral mine detection." In Aerospace/Defense Sensing and Controls, pp. 139-148. International Society for Optics and Photonics, 1996.

[41] A. P. Bowman, E. M. Winter, A. D. Stocker, and P. G. Lucey. "Hyperspectral infrared techniques for buried landmine detection." In Detection of Abandoned Land Mines, 1998. Second International Conference on the (Conf. Publ. No. 458), pp. 129-133. IET, 1998.

[42] A. M. Smith, A.C. Kenton, R. Horvath, L. S. Nooden, J. Michael, J. A. Wright, J. L. Mars et al. "Hyperspectral mine detection phenomenology program." In AeroSense'99, pp. 819-829. International Society for Optics and Photonics, 1999.

[43] A.C. Kenton, C. R. Schwartz, R. Horvath, J. N. Cederquist, L. S. Nooden, D. R. Twede, J. A. Nunez, J. A. Wright, J. W. Salisbury, and K. Montavon. "Detection of land mines with hyperspectral data." In AeroSense'99, pp. 917-928. International Society for Optics and Photonics, 1999.

[44] M. T. Eismann, C. R. Schwartz, J. N. Cederquist, J.A. Hackwell, and R. J. Huppi. "Comparison of infrared imaging hyperspectral sensors for military target detection applications." In SPIE's 1996 International Symposium on Optical Science, Engineering, and Instrumentation, pp. 91-101. International Society for Optics and Photonics, 1996.

[45] E. M. Winter, M. A. Miller, C. G. Simi, A. B. Hill, T. J. Williams, D. Hampton, M. Wood, J. Zadnick, and M. D. Sviland. "Mine detection experiments using hyperspectral sensors." In Proceedings of SPIE, vol. 5415, pp. 1035-1041. 2004.

[46] A. M Thomas., and J. Michael Cathcart. "Applications of grid pattern matching to the detection of buried landmines." IEEE Transactions on Geoscience and Remote Sensing 48, no. 9 (2010): 3465-3470.

[47] N. Playle, "Detection of landmines using hyperspectral imaging." In Defense and Security Symposium, pp. 62170A-62170A. International Society for Optics and Photonics, 2006.

[48] G. Suganthi, R. Korah, "Discrimination of Mine-Like Objects in Infrared Images Using Artificial Neural Network", Indian Journal Of Applied Research, Volume : 4 Issue : 12 , India, p 206-208, Dec 2014

[49] J.S. Groot, Y.H.L. Janssen, "Remote Land Mine(Field) Detection, an overview of techniques", TNO Physics and Electronics Laboratory ,September 7, 1994.

[50] N. Milisavljević and I. Bloch. "How can data fusion help humanitarian mine action?." International Journal of Image and Data Fusion 1, no. 2 (2010): 177-191.

[51] D. Letalick, I. Renhorn, O. Steinvall, "Multi-Optical Mine detection System (MOMS) final report", FOI Swedish Defence Research Agency, ISSN 1650-1942, December 2009.

[52] M.-A. Gagnon, P. Lagueux, J.-P. Gagnon, S. Savary, P. Tremblay, V. Farley, É. Guyot and M. Chamberland. "Airborne thermal infrared hyperspectral imaging of buried objects." In SPIE Security+ Defence, pp. 96490T-96490T. International Society for Optics and Photonics, 2015.

[53] J. M Bioucas-Dias, A. Plaza, G. Camps-Valls, P. Scheunders, N. Nasrabadi, and J. Chanussot. "Hyperspectral remote sensing data analysis and future challenges." IEEE Geoscience and Remote Sensing Magazine 1, no. 2 (2013): 6-36.

[54] V. A. Kotkar , S. S. Gharde, "Review Of Various Image Contrast Enhancement Techniques, International Journal of Innovative Research in Science, Engineering and Technology Vol. 2, Issue 7, July 2013.

[55] C. P.Lee, "Mine detection techniques using multiple sensors." The Project in Lieu of Thesis, Electrical and Computer Engineering The University of Tennessee at Knoxville (2000).

[56] N. Sengee, A. Sengee and H.K. Choi, "Image Contrast Enhancement using Bi-Histogram Equalization with Neighborhood Metrics" IEEE Transactions on Consumer Electronics, Vol 56, No.4. November 2010.

[57] Y. Wang, Q. Chen, and B. Zhang. "Image enhancement based on equal area dualistic sub-image histogram equalization method." IEEE Transactions on Consumer Electronics 45, no. 1 (1999): 68-75.

[58] S. Der Chen and R. Ramli, "Minimum Mean Brightness Error Bi-Histogram Equalization in Contrast Enhancement", IEEE Transactions on Consumer Electronics, Vol. 49, No. 4, pp.1310-1319, 2003.

[59] D. Chen and R. Ramli, "Contrast Enhancement Using Recursive Mean-Separate Histogram Equalization for Scalable Brightness Preservation", IEEE Transactions on Consumer Electronics, Vol. 49, No. 4, pp.1301-1309, 2003.

[60] D. Menotti, L. Najman, J. Facon and A. Araujo, "Multi-Histogram Equalization Methods for Contrast Enhancement and Brightness Preserving", IEEE Transactions on Consumer Electronics, Vol. 53, No. 3, pp.1186-1194, 2007.

[61] H. Ibrahim and N. S. P. Kong. "Brightness preserving dynamic histogram equalization for image contrast enhancement." Consumer Electronics, IEEE Transactions on 53, no. 4 (2007): 1752-1758.

[62] M. Kim and M. G. Chung. "Recursively separated and weighted histogram equalization for brightness preservation and contrast enhancement." Consumer Electronics, IEEE Transactions on 54, no. 3 (2008): 1389-1397.

[63] U.K. Sharma, K. Umesh and K. Kumawat. "Review Of Histogram Based Image Contrast Enhancement Techniques. International Journal of Research in Engineering & Technology ISSN(E): 2321-8843; ISSN(P): 2347-4599 Vol. 3, Issue 2, Feb 2015, 65-76

[64] J-M Gaucel, M. Guillaume and S. Bourennane. "Adaptive-3D-Wiener for hyperspectral image restoration: Influence on detection strategy." Signal Processing Conference, 2006 14th European. IEEE, 2006.

[65] Filtrage adaptatif: théorie et algorithmes. Hermes Science, 2005.

[66] N. Renard, S. Bourennane and J. Blanc-Talon. "Multiway filtering applied on hyperspectral images." Advanced Concepts for Intelligent Vision Systems. Springer Berlin Heidelberg, 2006.

[67] P.M. Mather and Magaly Koch. "Computer processing of remotely-sensed images: an introduction". John Wiley & Sons, 2011.

[68] G. Noyel, J. Angulo, and D. Jeulin. "Morphological segmentation of hyperspectral images." Image Anal. Stereol 26, no. 3 (2007): 101-109.

[69] L. Kaufman, and P. J. Rousseeuw. Finding groups in data: an introduction to cluster analysis. Vol. 344. John Wiley & Sons, 2009.

[70] J. P. Benzecri, 1973." L'analyse de données 2, Dunod (1973).

[71] J.M. Beaulieu, and M. Goldberg. "Hierarchy in picture segmentation: A stepwise optimization approach." Pattern Analysis and Machine Intelligence, IEEE Transactions on 11.2 (1989): 150-163.

[72] J. C Tilton. "Image segmentation by region growing and spectral clustering with natural convergence criterion." International geoscience and remote sensing symposium. Vol. 4. Institute Of Electrical & Electronicsengineers, Inc (Ieee), 1998.

[73] J.C. Tilton, "Split-remerge method for eliminating processing window artifacts in recursive hierarchical segmentation." U.S. Patent No. 7,697,759. 13 Apr. 2010.

[74] C. Rodarmel and J. Shan. "Principal component analysis for hyperspectral image classification." Surveying and Land Information Science 62.2 (2002): 115.

[75] J. Ye and S. Ji. "Discriminant analysis for dimensionality reduction: An overview of recent developments." Biometrics: Theory, Methods, and Applications. Wiley-IEEE Press, New York (2010).

[76] K. Fukunaga. "Introduction to statistical pattern recognition." Academic Press Professional, Inc., San Diego, CA, USA, 2nd edition, 1990.

[77] P.-H. Hsu, "Feature extraction of hyperspectral images using wavelet and matching pursuit." ISPRS Journal of Photogrammetry and Remote Sensing 62, no. 2 (2007): 78-92.

[78] P. Howland, M. Jeon, and H. Park. Structure preserving dimension reduction for clustered text data based on the generalized singular value decomposition. SIAM Journal on Matrix Analysis and Applications, 25(1):165–179, 2003.

[79] J. Khoder, R. Younes, H. Obeid, and M. Khalil. "Dimension Reduction of Hyperspectral Image with Rare Event Preserving." In Iberian Conference on Pattern Recognition and Image Analysis, pp. 621-629. Springer, Cham, 2015.

[80] J. Khoder, R. Younes, and F. Ben Ouezdou. "Potential of hybridization methods to reducing the dimensionality for multispectral biological images." In Engineering in Medicine and Biology Society (EMBC), 2013 35th Annual International Conference of the IEEE, pp. 6458-6461. IEEE, 2013.

[81] J. Khoder, R. Younes, and F. Ben Ouezdou. "Similarity of dimensionality reduction methods applied on artificial hyperspectral images." In Proceedings of the International Conference on Image Processing, Computer Vision, and Pattern Recognition (IPCV), p. 1. The Steering Committee of The World Congress in Computer Science, Computer Engineering and Applied Computing (WorldComp), 2012.

[82] R. Ablin, and C. H. Sulochana. "A survey of hyperspectral image classification in remote sensing." International Journal of Advanced Research in Computer and Communication Engineering 2.8 (2013): 2986-3000.

[83] V. N. Vapnick, Statistical Learning Theory. John Wiley and Sons Inc.,1998.

[84] J. A. Gualtieri and R. F. Cromp, "Support vector machines for hyperspectral remote sensing classification," in Proceedings of the SPIE, vol.3584, 1999, pp. 221–232.].

[85] G. Mercier and M. Lennon. "Support vector machines for hyperspectral image classification with spectral-based kernels." Geoscience and Remote Sensing Symposium, 2003. IGARSS'03. Proceedings. 2003 IEEE International. Vol. 1. IEEE, 2003.

[86] P.-N. Tan, M. Steinbach and V. Kumar, "Cluster Analysis: Basic Concepts and Algorithms", Chapter 8 in Introduction to Data Mining, Addison-Wesley, 2006, 487-567.

[87] J.C. Harsanyi and C.-I. Chang. "Hyperspectral image classification and dimensionality reduction: an orthogonal subspace projection approach." Geoscience and Remote Sensing, IEEE Transactions on 32.4 (1994): 779-785.

[88] J. Broadwater, and R. Chellappa. "Hybrid detectors for subpixel targets." IEEE transactions on pattern analysis and machine intelligence 29, no. 11 (2007)

[89] D. Manolakis, E. Truslow, M. Pieper, T. Cooley, and M. Brueggeman. "Detection algorithms in hyperspectral imaging systems: An overview of practical algorithms." IEEE Signal Processing Magazine 31, no. 1 (2014): 24-33.

[90] R.O. Duda, P. E. Hart and D. G. Stork. Pattern classification. John Wiley & Sons, 2012.

[91] H. Ren, Q. Du, C.-I. Chang, and J. O. Jensen. "Comparison between constrained energy minimization based approaches for hyperspectral imagery." In Advances in Techniques for Analysis of Remotely Sensed Data, 2003 IEEE Workshop on, pp. 244-248. IEEE, 2003.

[92] O.L. Frost, "An algorithm for linearly constrained adaptive array processing." Proceedings of the IEEE 60, no. 8 (1972): 926-935.

[93] L. Wang, and C. Zhao. Hyperspectral Image Processing. Springer, 2015, p236.

[94] D.C. Heinz, "Fully constrained least squares linear spectral mixture analysis method for material quantification in hyperspectral imagery." IEEE transactions on geoscience and remote sensing 39, no. 3 (2001): 529-545.

[95] C.-I Chang,. "Spectral information divergence for hyperspectral image analysis." In Geoscience and Remote Sensing Symposium, 1999. IGARSS'99 Proceedings. IEEE 1999 International, vol. 1, pp. 509-511. IEEE, 1999.

[96] T. Wang, Bo Du, and L. Zhang. "A kernel-based target-constrained interference-minimized filter for hyperspectral sub-pixel target detection." IEEE journal of selected topics in applied earth observations and remote sensing 6, no. 2 (2013): 626-637.

[97] A. Ertürk, D. Çeşmeci, M. K. Güllü, D. Gerçek, and S. Ertürk. "Endmember extraction guided by anomalies and homogeneous regions for hyperspectral images." IEEE Journal of Selected Topics in Applied Earth Observations and Remote Sensing 7, no. 8 (2014): 3630-3639.

[98] M. Axelsson, O. Friman, T.V. Haavardsholm, and I. Renhorn. "Target detection in hyperspectral imagery using forward modeling and in-scene information." ISPRS Journal of Photogrammetry and Remote Sensing 119 (2016): 124-134.

[99] Y. Zhang, Bo Du, and L. Zhang. "A sparse representation-based binary hypothesis model for target detection in hyperspectral images." IEEE Transactions on Geoscience and Remote Sensing 53.3 (2015): 1346-1354.

[100] R.M. Willett, M. F. Duarte, M. A. Davenport, and R. G. Baraniuk. "Sparsity and structure in hyperspectral imaging: Sensing, reconstruction, and target detection." IEEE signal processing magazine 31, no. 1 (2014): 116-126.

[101] O. Ahmad, C. Collet, and F. Salzenstein. "Spatio-spectral Gaussian random field modeling approach for target detection on hyperspectral data obtained in very low SNR." 2015 IEEE International Conference in Image Processing (ICIP), pp. 2090-2094. IEEE, 2015.

[102] I. Makki, R. Younes, C. Francis and M. Zucchetti, "Mathematical Methods for Hyperspectral Imaging in Landmine Detection", Transactions of the American Nuclear Society, Vol. 112, San Antonio, Texas, June 7–11, 2015.

[103] J.B. ZARE, P. GADER and M. SCHATTEN, "Vegetation Mapping for Landmine Detection Using LongWave Hyperspectral Imagery", IEEE Transactions On Geoscience And Remote Sensing, 46,1, 172 (2008)

[104] J. KHODER, R. YOUNES. "Proposal for Preservation Criteria to Rare Event. application on Multispectral/Hyperspectral Images". 25th IEEE International Conference on Microelectronics (2013)

[105] N. PLAYLE, "Detection of landmines using hyperspectral imaging". Proc. SPIE 6217, Detection and Remediation Technologies for Mines and Minelike Targets XI, 62170A (2006).

[106] www.ehu.es/ccwintco/index.php/Hyperspectral_Remote_Sensing_Scenes

[107] D. Manolakis, R. Lockwood, T. Cooley, and J. Jacobson. "Is there a best hyperspectral detection algorithm?." In SPIE Defense, Security, and Sensing, pp. 733402-733402. International Society for Optics and Photonics, 2009

[108] J. Yin, Y. Wang, Y. Wang, and Z. Zhao. "A modified algorithm for multi-target detection in hyperspectral image." In Informatics in Control, Automation and Robotics (CAR), 2010 2nd International Asia Conference on, vol. 3, pp. 105-108. IEEE, 2010.

[109] A. Plaza, P. Martínez, R. Pérez, and J. Plaza. "A new method for target detection in hyperspectral imagery based on extended morphological profiles." In Geoscience and Remote Sensing Symposium, 2003. IGARSS'03. Proceedings. 2003 IEEE International, vol. 6, pp. 3772-3774. IEEE, 2003.

[110] W. McCulloch, W. Pitts (1943). "A Logical Calculus of Ideas Immanent in Nervous Activity". Bulletin of Mathematical Biophysics. 5 (4): 115–133. doi:10.1007/BF02478259

[111] C.M. Bishop, "Pattern recognition and machine learning." springer, 2006 p228

[112] M.JL. Orr, "Introduction to radial basis function networks." (1996). http://twyu2.synology.me/htdocs/class_2008_1/nn/Slides/Introduction%20to%20Radial%20Basis%20Function%20Networks%20(1996).pdf

[113] Y. Chen, H. Jiang, C. Li, X. Jia, and P. Ghamisi. "Deep feature extraction and classification of hyperspectral images based on convolutional neural networks."

IEEE Transactions on Geoscience and Remote Sensing 54, no. 10 (2016): 6232-6251.

[114] P.-H. Hsu, "Feature extraction of hyperspectral images using wavelet and matching pursuit." ISPRS Journal of Photogrammetry and Remote Sensing 62, no. 2 (2007): 78-92.

[115] X. He, D.Cai, S. Yan and H.J. Zhang, "Neighborhood preserving embedding." Computer Vision, 2005. ICCV 2005. Tenth IEEE International Conference on. Vol. 2. IEEE, 2005.

[116] J.W. Sammon, "A nonlinear mapping for data structure analysis." IEEE Transactions on computers 5 (1969): 401-409.

[117] M. Khoder, S. Kashana, J. Khoder, and R. Younes. "Multicriteria classification method for dimensionality reduction adapted to hyperspectral images." Journal of Applied Remote Sensing 11, no. 2 (2017): 025001-025001.

[118] B.-C. Kuo, and D. A. Landgrebe. "Nonparametric weighted feature extraction for classification." Geoscience and Remote Sensing, IEEE Transactions on 42, no. 5 (2004): 1096-1105.

[119] J. Khodr, and R. Younes. "Dimensionality reduction on hyperspectral images: A comparative review based on artificial datas." In Image and Signal Processing (CISP), 2011 4th International Congress on, vol. 4, pp. 1875-1883. IEEE, 2011.

[120] H. Grahn, and P. Geladi, eds. "Techniques and applications of hyperspectral image analysis". John Wiley & Sons, 2007 p185.

[121] H. Ren and C.-I. Chang, "Automatic spectral target recognition in hyperspectral imagery," IEEE Transactions on Aerospace and Electronic Systems, vol. 39, no. 4, pp. 1232–1249, October 2003.

[122] http://aviris.jpl.nasa.gov

[123] I. Makki, R. Younes, C. Francis, T. Bianchi, and M. Zucchetti. "Classification algorithms for landmine detection using hyperspectral imaging." In Landmine: Detection, Clearance and Legislations (LDCL), 2017 First International Conference on, pp. 1-6. IEEE, 2017.

[124] W.F. Nanceb, E. Basenera, and J. Kerekesa. "The target implant method for predicting target difficulty and detector performance in hyperspectral imagery." In Proc. of SPIE Vol, vol. 8048, pp. 80481H-1. 2011.

[125] rsipg.dii.unipi.it

[126] C. M. Bishop, 1996, Neural Networks for Pattern Recognition. Oxford Univ. Press, Oxford

[127] O. Laurino, R. D'Abrusco, G. Longo, G. Riccio; "Astroinformatics of galaxies and quasars: a new general method for photometric redshifts estimation", Monthly Notices of the Royal Astronomical Society, Volume 418, Issue 4, 21 December 2011, Pages 2165–2195, https://doi.org/10.1111/j.1365-2966.2011.19416.x

[128] I. Nabney, "NETLAB: algorithms for pattern recognition.", Springer Science & Business Media, 2002.

[129] M. Zucchetti, M. Khoder, I. Makki, R. Younes, C. Francis and T. Bianchi, "Landmines: Crisis, legacy, international and local action," 2017 First International Conference on Landmine: Detection, Clearance and Legislations (LDCL), Beirut, 2017, pp. 1-6.doi: 10.1109/LDCL.2017.7976954

[130] http://www.icbl.org/en-gb/the-treaty/treaty-status.aspx

[131] https://www.asdi.com/products-and-services/accessories/illuminator-reflectance-lamp

[132] Fundamentals of remote sensing, Canada center for remote sensing chap 2.8. http://pages.csam.montclair.edu/~chopping/rs/CCRS/chapter2/chapter2_8_e.html

[133] E. Truslow, "Performance evaluation of the adaptive cosine estimator detector for hyperspectral imaging applications.", Diss. NORTHEASTERN UNIVERSITY, 2012.